University of Southampton

Faculty of Engineering and Physical Sciences

Physics and Astronomy

A Holographic Study of High-Density Matter and Astrophysical Applications

by

Jesús Cruz Rojas

ORCiD: 0000-0002-5614-0649

Thesis for the degree of Doctor of Philosophy

November 2020

University of Southampton

Abstract

Faculty of Engineering and Physical Sciences
Physics and Astronomy

Thesis for the degree of Doctor of Philosophy

A Holographic Study of High-Density Matter and Astrophysical Applications

by Jesús Cruz Rojas

In this thesis we study a variety of physical phenomena using the Gauge/Gravity duality to model the symmetries that mimic QCD in the field side at the strong regime, by studying weakly coupled fields in a fixed AdS space-time.

We compute the gauge dependent quark condensate in the colour superconducting phase. We construct a holographic dual of the condensate by arguing that near the chiral restoration transition, the strongly coupled gluons are gapped so that the colour quantum numbers of the quarks can be thought of below that gap as global indices. An AdS/superconductor model is then used to analyze the fermionic gap formation. We investigate the role of four fermion interactions to include the gapped QCD interactions. It turns out to be easiest to relate the interaction of the holographic superconductor to the strength of the gapped gluons. The result is a holographic description of the QCD colour superconducting phase diagram. We take a first look at how quark mass enters and causes a transition between the colour flavour locked phase and the 2SC phase.

Next we adjust the D3/D7 model to include a running anomalous dimension for the chiral quark condensate. This introduces a mechanism for chiral symmetry breaking, yet the model still has a deconfined massive phase at intermediate densities. We show that these systems, dependent on the running profile in the IR, generate stiffer equations of state than the base D3/D7 model, and a non-monotonic behaviour in the speed of sound. We show that this model support hybrid compact stars with quark cores.

Finally we present a model with a first order chiral restoration phase transition with chemical potential, μ, due to a discontinuity in the dual description as the quarks are integrated out below their constituent mass. The model predicts a deconfined, massive quark phase at intermediate densities (350MeV$< \mu <$ 550MeV). This phase, has a very stiff equation of state and a speed of sound close to the speed of light. We also include a holographic description of a colour superconducting condensate in the chirally restored vacuum which provides a first order transition from the deconfined massive quark phase at very high density ($\mu >$ 550MeV). We solve the TOV equations and find stable hybrid stars with quark cores and with values of the tidal deformabilities that provide an excellent fit to the gravitational wave data GW170817 of LIGO and Virgo.

Contents

List of Figures

List of Tables

Declaration of Authorship

I, Jesús Cruz Rojas , declare that the thesis entitled *A Holographic Study of High-Density Matter and Astrophysical Applications* and the work presented in the thesis are both my own, and have been generated by me as the result of my own original research. I confirm that:

- This work was done wholly or mainly while in candidature for a research degree at this University;
- Where any part of this thesis has previously been submitted for a degree or any other qualification at this University or any other institution, this has been clearly stated;
- Where I have consulted the published work of others, this is always clearly attributed;
- Where I have quoted from the work of others, the source is always given. With the exception of such quotations, this thesis is entirely my own work;
- I have acknowledged all main sources of help;
- Where the thesis is based on work done by myself jointly with others, I have made clear exactly what was done by others and what I have contributed myself;
- Parts of this work have been published as references: [1][2]

Signed:.....

Date:.....

Acknowledgements

First of all I would like extend my gratitude to my supervisor, Prof. Nick Evans for his kind willingness to share his knowledge and for his vast patience. He is always very approachable to discuss physics. Without his guidance I would have been unable to complete this work.

I am also very grateful to my collaborator Dr. Kazem Bitaghsir Fadafan, who co-authored two of the papers in which this thesis is based, for all that he taught me during our time spent working together and for his sincere friendship.

In the years I have lived in Southampton, I have meet a lot of great people with whom I have become friends. There are too many to name here, but special mention must be made (in alphabetical order) for David Arcia Anaya, Rafael Angel Gutierrez Nuo, Nicolas Kinich Hernandez Sanchez, Monserrat Kong, Erick Montes de Oca Valle, Diego Ojeda Pedraza and Preeti Prasanan. Without their friendship, my time in Southampton would not have been nearly so fun.

I would also like to profoundly thank my parents and my sister for their unconditional support. Specially to Norma Gabriela Rojas García, this thesis would not have been possible without her constant encouragement and affection.

Finally, I would like to thank Diana Franco Bocanegra, for all the moments we spent together, every one of them truthfully marvelous, for her kindness and for her loving care. She was the main reason I could consider Southampton my home during my time here.

This thesis was supported by Mexico's National Council of Science and Technology CONACyT Scholarship No. 439332.

Jesús Cruz Rojas
Southampton UK
September 2020

Into this wild abyss,
The womb of nature and perhaps her grave,
Of neither sea, nor shore, nor air, nor fire,
But all these in their pregnant causes mixed
Confusedly, and which thus must ever fight,
Unless the almighty maker them ordain
His dark materials to create more worlds,
Into this wild abyss the wary fiend
Stood on the brink of hell and looked a while,
Pondering his voyage...

John Milton: Paradise Lost, Book II

Chapter 1

Introduction

1.1 Motivation

Physics in the 20th century was built on two large pillars: General Relativity (GR) and Quantum Field Theory (QFT). GR describes the gravitational force in terms of the geometry of the space-time, whereas QFT aims to describe the quantum interactions observed among fundamental particles.

The two theories typically work for phenomena at very different energy scales, however, there are some situations in which both, the gravitational and the quantum interactions observed between subatomic particles need to be taken into account; such is the case of the study of the singularities in the interior of black holes, and the initial singularity before the big bang [3]. A theory of quantum gravity is needed to fully comprehend these limit cases.

On the other hand, within QFT there are several open questions. The more relevant for this thesis are the ones that have to do with the strong interaction. Since the early formulation of the theory that describes the strong interaction between quarks and gluons, Quantum Chromodynamics (QCD) [4], there have been problems in explaining some of its features such as confinement and the breaking of the chiral symmetry. There also have been problems in exploring the high density phase diagram of the theory in the strongly coupled regime. Many advances have been made with the introduction of computational approaches such as the Lattice Field Theory scheme, however, due to the sign problem [5] Lattice calculations are limited.

The Anti-de Sitter/Conformal Field Theory (AdS/CFT) duality proposed by Maldacena [6] is the most prominent realisation of the holographic principle. It has provided us with a possible solution to the apparently unrelated problems described before. Indeed, we may have a way to obtain a quantum description of Gravity if we use the duality in a way that we can explore the strongly coupled type IIB String Theory. On the

other hand, if we use the duality in the inverse regime where the gravity side is weakly coupled it provide us with the ability to rigorously compute observable quantities in the strong coupling regime of the QFT $\mathcal{N} = 4$ super Yang-Mills theory in the limit of a large number of colour charges N. Thus, in this second regime of the duality, one can study mechanisms and develop intuition about aspects of QFT at large coupling, using a weakly coupled dual gravitational theory based on the Anti-de Sitter (AdS) space-time.

In this thesis, we will take the later approach to the duality and seek for a holographic realisation of physical phenomena in QFT such as the breaking of the chiral symmetry and the change to the Colour Superconductivity (CSC) phase at high densities, which can be posed with the study of Conformal Field Theories (CFT) and their deformations that resemble QCD.

1.2 Gauge theories

In this section we provide a brief introduction to gauge field theories. Specifically, we focus on Quantum Chromodynamics, we review its Lagrangian and symmetries as well as the main characteristics of the theory. Finally, we also provide a review of the current understanding of the phase diagram and of the higher density phases of QCD, where chiral symmetry is restored and beyond, where quark condensation is expected to cause a colour superconductivity phase.

A non-comprehensive list of introductory texts for the study of gauge theories is [7, 8].

1.2.1 Quantum Chromodynamics

The Standard model is the most successful model to describe physical phenomena at high energies, typically higher than around 200 MeV[1] since we need to be able to use perturbative techniques. It is built from certain QFT, based on different special unitary groups $SU(N)$, which are called Yang-Mills theories. They describe the different forces with which the fundamental particles interact: the strong force which is described by Quantum Chromodynamics, and the electromagnetic together with the weak force which are described by the electroweak model. These three fundamental interactions are mediated by the exchange of vector bosons.

A Yang-Mills theory is constructed from a Lagrangian density $\mathcal{L}$ which is Lorentz invariant. $\mathcal{L}$ is also gauge invariant, which mean it have a non abelian Lie group G acting as a local symmetry. For example, for the case of the electroweak model, G is $U(1) \times SU(2)$,

[1] This is the approximate value of the scale Λ_{QCD} where the coupling of QCD diverges. The other theories in the standard model have Landau Poles at much larger energies and are weakly coupled for smaller energies

whereas for the case of QCD, G is the special unitary group $SU(3)$. Fields that differ by a gauge transformation are physically exactly the same.

Historically among the Standard Model, the study of strong interactions was a mayor challenge. The huge amount of hadrons discovered at the time were successfully classified by the quark model of Gell-Mann and Zweig [9, 10]; however, the dynamics of the quark model were unknown. Also, the observation of composite particles such as the Ω^- hyperon, composed of three strange quarks with parallel spins had no explanation; since quarks are fermions, such a combination is forbidden by Pauli's exclusion principle. This evidence led to the notion of the colour degrees of freedom [11]. In addition there was experimental observation in deep inelastic scattering of leptons on nucleons, of asymptotic freedom [7]. Together this gave rise to the emergence of ideas such as String Theory and ultimately QCD.

To this day QCD is the theory that provides the best description available for strong interactions. It explains how hadrons interact and decay, and also predicts its spectrum. This is a consequence of the more profound scope of the theory since QCD aims to explain the interaction between quarks and gluons. QCD is a non-abelian gauge theory since its symmetry group is $SU(3)$. The QCD analog of the electric charge in the theory that describes electromagnetism, Quantum Electrodynamics (QED), is a property called colour. Gluons are the force carriers of the theory, just as photons are for the electromagnetic force in QED. The matter degrees of freedom of the theory, called quarks, come in six flavours. The masses of the lighter and heavier quark flavours differ by two orders of magnitude, this is a fact still not explained, since the quark masses enter the standard model as free parameters. At very low energies only three quark flavours contribute, the up, down and strange quarks.

The Lagrangian of classical QCD is given by

$$\mathcal{L}_{\text{QCD}} = -\frac{1}{2}\,\text{tr}\left(G_{\mu\nu}G^{\mu\nu}\right) + \sum_{f=1}^{N_f} \bar{\psi}_f \left(i\not{D} - m_q \mathbb{1}_c\right) \psi_f \tag{1.1}$$

where $\not{D} = \gamma^\mu \left(\partial_\mu - igA_\mu\right)$ is the gauge covariant derivative contracted with a gamma matrix. We have suppressed the sum over the colour and flavour indices. We observe that $\mathcal{L}_{\text{QCD}}$ is Poincaré invariant; (1.1) also has the discrete symmetries CPT as well as the $SU(3)$ local gauge symmetry and the $U(1)$ baryon number symmetry. $G_{\mu\nu}$, the field strength tensor, which is analogous to the Faraday tensor for the electromagnetic field is defined as:

$$G^{\mu\nu} = G_a^{\mu\nu} T_a = \partial^\mu A^\nu - \partial^\nu A^\mu - ig\left[A^\mu, A^\nu\right] \tag{1.2}$$

$G_{\mu\nu}$ transforms in the adjoint representation of the gauge group $SU(3)$, which is called colour symmetry group. The explicit transformations of the fields under a local gauge transformation $\alpha(x) \in L(SU(3))$, where $L(SU(3))$ is the Lie algebra of the gauge group,

are:

$$\psi(x) \to e^{i\alpha(x)}\psi(x)$$
$$A^{\mu}(x) \to e^{i\alpha(x)}A^{\mu}e^{-i\alpha(x)} + \tfrac{1}{g}e^{i\alpha(x)}\partial^{\mu}e^{-i\alpha(x)} \tag{1.3}$$

The quanta of the gauge field are the gluons. The quark fields are given by Dirac spinors ψ_j transforming in the fundamental representation of the gauge group as we see in (1.3). For simplicity we have suppressed their spinorial indices. We have chosen all quark masses m_q to be equal. The Dirac spinors also transform in the fundamental representation of a global flavour symmetry $SU(N_f)$ with $f = 1, \ldots, N_f$. Since the strong interaction does not discriminate between different flavours of quark, QCD has the approximate global $SU(N_f) \times SU(N_f)$ flavour chiral symmetry when the mass of the quarks is small compared to some cut-off scale Λ.

As mentioned before, since the early years in the development of QCD the theory has not been completely understood and problems in explaining asymptotic freedom and chiral symmetry breaking are still unresolved. Also the fact that the coupling constant of the theory depends on the scale of energy make the computations in the strongly coupled regime very difficult, and solvable in reasonable time only in some cases and with the use of powerful computational techniques. For instance a standard approach to low-energy non-Abelian gauge theories, is lattice gauge theory.

Some of the most interesting phenomena in QCD, that are approached with holographic techniques, are the deconfinement of quarks from the nucleus at a certain scale of energy, the breaking of the chiral symmetry and the change of phase from deconfined quarks to colour superconductor matter. In the following subsections we shall discuss these important features of the theory.

1.2.2 Asymptotic freedom and deconfinement

It was for a long time completely obscure that a theory of exchanging vector bosons could correctly describe the strong interaction. Part of the problem was that quarks are never observed as isolated particles. The quarks and gluons can only exist in bound states with no overall colour. They are confined into hadrons; these can be baryons, with one of each of the three colours represented, or mesons which are formed by a quark and an anti-quark. Thus the existence of quarks, and all their properties, had to be deduced from the spectrum of observable strongly interacting particles.

Intuitively, we can understand confinement by considering that the effective potential between two quarks increases with their separation rather than decreasing as occurs in weakly coupled theories. If we attempt to take the quark and antiquark apart in a meson, at some point the potential energy exceeds the energy required to create a new

quark-antiquark pair. The meson will then split into two new mesons and at no point there would be a free quark.

The hint that the strong interactions is in fact mediated by a gauge boson arose from another mystery at the time: the observation that the strong interactions turn themselves off when the momentum transfer is very large.

This can be seen considering the beta function $\beta(g)$. This function encodes the running of a coupling parameter, g; it is defined by the relation:

$$\beta(g) = \mu \frac{\partial g}{\partial \mu} = \frac{\partial g}{\partial \ln \mu} \tag{1.4}$$

where μ here, is the energy scale of the given physical process.

In the quantized QCD theory, if the quark masses are taken to be equal, the one-loop β function for the gauge coupling is given by

$$\beta(g) = -\frac{g^3}{48\pi^2}(11N - 2N_{\mathrm{f}}) \tag{1.5}$$

The 1 loop diagrams that contribute to the beta function (1.5) are shown in Fig. 1.1

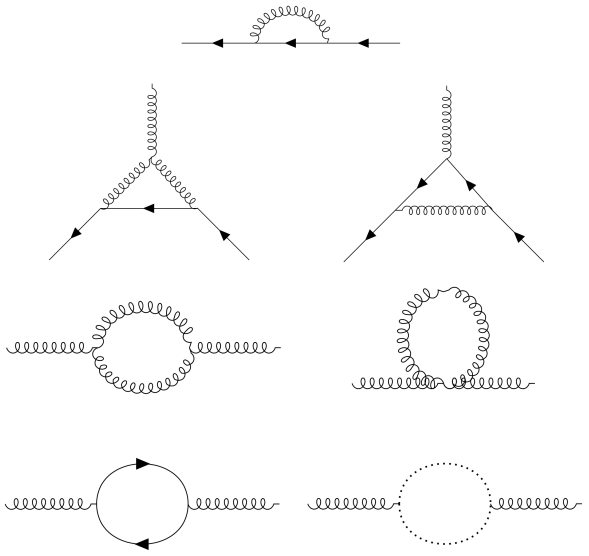

Figure 1.1: *Feynman diagrams that contribute to the 1 loop level beta function of QCD.*

The loop diagram at the bottom-right in Fig. 1.1 represent the Fadeev-Popov ghost fields c^a, where a is an index in the adjoint representation of the gauge group. This ghost fields are scalars under Lorentz transformations, but they are anti-commuting entities. Fadeev-Popov ghost fields are necessary to restrict the Path integral domain of integration to fixed gauge solutions [12].

In this case $N = 3$ is the number of colours and N_f is the number of flavours. For $11N > 2N_{\mathrm{f}}$, $\beta(g)$ is negative. This implies that there is a UV fixed point for $\mu \to \infty$,

with μ the renormalization scale, at which the theory is asymptotically free. Asymptotic freedom is a key feature of non-Abelian gauge theories. On the other hand, for low energies, the gluons, which also carry colour charge, make the coupling becomes large and perturbation theory breaks down.

1.2.3 Chiral symmetry breaking

Chiral symmetry and how it spontaneously breaks is one of the most important features of QCD at low energies. Chiral symmetry breaking is the mechanism for the mass generation of some light particles, such as the pion, which is a pseudo-Goldstone boson of this spontaneously broken symmetry. As we mentioned before, the QCD Lagrangian (1.1) has the approximate global $SU(N_f) \times SU(N_f)$ flavour chiral symmetry. This symmetry is exact in the case of massless QCD:

$$\mathcal{L}_{\mathrm{QCD}}|_{m=0} = -\frac{1}{4}F^a_{\mu\nu}F^{a\mu\nu} + i\bar{\psi}_{\mathrm{L}}\not{D}\psi_{\mathrm{L}} + i\bar{\psi}_{\mathrm{R}}\not{D}\psi_{\mathrm{R}} \tag{1.6}$$

In (1.6) ψ_{L} and ψ_{R} are the left-handed and right-handed chiral projections of the Dirac spinors ψ of (1.1) which in the massless case we can rewrite as

$$\psi = \begin{pmatrix} \psi_{\mathrm{L}} \\ \psi_{\mathrm{R}} \end{pmatrix} \tag{1.7}$$

In this case the chiral projections have separate invariances under the flavour symmetry, rotating the left-handed and the right-handed components independently makes no difference to the theory. For the case of three flavours u, d, s, i.e. $N_{\mathrm{f}} = 3$, we have

$$\psi_{\mathrm{L}} \mapsto e^{(-i\theta_{\mathrm{L}}\cdot\lambda)}\psi_{\mathrm{L}}, \quad \psi_{\mathrm{R}} \mapsto e^{(-i\theta_{\mathrm{R}}\cdot\lambda)}\psi_{\mathrm{R}} \tag{1.8}$$

where $\lambda_a, a = 1, \ldots, 8$ are the $SU(3)$ Gell-Mann matrices. These transformations can also be expressed as vector and axial-vector transformations,

$$\psi \mapsto e^{(-i\theta_V\cdot\lambda)}\psi, \quad \psi \mapsto e^{(-i\theta_A\cdot\lambda\gamma_5)}\psi \tag{1.9}$$

with $\theta_V = (\theta_{\mathrm{L}} + \theta_{\mathrm{R}})/2$, $\theta_{\mathrm{A}} = (\theta_{\mathrm{L}} - \theta_{\mathrm{R}})/2$. The Lagrangian (1.6) is thus invariant under $SU(3)_L \times SU(3)_R$ or equally under $SU(3)_V \times SU(3)_A$.

Given the transformations of the spinors as described in (1.9), we might have expected a $U(3)_V \times U(3)_A$ global symmetry, which then would be equivalent to $SU(3)_V \times SU(3)_A \times U(1)_V \times U(1)_A$. However, it turns out that in QCD, the $U(1)_A$ symmetry is anomalous [13], and thus not present in the quantized theory. We can see how this anomaly arises by considering the axial charge of the symmetry

$$Q_A \equiv \int \mathrm{d}^3x\psi^\dagger\gamma_5\psi \tag{1.10}$$

This is time independent, so axial symmetry is conserved classically. Under this symmetry the fermions transform as $\psi \to e^{i\gamma_5\theta}\psi$. When the theory is quantized, bilinears of the same fermion field at the same space-time point become ill defined. So Q_A, which depends on a local bilinear of the fermions becomes singular. This singularity can be solved through a renormalization procedure. However, it is not possible to construct a renormalization procedure that preserves the transformation rules so the symmetry is broken in the quantum theory.

The divergence of the associated axial current receives nontrivial quantum contributions through the triangle quark loop graph, $\langle \partial_\mu J_5^\mu \rangle \neq 0$. If we consider this for general values of N and N_f, then the only exception to the anomalous $U(1)_A$ symmetry breaking arises when $N_f \ll N$. In this case, the triangle graph gives a contribution

$$\langle \partial_\mu J_5^\mu \rangle = \frac{1}{16\pi^2}\frac{N_\mathrm{f}}{N}\tilde{F}F \tag{1.11}$$

The triangle graph becomes suppressed in the $1/N$ expansion. The $U(1)_A$ symmetry is thus not anomalous at the large N limit.

As the axial symmetry is not present at the quantum level, this leaves the theory with an $SU\,(3)_L \times SU\,(3)_R \times U(1)_B$ symmetry, where $U(1)_B$ is the symmetry associated with the conservation of baryon number.

Since QCD is strongly coupled in the infra-red (IR), e.g. at low energies, the vacuum is non-perturbative, this means it is not the vacuum of the free theory to which one would add the interactions by perturbation theory. The very strong interaction between quark anti-quark pairs in QCD leads to a ground state with a $\langle \bar{\psi}\psi \rangle$ condensate, just as in the BSC superconductor model [14] where electrons form Cooper pairs in the ground state of a metal. Expanding the condensate in terms of the left and right chiral components we obtain $\left\langle \bar{\psi}_L\psi_R + \bar{\psi}_R\psi_L \right\rangle$.

In other words, the dynamics of the strong force generates a vacuum expectation value for the operator $\langle \bar{\psi}\psi \rangle = \left\langle \bar{\psi}_\mathrm{L}\psi_\mathrm{R} \right\rangle + \text{h.c.} \neq 0$[2]. The vacuum is then no longer invariant under separate transformations of the left and right hand sectors $SU(3)_L$ and $SU(3)_R$ but only under a subset of these that acts on both sides equally. The flavour symmetry is broken down to a single vector $SU(3)_V$ factor

$$SU(3)_L \times SU(3)_R \to SU(3)_V \tag{1.12}$$

Goldstone's theorem [15] states that the spontaneous breaking of a symmetry group into a smaller one produces a set of Goldstone bosons. Eight massless Goldstone bosons are expected, one for each generator for which the associated symmetry is broken. In QCD

[2] h.c. is an abbreviation for "plus the Hermitian conjugate"; it means is that there are additional terms which are the Hermitian conjugates of all of the preceding terms.

these correspond to quark bound states, the pions and kaons $\pi^{\pm}, \pi^0, K^{\pm}, K^0, \bar{K}^0$ and the eta-particle η.

These eight Goldstone bosons correspond to the octet representation of $SU(3)$. As a meson consists of a quark and an anti-quark which live in the fundamental $\mathbf{3}$, and anti-fundamental $\overline{\mathbf{3}}$ representations of $SU(3)$ correspondingly, and as we can see from the weight diagrams; we have that the tensor product of this representation gives us

$$\mathbf{3} \otimes \overline{\mathbf{3}} = \mathbf{8} \oplus \mathbf{1} \tag{1.13}$$

where $\mathbf{8}$ is the octet representation and $\mathbf{1}$ is the singlet. The octet is identified with the observed pions, kaons and η^0 mesons. The singlet is the η' state which correspond to the anomalous axial symmetry described above. If the chiral symmetry were exact all these mesons would be massless however since it is only an approximate symmetry group we get massive, but light, pseudo-Goldstone bosons.

Since baryons consist of three quarks a similar analysis using three quarks in the fundamental representation give us

$$\mathbf{3} \otimes \mathbf{3} \otimes \mathbf{3} = \mathbf{1} \oplus \mathbf{8} \oplus \mathbf{8} \oplus \mathbf{10} \tag{1.14}$$

which provide the set of baryons.

1.2.4 High density phases in QCD

The phase diagram of quark matter is still not very well understood. QCD is an asymptotically free theory, thus at high temperatures (or densities), the quarks are deconfined because their mutual distances decrease and the exchanged momenta increase so the interaction becomes very weak, enough to release them [16]. The state of deconfined quarks is called the quark-gluon plasma (QGP). Lattice QCD calculations have established the existence of the QGP phase at temperatures larger than ~ 150MeV and zero density. Besides this, we know that the ground state of QCD breaks the chiral symmetry spontaneously. However, at sufficiently high temperature $T \gg \Lambda_{\mathrm{QCD}}$, due to the asymptotic freedom, perturbation theory around the approximation of the gas of free quarks and gluons should become applicable. In this regime chiral symmetry is not broken. Thus we must expect a transition from a broken chiral symmetry vacuum state to a chirally symmetric equilibrium state at some temperature $T_c \sim \Lambda_{\mathrm{QCD}}$.

On the other hand, at low energies, we know that there is a phase transition at zero temperature and around 308 MeV in the quark chemical potential μ axis, which separates the gaseous nuclear phase, which we consider vacuum, from the liquid nuclear phase. The transition from the gaseous to the liquid nuclear phase is a first order phase transition. It starts from this point at $T = 0$ and disappears in a critical endpoint at $T \sim 10$MeV

and slightly lower quark chemical potential. In this endpoint, the transition is of second order. Above this endpoint, there is no distinction between these two phases.

For temperatures below $\sim$ 160MeV and quark chemical potentials below $\sim$ 350MeV (corresponding to net-baryon densities which are a few times the nuclear saturation density $n_s \approx 0.16\ fm^{-3}$), strongly interacting matter is in the hadronic phase. In a very similar fashion to the nuclear liquid-gas transition, there is a line of first-order phase transition, which separates the hadronic phase from the QGP and terminates in a critical endpoint where the transition is of second order. This endpoint is approximately at $(T, \mu) \simeq (160, 240)$MeV [17]. For smaller quark chemical potentials, the transition becomes a crossover, and there is no real distinction between hadronic matter and the QGP. The position of the critical endpoint depends on the value of the quark masses. Finally, at large quark chemical potential and small temperature, quark matter becomes a color superconductor.

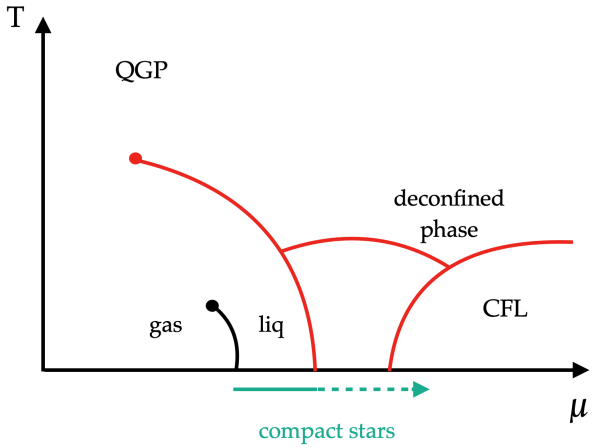

Figure 1.2: *The current of knowledge of the phase diagram of strongly interacting matter. This phase diagram is drawn schematically.*

It is known that a fermionic system at finite chemical potential μ is expected to develop a Fermi surface. A Fermi surface is the surface delimiting the fermionic, occupied states (with energy $E < \mu$) from the fermionic unoccupied ones in the momentum space at zero temperature. The existence of a Fermi surface is a direct consequence of the Pauli exclusion principle, which allows a maximum of one electron per quantum state.

Following Wilson's interpretation of the renormalization group, which views the cutoff scale as a way to divide the interesting degrees of freedom from uninteresting ones, the fixed point in the renormalization group flow founded for this kind of fermionic systems is the Landau's Fermi-liquid theory. From this it is known [18, 19, 20, 21] that if there is an attractive interaction of any kind between the fermions, condensation between two fermions, such as in Cooper pairs, will occur causing superconductivity or superfluidity.

This leads to the natural expectation that quarks will condense in high density QCD, and there has been considerable work on understanding the phase structure (see for

example the review [22]). Typically the preferred condensation is expected to break the colour gauge group of QCD, so the phenomenon is referred to as colour superconductivity (CSC).

Given that in the colour superconductivity phase quarks form Cooper pairs, we need to know who pairs with whom. In quark matter at sufficiently high densities, where u, d, s quarks can be treated equally and effects of the strange quark mass can be neglected, the most symmetric is the colour-flavour locked phase (CFL) [23], where quarks of all three colours and all three flavours form conventional zero-momentum spinless Cooper pairs. In this phase the quarks form Cooper pairs, whose color properties are correlated with their flavour properties in a one-to-one correspondence between three color pairs and three flavour pairs. This is encoded in the quark-quark self-energy

$$\langle \psi_i^\alpha C\gamma_5 \psi_j^\beta \rangle \propto \Delta_{CFL}\epsilon^{\alpha\beta A}\epsilon_{ijA} + \Delta_{CFL}\kappa(\delta_i^\alpha\delta_j^\beta + \delta_j^\alpha\delta_i^\beta) \tag{1.15}$$

where α, β are colour indices, and i, j run from 1 to 3 are flavour indices. Δ_{CFL} is the CFL gap parameter. This means that for example a Cooper pair of an up quark and a down quark must have colours red and green. The Dirac structure $C\gamma_5$ is a Lorentz singlet, and corresponds to parity-even spin-singlet pairing, so it is anti-symmetric in the Dirac indices. The two quarks in the Cooper pair are identical, so the remaining colour-flavour structure must be symmetric.

The dominant term in (1.15) transforms in the $\bar{3}$ channel, whereas the subdominant term multiplied by κ transforms in the 6 channel so in the case of modelling attractive interactions the second term will be neglected. There are many reasons to expect the $\bar{3}$ to be favoured; for example, it is the most attractive channel for quarks interacting via single-gluon exchange which is the dominant interaction at high densities, where the QCD coupling is weak.

At intermediate densities the CFL phase suffers from stresses induced by the strange quark mass. It can only survive down to the transition to nuclear matter if the pairing is strong enough. It is therefore quite possible that other pairing patterns occur at intermediate densities. The 2SC pattern occurs when only u and d quarks of two colours pair. In this phase only up and down quarks of two colours pair lock their Fermi momenta together, contrary to the CFL case in which all colours and flavours pair and have a common Fermi momentum. Therefore the 2SC pattern breaks the colour gauge group $SU(3)$ down to $SU(2)$.

1.3 AdS/CFT correspondence

In this section we shall give a first introduction to the Gauge/Gravity duality. For more details we refer to the books [24, 25, 26, 27] as well as to the review [28]. Before defining the duality in 1.3.4, we will review aspects of conformal field theory (CFT) and one notable example which is the $\mathcal{N} = 4$ Super Yang-Mills (SYM) theory. We will then discuss string theory and AdS space-time, which will be needed for the statement of the duality, and for understanding later chapters of this thesis. Finally, we introduce the probe brane approach to introduce flavour degrees of freedom and the AdS/QCD approach.

1.3.1 Conformal field theory

Conformal field theories, are field theories that are invariant under a specific set of transformation called conformal transformations. A conformal transformation is a coordinate transformation $x \to x'$ such that the metric changes by an overall scale factor $\Omega^2(x)$

$$g_{\mu\nu}(x) \to g'_{\mu\nu}\left(x'\right) = \Omega^2(x) g_{\mu\nu}(x) \tag{1.16}$$

a Weyl transformation can be applied then, which removes the scale factor. Conformal transformations can be visualized geometrically as transformations that change the lengths of vectors but preserving the angles between them. In a d-dimensional Minkowski space, where the metric tensor is $g_{\mu\nu} = \eta_{\mu\nu} = \text{diag}(-1, 1, ..., 1)$ we can define conformal transformations as the most general locally causality preserving transformations, i.e. space-like separated points are mapped to space-like separated points, the same happens with time-like and light-like separated points. For $d \geq 3$ conformal transformations form the group $\text{SO}(d, 2)$, which consist of Poincaré transformations i.e. translations and Lorentz transformations; dilatations; and special conformal transformations, $x^\mu \to \frac{x^\mu + b^\mu x^2}{1 + 2b\cdot x + b^2 x^2}$, where $b \in \mathbb{R}^{d-1,1}$.

The case $d = 2$ is notable in the context of String Theory, since it is the theory defined on the string world-sheet. In this conformal theory is encoded the type of string, the geometry of the space-time in which it propagates, and the presence of background fields. For $d = 2$, the conformal group is infinite-dimensional and has $\text{SO}(2, 2)$ as a subgroup.

To determine the conformal algebra first we need to derive the infinitesimal transformations. In flat space-time the components of the metric tensor are given by $g_{\mu v} = \eta_{\mu v}$. For an infinitesimal transformation $x^\mu \mapsto \tilde{x}^\mu = x^\mu + \epsilon^\mu(x)$, the metric transforms as $\eta_{\mu v} \mapsto \eta_{\mu v} + \partial_\mu \epsilon_v + \partial_v \epsilon_\mu$.

Using the definition (1.16), an infinitesimal conformal transformation needs to satisfy the equation

$$\partial_\mu \epsilon_v + \partial_v \epsilon_\mu = 2\sigma(x)\eta_{\mu v} \tag{1.17}$$

where we have used $\Omega(x) = e^{\sigma(x)} = 1 - \sigma(x) + \mathcal{O}\left(\sigma^2\right)$. Contracting the indices of both sides with $\eta^{\mu\nu}$, we obtain that $\partial \cdot \epsilon = \partial_\mu \epsilon^\mu = \sigma(x) \cdot d$ in d dimensions. Therefore the infinitesimal transformation is conformal if $\epsilon(x)$ satisfies

$$\left(\eta_{\mu\nu}\partial_\rho\partial^\rho + (d-2)\partial_\mu\partial_v\right)\partial \cdot \epsilon = 0 \tag{1.18}$$

We note that equation (1.18) simplifies at $d = 2$. Therefore, we have to distinguish between the cases $d = 2$ and $d > 2$. Let us first consider the case $d > 2$. For $d > 2$, the conformal Killing equation (1.18) is solved if $\epsilon(x)$ is at most of second order in x giving us

$$\epsilon^\mu(x) = a^\mu + \omega^\mu_v x^v + \lambda x^\mu + b^\mu x^2 - 2(b \cdot x)x^\mu \tag{1.19}$$

Then if ϵ^μ is given by (1.19) we have $\sigma = \lambda - 2b \cdot x$. The parameters $a^\mu, \omega^\mu_v, \lambda$ and b^μ have a finite number of components so this tells us that the conformal algebra and the associated symmetry group are finite dimensional. The generators corresponding to a_μ and $\omega_{\mu\nu}$ are the momentum vector P^μ and $J^{\mu\nu}$. The operators D and K^μ, corresponds to dilatations parametrized by λ, and special conformal transformations b^μ. The conformal algebra consisting of $J^{\mu\nu}, P^\mu, D$ and K^μ is given by the commutation relations:

$$\begin{aligned}
[J_{\mu v}, J_{\rho\sigma}] &= i\left(\eta_{\mu\rho}J_{v\sigma} + \eta_{v\sigma}J_{\mu\rho} - \eta_{v\rho}J_{\mu\sigma} - \eta_{\mu\sigma}J_{v\rho}\right) \\
[J_{\mu v}, P_\rho] &= i\left(\eta_{\mu\rho}P_v - \eta_{v\rho}P_\mu\right), \quad [P_\mu, P_v] = 0 \\
[J_{\mu v}, K_\rho] &= i\left(\eta_{\mu\rho}K_v - \eta_{v\rho}K_\mu\right) \\
[D, P_\mu] &= iP_\mu, \quad [D, K_\mu] = -iK_\mu, \qquad [D, J_{\mu\nu}] = 0 \\
[K_\mu, K_\rho] &= 0, \quad [K_\mu, P_v] = -2i\left(\eta_{\mu\nu}D - J_{\mu\nu}\right)
\end{aligned} \tag{1.20}$$

Fields in a CFT transform in irreducible representations of the conformal algebra. In order to construct the transformation representations for general dimensions, first, we analyse how the fields ϕ transform at $x = 0$. Then, using the momentum vector P^μ, we can shift the argument of the field to an arbitrary point x in order to obtain the general transformation. First we have for the Lorenz transformations the following commutation relation:

$$[J_{\mu\nu}, \phi(0)] = -\mathcal{J}_{\mu\nu}\phi(0) \tag{1.21}$$

where $\mathcal{J}_{\mu v}$ is a finite-dimensional representation of the Lorentz group that determines the spin for the field $\phi(0)$. For the conformal algebra, in addition we have commutation relations with the dilatation operator D,

$$[D, \phi(0)] = -i\Delta\phi(0) \tag{1.22}$$

This implies that ϕ has scaling dimension Δ; this means that under the action of dilatations $x \mapsto x' = \lambda x$, it transforms as

$$\phi(x) \mapsto \phi'\left(x'\right) = \lambda^{-\Delta}\phi(x) \tag{1.23}$$

In particular, a field ϕ which transforms covariantly under an irreducible representation of the conformal algebra has a fixed scaling dimension and is therefore an eigenstate of the dilatation operator D.

In a conformal algebra it is sufficient to consider only the conformal primary fields, which are a particular set of fields that satisfy the commutation relation

$$[K_\mu, \phi(0)] = 0 \tag{1.24}$$

By applying the commutation relations of D with P_μ and K_μ to the eigenstates of D, we see that P_μ increases the scaling dimension while K_μ decreases it. In a unitary CFT, there is a lower bound on the scaling dimension of the fields. This implies that any conformal representation must contain operators of lowest dimension which due to (1.24) are annihilated by K_μ at $x^v = 0$. In a given irreducible multiplet of the conformal algebra, the conformal primary fields are the fields of lowest scaling dimension determined by (1.24). All other fields called the conformal descendants of ϕ, are obtained by acting with P_μ on the conformal primary fields.

Using the operator $\mathcal{T}(x) = \exp\left(-iP_\mu x^\mu\right)$ we can write $\phi(x) = \mathcal{T}(x)\phi(0)\mathcal{T}^{-1}(x)$ and thus we can obtain the commutation relations for a conformal primary field $\phi(x)$

$$\begin{aligned}
[P_\mu, \phi(x)] &= -i\partial_\mu\phi(x) \equiv \mathcal{P}_\mu\phi(x) \\
[D, \phi(x)] &= -i\Delta\phi(x) - ix^\mu\partial_\mu\phi(x) \equiv \mathcal{D}\phi(x) \\
[J_{\mu\nu}, \phi(x)] &= -\mathcal{J}_{\mu\nu}\phi(x) + i\left(x_\mu\partial_\nu - x_\nu\partial_\mu\right)\phi(x) \equiv \tilde{\mathcal{J}}_{\mu\nu}\phi(x) \\
[K_\mu, \phi(x)] &= \left(i\left(-x^2\partial^\mu + 2x_\mu x^\rho\partial_\rho + 2x_\mu\Delta\right) - 2x^\nu\mathcal{J}_{\mu\nu}\right)\phi(x) \equiv \mathcal{K}_\mu\phi(x)
\end{aligned} \tag{1.25}$$

Now we discuss what is probably the most important example of a CFT, $\mathcal{N} = 4$ super Yang-Mills in $d = 4$. This is also a gauge, supersymmetric theory, thus generators of its symmetry group include those we have already mentioned; the Poincare generators, as well as dilatation and special conformal transformations . We also have the additional supersymmetry generators Q^I_α and $\bar{Q}^I_{\dot{\alpha}}$.

In addition to these we also have the 15 generators T^A of the $SU(4)$ R-symmetry, and two new superconformal supersymmetries S^I_α and $\bar{S}^I_{\dot{\alpha}}$ which arise from the commutators of the Poincaré supersymmetries with the conformal symmetry generators. The complete superconformal group is $SU(2,2|4)$, of which both $SO(4,2)$, which is the conformal symmetry group, and $SU(4)$ are bosonic subgroups. The Lagrangian for this theory is:

$$\mathcal{L} = \mathrm{Tr}\left\{-\frac{1}{2g^2}F_{\mu\nu}F^{\mu\nu} + \frac{\theta_I}{8\pi^2}F_{\mu\nu}\bar{F}^{\mu\nu} - \bar{\lambda}^a\bar{\sigma}^\mu D_\mu\lambda_a - D_\mu X^i D^\mu X^i \right.$$
$$\left. + gC_i^{ab}\lambda_a\left[X^i,\lambda_b\right] + g\bar{C}_{iab}\bar{\lambda}^a\left[X^i,\bar{\lambda}^b\right] + \frac{g^2}{2}\left[X^i,X^j\right]^2\right\} \tag{1.26}$$

where $F_{\mu\nu}$ is the Maxwell tensor for the gauge field A_μ which is a singlet of the $SU(4)$ global R symmetry group, λ_a are a set of 4 Weyl fermions in the adjoint representation of the gauge group, X^i are a set of 6 scalars again in the adjoint representation. D_μ is the covariant derivative, g is the gauge coupling, σ^μ are the Pauli matrices and C_i^{ab} and θ_I are constants. C_i^{ab} arise from the Clifford Dirac matrices and θ_I is a parameter known as the real instanton angle.

This theory has the property that the beta function of its unique coupling vanishes to all orders in perturbation theory. This confirms the theory is conformal also at the quantum level.

We can illustrate why the beta function of this theory is zero at one loop level, by considering the QCD beta function. Equation (1.5) can be put in terms of the constants $C_2(R)$ and $C(R)$ which depend on the representation R of the gauge group and also on the normalisation of the generators of the corresponding Lie algebra T_a, and are defined by:

$$\begin{aligned} T^aT^a &= C(R)I \\ \mathrm{Tr}\left(T_aT_b\right) &= C(R)\delta_{ab} \end{aligned} \tag{1.27}$$

For the case of a Yang-Mills theory coupled to n_f fermions and n_s scalars with representations R_f and R_s respectively, we can obtain a similar expression:

$$\beta(g) = \frac{g^3}{16\pi^2} \times \left(-\frac{11}{3}C_2(G) + \frac{2}{3}n_f C(R_f) + \frac{1}{6}n_s C(R_s)\right) \tag{1.28}$$

In $\mathcal{N} = 4$ super Yang-Mills we have $n_f = 4$ Weyl fermions and $n_s = 6$ real scalars. In this case all particles are in the adjoint representation of $SU(N)$ since they all belong to the vector multiplet. Then we can see that the beta function (1.28) vanishes.

1.3.2 Anti-de Sitter space

General Relativity is based on the idea that gravitational interactions are due to the geometry of the space-time, and that matter itself curves the space-time. The space-time is modelled in terms of differentiable manifolds $\mathcal{M}$. This is physically reasonable since this allows invariance under coordinate transformations.

Of central importance is the role is played by the metric, which is a $(0,2)$ tensor field g i.e. at each point $p \in \mathcal{M}$ g is a non-degenerate symmetric bilinear form $g : T_p(\mathcal{M}) \times T_p(\mathcal{M}) \to \mathbb{R}$.

The metric may be expressed in terms of the basis covectors $\mathrm{d}x^\mu \otimes \mathrm{d}x^\nu$ of $T_p^*(\mathcal{M}) \times T_p^*(\mathcal{M})$ using the components $g_{\mu\nu}(x)$ as

$$\mathrm{d}s^2 \equiv g_{\mu\nu}(x)\mathrm{d}x^\mu \otimes \mathrm{d}x^\nu \tag{1.29}$$

Usually one suppresses $\otimes$ and writes $g_{\mu\nu}\mathrm{d}x^\mu\mathrm{d}x^\nu$ as a shorthand notation. Equation (1.29) introduces the notion of an infinitesimal line element. If $g_{\mu\nu}$ has only positive eigenvalues the manifold is Riemannian while if it has one negative eigenvalue the manifold is Lorentzian. For Lorentzian manifolds, the infinitesimal line element $\mathrm{d}s^2$ determines whether a vector $\mathrm{d}x^\mu$, viewed as an infinitesimal distance between points on a manifold, is space-like, time-like or light-like depending on the sign of $\mathrm{d}s^2$.

Einstein introduced the field equations

$$R_{\mu\nu} - \frac{1}{2}Rg_{\mu\nu} + \Lambda g_{\mu\nu} = \kappa^2 T_{\mu\nu} \tag{1.30}$$

which relate the matter content, given by the energy momentum tensor $T_{\mu\nu}$ on the right-hand side, to the space-time geometry on the left-hand side given by the Ricci tensor $R_{\mu\nu}$. The parameter Λ is the cosmological constant and κ is related to Newton's gravitational constant G by $\kappa^2 = 8\pi G$.

The Einstein equations can be derived from an action principle. The appropriate action of the gravitational system is given by

$$\mathcal{S}\left[g_{\mu\nu}, \varphi\right] = \mathcal{S}_{\mathrm{EH}}\left[g_{\mu\nu}\right] + \mathcal{S}_{\mathrm{matter}}\ \left[g_{\mu\nu}, \varphi\right] \tag{1.31}$$

where $\mathcal{S}_{\mathrm{matter}}$ is the matter action; φ denotes any possible field, such as a matter field or a gauge field. $\mathcal{S}_{\mathrm{EH}}\left[g_{\mu\nu}\right]$ is the Einstein-Hilbert action with cosmological constant Λ

$$\mathcal{S}_{\mathrm{EH}}\left[g_{\mu\nu}\right] = \frac{1}{2\kappa^2}\int \mathrm{d}^d x\sqrt{-g}(R - 2\Lambda) \tag{1.32}$$

By varying the action $\mathcal{S}_{\mathrm{EH}}$ with respect to the metric $g_{\mu\nu}$ we obtain

$$\frac{\delta\mathcal{S}_{\mathrm{EH}}}{\delta g^{\mu\nu}} = \frac{\sqrt{-g}}{2\kappa^2}\left(R_{\mu\nu} - \frac{1}{2}g_{\mu\nu}R + \Lambda g_{\mu\nu}\right) \tag{1.33}$$

Then, defining the energy-momentum tensor $T_{\mu\nu}$ in curved space-time by

$$T_{\mu\nu} \equiv -\frac{2}{\sqrt{-g}}\frac{\delta\mathcal{S}_{\mathrm{matter}}}{\delta g^{\mu\nu}} \tag{1.34}$$

we arrive to Einstein's field equations (1.30).

A manifold of dimension d can only have at most $d(d+1)/2$ linearly independent Killing vector fields. The space-times which satisfy this upper bound are called maximally symmetric space-times. Minkowski space-time is an an example since it has d translational

isometries and $d(d-1)/2$ rotational isometries, which include boosts.

In the case of a Lorentzian manifold there are three maximally symmetric spacetimes classified by the sign of the Ricci scalar R. For $R = 0$, the maximally symmetric space-time is Minkowski space-time, for $R > 0$, the space-time is de Sitter space, and for $R < 0$ the maximally symmetric space-time turns out to be Anti-de Sitter (AdS) space.

AdS space-time is of central importance for the gauge/gravity duality. $(d+1)$-dimensional Anti-de Sitter space, which we abbreviate as AdS_{d+1}, may be embedded into a $(d+2)$-dimensional Minkowski space-time with line element:

$$\mathrm{d}s^2 = -\left(\mathrm{d}X^0\right)^2 + \left(\mathrm{d}X^1\right)^2 + \cdots + \left(\mathrm{d}X^d\right)^2 - \left(\mathrm{d}X^{d+1}\right)^2 \equiv \bar{\eta}_{\mu\nu}\mathrm{d}X^\mu \mathrm{d}X^\nu \tag{1.35}$$

where $\mu, \nu \in \{0, \ldots, d+1\}$. AdS_{d+1} is given then by the hypersurface

$$\bar{\eta}_{\mu\nu}X^\mu X^\nu = -\left(X^0\right)^2 + \sum_{i=1}^{d}\left(X^i\right)^2 - \left(X^{d+1}\right)^2 = -L^2 \tag{1.36}$$

inside $\mathbb{R}^{d,2}$. L is the radius of curvature of the AdS space. Note that the hypersurface given by (1.36) is invariant under $O(d,2)$ transformations acting on $\mathbb{R}^{d,2}$. This means that the isometry group of AdS_{d+1} is $O(d,2)$. Using the isometry group $SO(d,2)$, we may write AdS_{d+1} space as the coset space $SO(d,2)/SO(d,1)$ since a maximally symmetric space-time may be represented as a coset space. The coset is obtained by modding out the isometry group of the space-time by the stabiliser group, which contains those isometries which leave p invariant, for each point $p \in AdS_{d+1}$.

The AdS space has a conformal boundary since for large X^μ, the hyperboloid given by (1.36) approaches the light-cone in $\mathbb{R}^{d,2}$ given by $\bar{\eta}_{\mu\nu}X^\mu X^\nu = 0$.

We may define the conformal boundary of AdS space through a conformal compactification. In the conformal compactification construction, one maps the manifold being considered, in this case (1.36) onto the interior of a compact manifold with boundary, and then one calls the boundary of this manifold the conformal boundary of the original manifold. Thus we define $\partial AdS_{d+1}$by the set of all lines on the light-cone originating from $0 \in \mathbb{R}^{d,2}$, i.e.

$$\partial AdS_{d+1} = \left\{ [X] \quad | \quad X \in \mathbb{R}^{d,2}, X \neq 0, X_\mu X^\mu = 0 \right\} \tag{1.37}$$

where we identify $[X]$ with $[\tilde{X}]$ if $\left(X^0, X^1, \ldots, X^{d+1}\right) = \lambda\left(\tilde{X}^0, \tilde{X}^1, \ldots, \tilde{X}^{d+1}\right)$ for $\lambda \in \mathbb{R}$.

∂AdS_{d+1} is a compactification of d-dimensional Minkowski space-time. To verify this, we can consider a point $X \neq 0$ satisfying $\bar{\eta}_{\mu\nu}X^\mu X^\nu = 0$. Introducing the coordinates (u, v) as following

$$u = X^{d+1} + X^d, \quad v = X^{d+1} - X^d \tag{1.38}$$

we have that the condition $\bar{\eta}_{\mu\nu}X^\mu X^\nu = 0$ becomes $uv = \eta_{\mu v}X^\mu X^v$, where here μ and ν take values in $\{0,\dots,d-1\}$ and $\eta_{\mu\nu}$ is the diagonal matrix with entries $\mathrm{diag}(-1,1,\dots,1)$. If $v \neq 0$ we can rescale X so that $v = 1$ without loss of generality. For a given X^μ with $\mu \in \{0,\dots,d-1\}$ we can solve $uv = \eta_{\mu v}X^\mu X^v$ for u. Therefore for $v \neq 0$ we obtain d-dimensional Minkowski space-time. The points with $v = 0$ correspond to infinities added to d-dimensional Minkowski space-time. With the condition $uv = \eta_{\mu v}X^\mu X^v$ a light-cone is added to Minkowski space-time, this is necessary to define conformal transformations. This also explains why ∂AdS_{d+1} is a conformal compactification of $d-$dimensional Minkowski space-time.

A useful parametrization of the hyperboloid (1.36) is given by

$$\begin{aligned} X^0 &= \frac{L^2}{2r}\left(1 + \frac{r^2}{L^4}\left(\vec{x}^2 - t^2 + L^2\right)\right) \\ X^i &= \frac{rx^i}{L} \quad \text{for } i \in \{1,\dots,d-1\} \\ X^d &= \frac{L^2}{2r}\left(1 + \frac{r^2}{L^4}\left(\vec{x}^2 - t^2 - L^2\right)\right) \\ X^{d+1} &= \frac{rt}{L} \end{aligned} \tag{1.39}$$

Where $t \in \mathbb{R}$, $\vec{x} = \left(x^1,\dots,x^{d-1}\right) \in \mathbb{R}^{d-1}$ and $r \in \mathbb{R}^+$. Due to the restriction $r > 0$, only one-half of the AdS_{d+1} spacetime is covered. These local coordinates are called the Poincaré patch coordinates. In these coordinates, the metric of AdS_{d+1} reads as

$$\mathrm{d}s^2 = \frac{L^2}{r^2}\mathrm{d}r^2 + \frac{r^2}{L^2}\left(-\mathrm{d}t^2 + \mathrm{d}\vec{x}^2\right) \tag{1.40}$$

An explicit calculation of the Ricci scalar for AdS_{d+1} gives $R = -\frac{d(d+1)}{L^2}$. This means that the curvature is negative and constant. This also confirms that L is the radius of curvature.

In the Poincaré patch we can see the AdS space as flat space-time, parametrized by the coordinates $t, \vec{x}$, plus an extra warped direction denoted by r. For a fixed value of r, the d-dimensional transverse slice is flat Minkowski space-time $\mathbb{R}^{d-1,1}$. For $r \to 0$ we have a degenerate Killing horizon, also known as a Poincaré horizon. A Killing horizon is a null hypersurface uniquely defined by $k_\mu k^\mu = 0$, where k_μ is a Killing vector. Note that the Poincaré horizon is only a coordinate singularity, not a curvature singularity since on the other side of the horizon, for $r < 0$, there is another Poincaré patch, which is needed to cover the whole of AdS space-time. We note on the other hand that the metric (1.40) has a second order pole for $r \to \infty$, i.e. g_{ii} diverges quadratically for $r \to \infty$. It is possible to show that any metric of asymptotically AdS spaces always has such a quadratic divergence for a particular value r^* of the radial direction. The slice of space-time for fixed $r = r^*$ is the conformal boundary of the AdS space, in particular for the coordinates used in (1.40) the conformal boundary is at $r \to \infty$.

To continue the metric to the boundary of AdS space, we have to ensure its finiteness. This is done by multiplying the metric by a defining function $g(r,t,\vec{x})$, which has to be a positive smooth function of the coordinates r,t and $\vec{x}$. Also, $g(r,t,\vec{x})$ need to have a second order zero at $r=\infty$. For example $g(r,t,\vec{x}) = \left(L^2/r^2\right)\omega(t,\vec{x})$, with ω a smooth and positive function of $\vec{x}$ and t. Multiplying (1.40) with this example of g and taking the limit $r\to\infty$ allows us to define a finite boundary metric given by $\mathrm{d}s^2_{\partial AdS} = \omega(t,\vec{x})\left(-\mathrm{d}t^2+\mathrm{d}\vec{x}^2\right)$. Different choices of $\omega(t,\vec{x})$, or generally speaking different choices of $g(r,t,\vec{x})$, define different boundary metrics. Therefore the bulk metric determines a class of boundary metrics which are related by conformal transformations. This class is called conformal structure.

From the defining equation for the AdS hypersurface (1.36) is clear that the isometry group of AdS_{d+1} is $SO(d,2)$, but only for the metric in Poincaré coordinates the subgroups $\mathrm{ISO}(d-1,1)$ (Poincaré transformations acting on $(t,\vec{x})$), and $SO(1,1)$ (acting on $t,\vec{x}$ and r as $(t,\vec{x},r)\mapsto(\lambda t,\lambda\vec{x},r/\lambda)$) of $SO(d,2)$ are manifest. It can be shown that the isometry group $SO(d,2)$ acts on the boundary of AdS as the conformal group of Minkowski space.

To formulate the AdS/CFT correspondence we will need to define an Euclidean signature version of AdS_{d+1} by Wick rotating the component X^0 in (1.36) then the isometry group of Euclidean AdS_{d+1} is given by $SO(d+1,1)$ instead of $SO(d,2)$.

1.3.3 String theory

The basic idea behind String Theory is that we consider one-dimensional extended strings as the fundamental objects. The strings give a $(1+1)$ dimensional worldsheet Σ in the space-time when they propagate, this in juxtaposition of the worldline in the case of the propagation of point-like particles.

The worldsheet Σ is parametrized by the proper time τ and the spatial extension σ of the string. The coordinate σ takes values in the interval $[0,\sigma_0]$, where σ_0 will be chosen later in a convenient way depending if the string is closed or open. The embedding of the worldsheet of the fundamental string into a D-dimensional target space-time is given by functions $X^M(\tau,\sigma)$.

The physics does not depend on the parametrization of the worldsheet. The action of a relativistic string is given by the area of the world-sheet, this is the simplest action that is invariant under parametrization of Σ and it is called the Nambu-Goto action:

$$S = T\int d\tau d\sigma\sqrt{\det P\left[G_{ab}\right]},\quad P\left[G_{ab}\right] = G_{MN}\frac{dX^M}{d\sigma^a}\frac{dX^N}{d\sigma^b} \tag{1.41}$$

Here $T \equiv 1/2\pi\alpha'$ is the string tension, α' is related to the string length l_s as $\alpha' = l_s^2$; $\sigma^a = (\tau, \sigma)$ are the time and space coordinates on the worldsheet; P represents the pullback of the metric; and G_{MN} is the background metric of the target space-time.

The Nambu-Goto action (1.41) can be rephrased as the Polyakov action (1.42) by introducing a worldsheet metric h_{ab}.

$$S = -\frac{1}{4\pi\alpha'} \int d^2\sigma \sqrt{-h} h^{ab} \partial_a X^M \partial_b X^N G_{MN} \tag{1.42}$$

but there is also a constraint. Using the equations of motion for h_{ab} which are obtained by computing $\delta S/\delta h^{\alpha\beta} = 0$, we conclude that the worldsheet energy-momentum tensor T_{ab} has to vanish,

$$T_{ab} = \partial_a X^M \partial_b X_M - \frac{1}{2} h_{ab} h^{cd} \partial_c X^M \partial_d X_M = 0 \tag{1.43}$$

The equation $T_{ab} = 0$ puts constraints on the dynamical fields X^M of the Polyakov action which are known as Virasoro constraints. The symmetries preserved by the action (1.42) allows us to make the worldsheet metric flat by a Weyl transformation and reparametrization of the worldsheet coordinates.

Analyzing the string spectrum, there are different possibilities to satisfy the boundary conditions of the equations of motion of the Polyakov action (1.42). For free strings the worldsheet topology is either a cylinder in the case of closed strings, or a strip in the case of open strings.

For closed strings we set $\sigma_0 = 2\pi$ and thus the embedding functions X^M has to satisfy periodic boundary conditions. On the other hand for open strings we set up $\sigma_0 = \pi$, in this case there are two different alternatives; Neumann boundary conditions $\partial_\sigma X^M(\tau, \sigma^*) = 0$, or Dirichlet boundary conditions $\delta X^M(\tau, \sigma^*) = 0$, where σ^* is one of the two endpoints of the string. Both boundary conditions can be implemented for each string endpoint independently and for each target space-time dimension. The only exception is the time direction, in which we have to impose Neumann boundary conditions.

Let us consider the boundary conditions in which we take Dirichlet boundary conditions for both ends of the string. We refer to this as DD boundary conditions for X^M. X^M has to satisfy $X^M(\tau, 0) = x_{\mathrm{i}}^M$ and $X^M(\tau, \pi) = x_{\mathrm{f}}^M$ where x_{i}^M and x_{f}^M are the coordinates of the string endpoints. In this case the momentum of the open string p^M given by $p^M = \int_0^\pi \mathrm{d}\sigma \Pi^M(\tau, \sigma)$, with canonical momentum $\Pi^M(\tau, \sigma) = \frac{\partial_\tau X^M(\tau, \sigma)}{2\pi\alpha'}$ is not conserved. By imposing the Dirichlet boundary conditions we have broken translational invariance in this direction, and momentum is no longer conserved.

Since the open string endpoints end on two hypersurfaces parametrised by $x^M = x_i^M$ and $x^M = x_{\mathrm{f}}^M$, these hypersurfaces have to absorb the momentum of the open string

and therefore have to be dynamical. These dynamical objects are referred to as Dirichlet branes, or D-branes for short. D-branes are extended in those directions in which we impose Neumann boundary conditions, and are transverse to those directions in which we impose Dirichlet boundary conditions. We will discuss more profoundly D-branes later in this section.

Classically, the base state of the string is massless, but excited states, which can be visualized as oscillations of the string, form a tower of states with masses in units of $\sqrt{T}$. The zero point energies of these oscillations contribute with a constant negative shift of this spectrum when we consider the quantum string. The only known way to remove the tachyonic modes is to impose supersymmetry.

Supersymmetry also add the fermionic degrees of freedom to the theory which are necessary to model the particles observed in nature. In order to obtain a supersymmetric string worldsheet, a two-component real fermion $\Psi^M = \left(\psi_-^M, \psi_+^M\right)^T$ is added to the Polyakov action. Integrating by parts the fermionic part of the action, we obtain a boundary term that oblige us to choose either open or closed strings boundary conditions.

In order to get rid of the tachyon in the Neveu-Schwarz sector as well as one of the chiralities in the vacuum of the Ramond sector that contains both chiralities, we introduce the fermion number $\exp(i\pi F)$ which counts how often a fermionic creation operator is applied to the vacuum. We keep only those states with an odd number of creation operators applied to $|0\rangle_{\mathrm{NS}}$. In the Ramond sector we have the choice of whether keep only the states with an even or with an odd number of creation operators acting on the vacuum. Depending on the choice, the physical massless string state in the Ramond sector has a definite chirality and is real, i.e. a Majorana-Weyl spinor.

This truncation prescription, known as GSO projection due to Gliozzi, Scherk and Olive [29] leaves an equal number of fermions and bosons at each mass level, leaving a supersymmetric space-time theory. We also see that the worldsheet conformal invariance is anomalous in the quantum theory, unless the theory lives in 10 space-time dimensions.

Oscillations of open strings give rise to massless gauge multiplets. Multiple charges are included via Chan-Paton factors, which are global charges, attached to the ends of the strings, such that non-abelian gauge symmetries may be realized.

Closed strings have both left and right moving modes, such that they naturally generate a massless field that looks like the Lorentz product of two gauge fields, i.e. like a graviton multiplet. The spectrum of closed super-string theory contains the metric, G^{MN}, the scalar dilaton Φ, and a two index antisymmetric tensor B^{MN}. The GSO projection acts as a chiral projection on the space-time fermions emerging from each of the left and right moving modes of a theory of closed strings. If the same chirality is projected in each case, then one obtains type IIA string theory. Its bosonic field content consists

of a gauge field A_1 and a 3-form C_3. If the chiral projections are opposite, then one obtains type IIB theory, with bosonic field content consisting of a scalar, a two-form C_2, and a four-form C_4. Both the type IIA and the type IIB theories possess $\mathcal{N} = 2$ supersymmetry.

Open strings can also be included into type II string theory, breaking the supersymmetry to $\mathcal{N} = 1$. Interactions between strings can be introduced by allowing the string worldsheet to have holes and handles. The dilaton Φ acts as a measure of these topology changes and then the quantity e^{Φ} plays the role of the theory's coupling constant. When open and closed string sectors are combined the Yang-Mills coupling from the open string sector has $g_{YM}^2 = e^{\Phi}$.

Supergravity

For the AdS/CFT correspondence applied to $3+1$-dimensional field theories, type IIB String Theory is crucial and in particular its low-energy limit, which is supergravity. We obtain actions for type II supergravity in the string frame, writing out only the bosonic part of the supergravity actions. Supergravity may also be constructed independently of string theory by requiring local supersymmetry. Supergravity theories may be formulated in any dimension less than or equal to $D = 11$. There exists no completely satisfactory action for the type IIB supergravity, since it involves an antisymmetric field C_4 with self-dual field strength F_5. However, it is possible to write down an action involving both dualities of C_4, and then impose the self-duality as a supplementary field equation. In this way one obtains

$$\begin{aligned} S_{IIB} =& \frac{1}{4\kappa_B^2}\int d^{10}X\sqrt{G}e^{-2\Phi}\left(2R_G + 8\partial_\mu\Phi\partial^\mu\Phi - |H_3|^2\right) \\ & - \frac{1}{4\kappa_B^2}\int\left[\sqrt{G}\left(|F_1|^2 + \left|\tilde{F}_3\right|^2 + \frac{1}{2}\left|\tilde{F}_5\right|^2\right) + C_4\wedge H_3\wedge F_3\right] + \text{ fermions} \end{aligned} \tag{1.44}$$

where $\kappa_B^2 = (2\pi)^7\alpha'^4$ is the ten-dimensional gravitational constant, and the field strengths are defined by

$$\begin{gathered} F_1 = dC, \quad H_3 = dB, \quad F_3 = dC_2, \quad F_5 = dC_4 \\ \tilde{F}_3 = F_3 - CH_3, \quad \tilde{F}_5 = F_5 - \tfrac{1}{2}A_2\wedge H_3 + \tfrac{1}{2}B\wedge F_3 \end{gathered} \tag{1.45}$$

and we have the additional self-duality condition $*\tilde{F}_5 = \tilde{F}_5$.

D-Branes

As we mentioned before when we considered open strings, it is consistent to constrict the string end points to move in a subspace of the full ten dimensions. The resulting hyperplanes, on which the strings' ends are confined, are called D-branes [30]. Some

solitonic solutions of the supergravity actions also exist that are naturally sourced by these branes.

D-branes are the fundamental electric and magnetic sources of many of the supergravity antisymmetric forms. In particular in type IIA String Theory, the theory allows branes of even dimension that are electric and magnetic sources for A_1 and C_3. Type IIB theory includes odd dimension branes that are electric and magnetic sources for the dilaton, two and four index fields.

The action for a Dp-brane (p is the spatial direction of the brane) is given by the Dirac-Born-Infeld (DBI) action which is an extension of the Nambu-Goto form for the fundamental string, the geometric interpretation is that one minimises its world-volume. In the DBI action there are extra terms originating from the role of the D-branes as sources for an antisymmetric two-form F, including Chern-Simons terms. F is the gauge field strength tensor describing gauge fields on the Dp-brane probe and ϕ the dilaton. The action, in String frame is given by:

$$\begin{aligned} S_{Dp} = -\mu_p \int d^{(p+1)}\xi e^{-\phi} \sqrt{-\det\left(P\left[G + 2\pi\alpha' B\right]_{ab} + 2\pi\alpha' F_{ab}\right)} \\ + \frac{\left(2\pi\alpha'\right)^2}{2} \mu_p \int P\left[C^{(p+1)}\right] \wedge F \wedge F \end{aligned} \tag{1.46}$$

where $\mu_p = (2\pi)^{-p}\alpha'^{\left(\frac{p+1}{2}\right)}$ and B is an external antisymmetric two-form which may be present in the supergravity background. In principle, B may also contribute terms of Chern-Simons form, which are however not relevant for the examples described in this thesis.

$\mathcal{N} = 4$ super Yang-Mills theory naturally emerges on the surface of a $D3$-brane in type IIB superstring theory. Open strings generate a massless gauge field in ten dimensions. When the open string ends are restricted to a $3+1$ dimensional subspace the ten components of the gauge field naturally break into a $3+1$ dimensional gauge field and 6 scalar fields. The fermionic super-partners naturally separate to complete the $3+1$ dimensional super-multiplets.

1.3.4 Gauge/Gravity duality

String theory was born from the attempt to understand interactions between hadrons. At the time it was known that the plot of the angular momentum J of hadronic excitations against their energy-squared followed straight lines $J = \alpha E^2$ called Regge trajectories. String Theory seemed to be a reasonable candidate for a theory of strong interactions because the relationship between J and E^2 emerges naturally from a rotating classical open string. Despite this, the early attempts to use relativistic strings to describe hadrons faced a lot of problems, for example the presence of unwanted massless vectors

and massless tensors, which are precisely the particles needed to make string theory a candidate for a unified theory of physics. The string approach to strong interactions was abandoned and QCD was adopted.

However it turns out that certain strongly interacting gauge theories have an exact string picture, but with strings not propagating in the space-time where the strongly interacting theory lives. Instead the gauge theory lives on the boundary of this space-time. The equivalence of a gauge theory and a string theory was first explicitly exhibited in the AdS/CFT correspondence [6]. In this correspondence, a maximally supersymmetric $SU(N)$ Yang-Mills theory in four-dimensional Minkowski spacetime is conjectured to be equivalent to type IIB closed superstring theory. The ten-dimensional space-time in this superstring theory takes a particular form; five dimensions are in the form of a sphere S^5 and the other five dimensions take the form of AdS_5 space-time. One can view the Minkowski space-time of the field theory as the conformal boundary of AdS_5. Then the Yang-Mills theory turns to be a CFT.

There are many specific examples of the AdS/CFT duality. In this thesis we will focus on the most prominent example which relates $\mathcal{N} = 4$ Super Yang-Mills theory in 3+1 dimensions and IIB superstring theory on $AdS_5 \times S^5$. The strongest form of the $\mathrm{AdS}_5/\mathrm{CFT}_4$ correspondence states that $\boldsymbol{\mathcal{N} = 4}$ ***Super Yang-Mills theory with gauge group*** $\boldsymbol{SU(N)}$ ***and coupling constant*** $\boldsymbol{g_{YM}}$ ***is dynamically equivalent to type IIB superstring theory with string length*** $\boldsymbol{l_s = \sqrt{\alpha'}}$ ***and coupling constant*** $\boldsymbol{g_s}$ ***on*** $\boldsymbol{AdS_5 \times S^5}$ ***with radius of curvature*** $\boldsymbol{L}$ ***and*** $\boldsymbol{N}$ ***units of*** $\boldsymbol{F_{(5)}}$ ***flux on*** $\boldsymbol{S^5}$.

The two free parameters on the field theory side, i.e. g_{YM} and N, are mapped to the free parameters g_{s} and $L/\sqrt{\alpha'}$ on the string theory side by

$$g^2_{\mathrm{YM}} = 2\pi g_{\mathrm{s}} \quad \text{and} \quad 2g^2_{\mathrm{YM}} N = L^4/\alpha'^2 \tag{1.47}$$

It is not currently possible to test this strongest version of the correspondence since it isn't known how to quantize String Theory on curved space backgrounds with Ramond-Ramond flux, therefore it is necessary to ease the strength of the correspondence by taking certain limits on both sides of the duality. String Theory is best understood in the perturbative regime, so we can take the string side of the correspondence to be weakly coupled, which means to take $g_{\mathrm{s}} \ll 1$, while keeping $L/\sqrt{\alpha'}$ constant. At leading order in g_{s}, the AdS side of the duality reduces to tree level string theory as we don't take the entire string genus expansion. The string length l_{s} as measured in units of L is kept constant. Using the map between parameters as stated in (1.47), we see that this means take $g_{\mathrm{YM}} \ll 1$ while keeping $g^2_{\mathrm{YM}} N$ finite. In order to do this we have to take the large N limit $N \to \infty$ for fixed 't Hooft constant $\lambda = g^2_{\mathrm{YM}} N$. This is known as the 't Hooft limit and corresponds to the planar limit of the gauge theory. The AdS/CFT in the 't Hooft limit is a concrete realisation of 't Hooft's idea that the planar limit of

a quantum field theory is a string theory. In this sense a $1/N$ expansion on the CFT side can then be mapped to an expansion in the genus of the string worldsheet, on the string theory side, since $1/N \propto g_s$ for fixed λ

In the 't Hooft limit there is only one free parameter on both sides of the duality. On the CFT side it is the 't Hooft coupling λ, whereas on the string theory side it is the radius of curvature $L/\sqrt{\alpha'}$. The two parameters are related by $L^4/\alpha'^2 = 2\lambda$. Since we are interested in strongly coupled CFT, we take the limit $\lambda \to \infty$, which corresponds to $\sqrt{\alpha'}/L \to 0$. The string length is then very small compared to the radius of curvature. Thus, for $\sqrt{\alpha'}/L \to 0$ we obtain the limit in which the string ca be seen as a point particle, which is given by type IIB supergravity on $AdS_5 \times S^5$. This leads to a strong/weak duality in the sense that strongly coupled $\mathcal{N} = 4$ SYM is mapped to type IIB supergravity on weakly curved $AdS_5 \times S^5$ space. This weak form of the AdS/CFT conjecture is the one that we are using in the following chapters of this thesis.

D3-Branes origin of the duality

The string theory origin of the AdS/CFT correspondence is based in the fact that D3-branes in 10 dimensions can be interpreted from two different points of view. On one side, D3-branes are hyperplanes in 10-dimensional space on which open strings can end. In the low-energy limit where only massless string degrees of freedom contribute, these open string degrees of freedom correspond to $\mathcal{N} = 4$ Super Yang-Mills theory with gauge group $U(N)$, where N corresponds to the number of superposed D3-branes. The gauge group $U(N)$ factorizes into $SU(N) \times U(1)$. The $U(1)$ factor corresponds to the motion of the center of mass of the D3 branes. The global symmetries of the theory are the $SO(4,2)$ superconformal group and the $SU(4)$ R-symmetry, which is isomorphic to $SO(6)$.

On the other hand, D3-branes are also solitonic solutions of 10-dimensional type IIB supergravity, with a metric of the form

$$ds^2 = \left(1 + \frac{R^4}{y^4}\right)^{-\frac{1}{2}} \eta_{ij} dx^i dx^j + \left(1 + \frac{R^4}{y^4}\right)^{\frac{1}{2}} \left(dy^2 + y^2 d\Omega_5^2\right) \tag{1.48}$$

where $R^4 = 4\pi g_s N \alpha^2$, N again is the number of D3-branes and η_{ij} is the standard $3+1$ dimensional Minkowski metric. The x^i are the coordinates on the stack of D3-branes, whereas $\vec{y}$ denotes the six spatial coordinates perpendicular to the brane, $y \equiv \sqrt{y_M y^M}$, with $M \in \{4, ..., 9\}$. For $y \gg R$ this metric returns to flat $9+1$ dimensional Minkowski space, but in the near-horizon limit $\ll R$, which is again a low-energy limit, we can perform a coordinate transformation $u = R^2/y$ on (1.48) and obtain the metric of $AdS_5 \times S^5$. Here we can identify R as the Anti-de Sitter radius L. Anti-de Sitter space has negative constant curvature $\mathcal{R} = -\frac{d(d-1)}{L^2}$, and its conformal boundary is located at $u = 0$.

Another ingredient contributed by D3-branes is that they carry charge that source a four-form antisymmetric tensor field C_4 in IIB supergravity. The D3 brane supergravity solution also has a self-dual five-form $F_5 = dC_4$, which satisfies

$$\int_{S^5} F_5 = N \tag{1.49}$$

As we mentioned in subsection 1.3.2 the isometry group of AdS_5 is $SO(4,2)$. The isometry of the five sphere is $SO(6)$. This product group matches the maximal bosonic subgroup of the supergroup $SU(2,2|4)$, which encodes the symmetries of the $\mathcal{N} = 4$ SYM theory. In particular we can note that $SO(6) \simeq SU(4)$, which is the R symmetry group of $\mathcal{N} = 4$ supersymmetry. Since the global symmetries match we are in position to say that these two theories are dual.

From (1.40) we can see that the gravitational side of the correspondence has an extra non-compact direction r, with respect to the gauge theory. This is why the correspondence is described as being holographic since the contents of the $4+1$ dimensional theory are encoded by the degrees of freedom in the $3+1$ dimensional gauge theory. To understand what this extra direction means in the gauge theory it is useful to look at the action of dilatations. The action of a massless scalar in 3+1 dimensions looks like $\int d^4x(\partial\phi)^2$ and is invariant under the transformations $x \to e^{\alpha}x$ and $\phi \to e^{-\alpha}\phi$, with $\alpha \in \mathbb{R}$ some arbitrary parameter. From the power of the scaling we can see that ϕ has energy dimension one and x energy dimension minus one. On the gravitational side of the duality this is a symmetry of the metric and for (1.40) to be invariant we require that the radial direction in AdS scales like a scalar field under the gauge theory's dilatations. Thus we can conclude that the radial direction is an energy scale. This leads to the natural interpretation that the Holographic direction r as a representation of the renormalization group scale in the gauge theory.

Field-Operator Map

In [31, 32] a field-operator map has been established between the two sides of the AdS/CFT duality. This maps gauge invariant operators in the $\mathcal{N} = 4$ SYM theory in a particular irreducible representation of $SU(4)$ to supergravity fields in the same representation. These five-dimensional supergravity fields are obtained by Kaluza-Klein reduction of the original ten-dimensional supergravity fields on the five-sphere S^5. To illustrate this consider a scalar field in AdS_5 with action

$$S = \int d^4x du \sqrt{-g} \left(g^{ab}\partial_a\phi\partial_b\phi - m^2\phi^2 \right) \tag{1.50}$$

Here we have transformed the radial coordinate of AdS as $u \equiv L^2/r$, and g is the determinant of the metric. The equation of motion for the scalar ϕ is the Klein-Gordon

equation with the d'Alembert operator in AdS given by

$$\Box_g|_{\text{AdS}} = \frac{1}{\sqrt{-g}}\partial_m\left(\sqrt{-g}g^{mn}\partial_n\phi\right) = \frac{1}{L^2}\left(u^2\partial_u^2 - (d-1)u\partial_u + u^2\eta_{\mu\nu}\partial^\mu\partial^\nu\right) \tag{1.51}$$

it is convenient to perform a Fourier decomposition in the x^μ directions and to consider a plane wave ansatz of the form $\phi(u,x) = e^{ip^\mu x_\mu}\phi_p(u)$. Then, the Klein Gordon equation for the modes $\phi_p(u)$ becomes

$$u^2\partial_u^2\phi_p(u) - (d-1)u\partial_u\phi_p(u) - \left(m^2L^2 + p^2u^2\right)\phi_p(u) = 0 \tag{1.52}$$

Near the boundary, $u \to 0$, we can expand $\phi(u,x)$ and then the solutions of the equation of motion, for which we drop the spatial dependence by setting $p = 0$, have the form

$$\phi(u) \sim u^{d-\Delta}\phi_0 + u^\Delta\langle\mathcal{O}\rangle \tag{1.53}$$

with $m^2L^2 = \Delta(\Delta - d)$. Since the roots of this equation are given by

$$\Delta_\pm = \frac{d}{2} \pm \sqrt{\frac{d^2}{4} + m^2L^2} \tag{1.54}$$

we see that a term $m^2L^2 < -d^2/4$ leads to an imaginary Δ. Thus in $(d+1)$-dimensional Anti-de Sitter space scalar fields are still stable even for a negative mass squared provided it satisfies $m^2L^2 \geq d^2/4$, this is called the Breitenlohner-Freedman (BF) bound [33].

Since supergravity fields do not transform under the CFT dilatations and u can be seen as an inverse mass scale, we see that ϕ_0 and $\langle\mathcal{O}\rangle$ carry dimension $(d-\Delta)$ and Δ respectively. Therefore, the boundary value ϕ_0 may be identified with the source of the gauge theory operator $\mathcal{O}$; $\langle\mathcal{O}\rangle$ is the vacuum expectation value (vev) of $\mathcal{O}$. Thus the AdS/CFT correspondence is stated as

$$\left\langle e^{\int d^4x\phi_0(\vec{x})\mathcal{O}(\vec{x})}\right\rangle_{\text{CFT}} = Z_{\text{Sugra}}|_{\phi(0,\vec{x})=\phi_0(\vec{x})} \tag{1.55}$$

Equation (1.55) means that the generating functional of particular gauge-invariant operators in the CFT correspond with the generating functional for tree diagrams in supergravity, with the boundary values of the supergravity fields coinciding with the sources. The equation $m^2 = \Delta(\Delta - d)$ provides a relation between the conformal dimension of the field theory operator Δ and the mass m of the dual supergravity field.

This suggests that the AdS/CFT correspondence can be tested by the comparison of correlation functions of the quantized $\mathcal{N} = 4$ SYM theory with classical correlation functions on AdS_5. This is not possible in general for any correlation function even in the large N limit, since the supergravity dual describes $SU(N)$ $\mathcal{N} = 4$ SYM theory at strong coupling. However, for selected correlation functions which satisfy non-renormalization theorems such that they are independent of the coupling, direct comparison is possible. In particular this is the case of to the two and three-point functions of 1/2 BPS operators

which are annihilated by half of the supersymmetry generators [34]. Another remarkable test of the AdS/CFT correspondence that we can mention is the calculation of the conformal trace anomaly of the $\mathcal{N} = 4$ theory from $AdS_5 \times S^5$ supergravity [35].

1.3.5 Probe branes and the D3/D7 model

As we have seen in the previous section (1.3.4) the AdS/CFT correspondence only involves fields in the adjoint representation of the gauge group. To generalize the correspondence to include quark degrees of freedom, which are in the fundamental representation of the gauge group, the simplest way of proceed is to add a new type of D-brane into the configuration, in addition to the stack of D3-branes.

Open strings that have both ends on the D3-branes generate adjoint degrees of freedom, whereas strings with ends between the D3-branes and the new added branes, of which we will add N_f of them, have only one end on the N D3-branes. This implies that the fields transform under the fundamental representation. These fundamental fields come in the form of quark supermultiplets because of the supersymmetry of the string theory. If supersymmetry is broken then one expects the scalar squarks to become massive on the scale of the supersymmetry breaking whilst the fermionic quarks will be kept massless by their chiral symmetries.

If the new branes, which we call now flavour branes, are separated a distance s from the D3-branes in a direction transverse to both branes, then the minimum length string between the two branes has none zero energy and hence the quark is massive with mass $m_q = s/2\pi\alpha'$. Strings with both ends on the flavour brane are in the adjoint of the $U(N_f)$ flavour symmetry of the quarks and hence naturally describe mesonic degrees of freedom. In string theory these states describe fluctuations of the brane in the background geometry. Small oscillations of the branes are therefore dual to the gauge theory mesons.

The need for separating the new flavour branes from the D3-brane stack in a transverse direction excludes D9-branes. D3 and D5-brane probes lead to defect field theories if supersymmetry is to be preserved. This leaves D7-brane probes for adding flavour states to the dual CFT.

The simplest way to obtain quark bilinear operators in the context of the gauge/gravity duality is to add D7-branes [36]. D7-branes are added in such a way that they extend in space-time as given in table 1.1 where 0 corresponds to the time direction. We then consider a stack of N coincident D3-branes along the usual 0123 space-time directions, embedded into the world volume of N_F D7-branes which extend along the 01234567 directions

	0	1	2	3	4	5	6	7	8	9
D3	X	X	X	X						
D7	X	X	X	X	X	X	X	X		

Table 1.1: *The* D3/D7 *-brane intersection in* $9+1$ *dimensional space-time. The X means that the correspondent brane extends in that particular direction.*

The D3/D7-brane intersection preserves 1/4 of the total amount of the supersymmetry in type IIB string theory, that correspond to 8 supercharges, and has an $SO(4) \times SO(2)$ isometry in the directions transverse to the D3-branes. The $SO(4)$ is present in the x^4, x^5, x^6, x^7 space-time directions, while the $SO(2)$ group acts on x^8, x^9. The separation of the D3-branes from the D7-branes in the 8-9 directions explicitly breaks the $SO(2)$ group. These geometrical symmetries are also realized in the dual field theory.

The field theory corresponding to the D3/D7 intersection is a $\mathcal{N} = 2$ supersymmetric $U(N)$ gauge theory which, in addition to the degrees of freedom of the $\mathcal{N} = 4$ SYM theory, now also contains N_f hypermultiplets in the fundamental representation of the gauge group.

The $\mathcal{N} = 4$ SYM multiplet is generated by massless open string modes with both ends on the D3-branes, we call these 3-3 strings. On the other hand the $\mathcal{N} = 2$ hypermultiplets descend from strings stretching between the D3 and the D7-branes, we call these 3-7 strings. We take a limit in which the 7-7 strings decouple, leaving a purely four-dimensional theory. This decoupling is achieved by taking the large N limit while keeping the four-dimensional 't Hooft coupling $\lambda = g_{YM}^2 N$, as well as N_f fixed. The eight-dimensional 't Hooft coupling that we call λ', that correspond to the N_f D7-branes is given by

$$\lambda' = \lambda \left(2\pi l_s\right)^4 N_f / N \tag{1.56}$$

λ' vanishes in the low-energy limit $\alpha' \to 0$ i.e. the limit $l_s \to 0$. The 7-7 strings therefore do not interact with the 3-3 or 3-7 strings anymore, and the $U\left(N_f\right)$ gauge group on the D7-branes plays the role of a global flavour group in the four-dimensional theory.

The Lagrangian of the $\mathcal{N} = 2$ field theory in the world-volume can be written in $\mathcal{N} = 1$ superspace formalism. Under $\mathcal{N} = 1$ supersymmetry the $\mathcal{N} = 4$ vector multiplet decomposes into the vector multiplet W_α and the three chiral superfields Φ_1, Φ_2, Φ_3. The $\mathcal{N} = 2$ fundamental hypermultiplets can be written in terms of the $\mathcal{N} = 1$ chiral multiplets $Q^r, \tilde{Q}_r \left(r = 1, \ldots, N_f\right)$. The Lagrangian is thus given by

$$\begin{aligned} \mathcal{L} = \mathrm{Im} \Big[\tau \int d^4\theta \left(\mathrm{tr} \left(\bar{\Phi}_I e^V \Phi_I e^{-V} \right) + Q_r^\dagger e^V Q^r + \tilde{Q}_r^\dagger e^{-V} \tilde{Q}^r \right) \\ + \tau \int d^2\theta \left(\mathrm{tr} \left(W^\alpha W_\alpha \right) + W \right) + c.c. \Big] \end{aligned} \tag{1.57}$$

c.c. refers to the complex conjugate and τ is the complex gauge coupling. The superpotential is given by

$$W = \mathrm{tr}\left(\varepsilon_{IJK}\Phi_I\Phi_J\Phi_K\right) + \tilde{Q}_r\left(m_q + \Phi_3\right)Q^r \tag{1.58}$$

The beta function of this theory $\beta \propto \lambda^2 N_f/N$ goes to zero for N_f small, fixed 't Hooft coupling λ and $N \to \infty$, making the theory conformal in this limit.

The $SO(2) \simeq U(1)$ isometry corresponds to a $U(1)_R$ R-symmetry in the field theory and as we mentioned before it is explicitly broken by a quark mass m_q proportional to the separation s of the D3-branes and the D7-branes. The global $SO(4) \approx SU(2)_\Phi \times SU(2)_\mathcal{R}$ symmetry can be seen as consisting of a $SU(2)_\Phi$ symmetry and a $\mathcal{N} = 2SU(2)_\mathcal{R}$ R-symmetry. The global symmetry $SU(2)_\Phi$ rotates the scalars in the adjoint hypermultiplet. There is also a baryonic $U(1)_B$ which is a subgroup of the $U\left(N_f\right)$ flavour group. The fundamental superfields Q^r and $\tilde{Q}_r$ are charged $+1$ and -1 under this $U(1)_B$ group.

In general, the presence of Flavour branes gives rise to source terms in the equations of motion of type IIB supergravity, such that $AdS_5 \times S^5$ is no longer a solution. This is referred to as backreaction of the flavour branes on the D3-brane geometry. The simplest way to analyze the D3/D7 system is to work in the limit where the D7-branes are treated as probes, following the reference [36]. By a probe brane we refer to the fact that only a very small number of D7-branes, compared to the number of D3-branes N, is added to the setup. In this limit we neglect the backreaction of the D7-branes on the near-horizon geometry of the D3-branes. As we are in the $N \to \infty$ limit, the D3-branes dominate. On the field theory side the probe limit means that this corresponds to the quenched approximation in which quark loops are neglected.

On the supergravity side of the duality, in addition to the $\mathcal{N} = 4$ degrees of freedom , there are new degrees of freedom corresponding to the D7-brane probe within the ten-dimensional space. The low-energy degrees of freedom of this brane are described by the Dirac-Born-Infeld action (1.46). These correspond to open string fluctuations on the D7-probe. The minimum action configuration for the D7-brane probe corresponds to a probe configuration which asymptotically near the boundary wraps an $AdS_5 \times S^3$ subspace of $AdS_5 \times S^5$.

The duality conjectured in [36] for the strings that end in the flavour branes is an open-open string duality, in contrast to the initial AdS/CFT correspondence stated in 1.3.4 which is an open-closed string duality. In addition to the original AdS/CFT duality, gauge invariant field theory operators involving fundamental fields are mapped to fluctuations of the D7-brane probe inside $AdS_5 \times S^5$.

The dynamics of the D7-brane probe is described by (1.46) in this case looks like

$$S_{D7} = -\mu_7 \int d^8\xi \sqrt{-\det\left(P[G]_{ab} + 2\pi\alpha' F_{ab}\right)} + \frac{\left(2\pi\alpha'\right)^2}{2}\mu_7 \int P\left[C^{(4)}\right] \wedge F \wedge F \tag{1.59}$$

If we write the 10 dimensional $AdS_5 \times S^5$ metric in the form

$$ds^2 = \frac{r^2}{L^2}\eta_{ij}dx^i dx^j + \frac{L^2}{r^2}\left(d\rho^2 + \rho^2 d\Omega_3^2 + dw_5^2 + dw_6^2\right) \tag{1.60}$$

with $\rho^2 = w_1^2 + \ldots + w_4^2$, $r^2 = \rho^2 + w_5^2 + w_6^2$ and (ρ, Ω_3) spherical coordinates in the 4567 plane. Then, the induced metric obtained from the pullback of the metric to the worldvolume of the D7-brane is given by

$$\mathrm{d}s^2_{\mathrm{ind}} = \frac{\rho^2 + w_5^2 + w_6^2}{L^2}\eta_{\mu\nu}\mathrm{d}x^\mu \mathrm{d}x^\nu + \frac{L^2}{\rho^2 + w_5^2 + w_6^2}\mathrm{d}\rho^2 + \frac{L^2\rho^2}{\rho^2 + w_5^2 + w_6^2}\mathrm{d}\Omega_3^2 \tag{1.61}$$

with $w_5 = w_5(\rho)$ and $w_6 = w_6(\rho)$. Then the action (1.59) for a static D7-brane embedding with $F = 0$ on its world-volume is given, up to angular factors by

$$S_{D7} = -\mu_7 \int d^8\xi \rho^3 \sqrt{1 + \dot{w}_5^2 + \dot{w}_6^2} \tag{1.62}$$

where a dot indicates a derivative with respect to ρ. The ground state configuration of the D7-brane then corresponds to the solution of the equation of motion

$$\frac{d}{d\rho}\left[\frac{\rho^3}{\sqrt{1 + \dot{w}_5^2 + \dot{w}_6^2}}\frac{dw}{d\rho}\right] = 0 \tag{1.63}$$

where w denotes either w_5 or w_6. From (1.63) we can see that the action is minimized by w constant. The D7-brane probe therefore lies flat in the space. The choice of the position in the w_5, w_6 plane corresponds to choosing the quark mass in the gauge theory action. That w is constant at all values of ρ is a statement of the non-renormalization of the mass. As we mentioned before the coordinate ρ is a holographic radial direction of the background AdS space that corresponds to the renormalization group scale. The non-renormalization of the mass is an expected characteristic of supersymmetric gauge theories. In general, the equations of motion have asymptotic solutions at $\rho \to \infty$ of the form

$$w = s + \frac{c}{\rho^2} + \ldots \tag{1.64}$$

In equation (1.64) s is proportional to the quark mass as discussed previously. In agreement with the AdS/CFT result (1.53) the extra parameter c correspond to the vev of an operator with the same symmetries as the mass and of dimension 3, since ρ carries energy dimension. Therefore we conclude that c is a measure of the quark condensate $\bar{\psi}_L\psi_R$. Solutions with $c \neq 0$ are not regular in AdS space and these solutions are excluded. This corresponds to a vev for this operator being forbidden by supersymmetry since it is an F-term of a chiral superfield, i.e. $\langle\bar{\psi}\psi\rangle \sim \left\langle \int \mathrm{d}^2\theta \tilde{Q}Q \right\rangle$.

The scalar operator with dimension $\Delta = 3$ have a supergravity mass given by $M^2_{\mathrm{sugra}} = \Delta(\Delta - 4) = -3$. It maps to the fermion bilinear $\bar{\psi}\psi$ in the dual field theory. This mode

corresponds to an imaginary AdS mass. However this mass is above the Breitenlohner-Freedman bound for AdS_5 [33] $\left(M^2_{\rm BF} = -4\right)$ and thus guarantees stability.

Therefore one usually considers regular supersymmetric embeddings of the D7-brane probe for which the quark mass m_q may be non-zero, but the condensate $\langle\bar{\psi}\psi\rangle$ vanishes. For massive embeddings, as mentioned before, the D7-brane probe is separated by a distance s from the stack of D3-branes in either the w^5 or w^6 directions. This corresponds to giving a mass $m_q = s/\left(2\pi\alpha'\right)$ to the hypermultiplet $(Q, \tilde{Q})$ in the fundamental representation. In this case the radius of S^3 becomes a function of the radial coordinate r in AdS_5. We can see this from the induced metric (1.61) in which if we have that $w_5 = s$, $w_6 = 0$, it becomes

$$\mathrm{d}s^2_{ind} = \frac{\rho^2 + s^2}{L^2}\eta_{\mu\nu}\mathrm{d}x^\mu \mathrm{d}x^\nu + \frac{L^2}{\rho^2 + s^2}\mathrm{d}\rho^2 + \frac{L^2\rho^2}{\rho^2 + s^2}\mathrm{d}\Omega_3^2 \tag{1.65}$$

We see in (1.65) that for $\rho = 0$, the radius of S^3 shrinks to zero. since ρ is related to the radial coordinate r by $r^2 = \rho^2 + s^2$, this implies that there exists a minimal value $r_{\rm min} = s$, and for $r < r_{\rm min}$ the D7-brane probe cannot go further into the interior of the AdS space. In the contrary regime, at $\rho \to \infty$ the induced metric asymptotes to the metric of $AdS_5 \times S^3$.

As we would like to use the AdS/CFT duality to obtain information about physical phenomena that at the moment do not have a satisfactory explanation, being able to study QFT at finite temperature is of great relevance. The gravity dual of a QFT at finite temperature can be obtained by considering a black hole in an asymptotically AdS space [37]. Black holes have the right properties to describe the thermodynamics of the gauge theory. Furthermore, the event horizon denoted by the radial distance r_H cuts off the holographic radial direction. This corresponds to cutting off energy scales below the temperature in the field theory.

The high temperature, deconfined, phase of the $\mathcal{N} = 4$ gauge theory is described by the AdS- Schwarzschild solution, given by

$$ds^2 = \frac{r^2 f(r)}{L^2}d\tau^2 + L^2\frac{dr^2}{r^2 f(r)} + \frac{r^2}{L^2}d\vec{x}^2 + L^2 d\Omega_5^2 \tag{1.66}$$

where

$$f(r) = 1 - \frac{r_H^4}{r^4} \tag{1.67}$$

Asymptotically for $r \gg r_H$, the black hole solution approaches $AdS_5 \times S^5$ whose radius is related to the 't Hooft coupling of the dual gauge theory by $L^4 = 4\pi\lambda\alpha'^2$. This space-time is smooth and complete if τ is periodic with period πr_H. The S^1 parameterized by τ collapses at the horizon $r = r_H$. The temperature of the field theory corresponds to the Hawking temperature of the black hole which is given by the radius of the event

horizon,

$$T_H = \frac{r_H}{L^2\pi}. \tag{1.68}$$

At finite temperature the fermions have anti-periodic boundary conditions in the Euclidean time direction [37, 38] and supersymmetry is broken. The black hole solution thus describes a strongly interacting quark-gluon plasma which is non-supersymmetric and non-conformal. It is therefore believed that, despite the presence of other fields not contained in QCD, this plasma shares some properties with the quark-gluon plasma of QCD.

In addition to finite temperature, it is also possible to describe a finite density ρ and the associated quark chemical potential μ [39, 40]. Consider the Lagrangian of a certain QFT with a $U(1)$ gauge symmetry, a scalar ϕ and a Dirac fermion ψ charged under this symmetry,

$$\mathcal{L} = -\left(D_\mu\phi\right)^* D^\mu\phi + i\bar{\psi}\gamma^\mu D_\mu\psi - \frac{1}{4g^2}F^{\mu\nu}F_{\mu\nu} \tag{1.69}$$

With covariant derivative $D_\mu = \partial_\mu + iA_\mu$. Consider a background field $\tilde{A}_0 = \mu$ for the time component of the gauge field A_μ, such that $A_0 = \tilde{A}_0 + \delta A_0$. This generates a potential of the form

$$V = -\mu^2\phi^*\phi - \mu\psi^\dagger\psi \tag{1.70}$$

where μ is the chemical potential and $\psi^\dagger\psi = \hat{N}$ gives the number density operator. Moreover, from (1.70) we can see that $-\mu^2$ is the mass square of the scalar field which may lead to instabilities as it is negative.

Now if we take this as the description we would obtain in the gauge theory side of the duality, on the gravity side it is natural to propose for a non-trivial form for the time component of the gauge field in the radial direction of the gravity theory, $A_t(r)$. Then the field-operator dictionary implies that near the boundary at $r \to \infty$, A_t behaves as

$$A_t(r) \sim \mu + \frac{d}{r^2} \tag{1.71}$$

with μ the chemical potential and d proportional to the density. This construction is observed when considering a D7-brane probe with action given by (1.59). For a single D7-brane probe leading to a $U(1)$ symmetry, A_t is dual to the quark charge density. For the field theory given by the D3/D7 system, this charge density operator is given by the $\nu = t$ component of the $U(1)$ current J^ν

$$J^t = \psi^\dagger\psi + \bar{\psi}\bar{\psi}^\dagger + i\left(q^\dagger D_t q - q\left(D_t q\right)^\dagger\right) + i\left(\bar{q}\left(D_t\bar{q}\right)^\dagger - \left(D_t\bar{q}\right)\bar{q}^\dagger\right) \tag{1.72}$$

where D_t is the time component of the covariant derivative in the $SU(N)$ gauge theory and the q^m are squarks. This operator is normalised so that when acting on a state, it gives precisely the quark density. According to the field/operator dictionary, its source is given by $A_t(\infty)$ such that $\mathcal{L}'_{\mathcal{N}=2} = \mathcal{L}_{\mathcal{N}=2} + A_t(\infty)J^t$. From the grand canonical potential

expression $\Omega = \left\langle \hat{H} \right\rangle - ST - \mu \left\langle \hat{J} \right\rangle$ we have $A_t(\infty) = \mu$. Also the expectation value of J^t coincides with the quark density, $n_q = \langle J^t \rangle$.

Following [41] we obtain the equations of motion from the DBI action for a D7-brane with non-trivial profile for A_t, setting the temperature to zero for simplicity. For N_f probe D7-branes, the action is

$$\mathcal{S}_{\rm D7} = -N_{\rm f}\mu_7 \int \mathrm{d}^8\xi \sqrt{-\det\left(P[g]_{ab} + (2\pi\alpha')\, F_{ab}\right)} \tag{1.73}$$

The contribution from the Chern-Simons term that appear in the general action (1.46) vanishes. With $F_{\rho t} = \partial_\rho A_t \equiv \dot{A}_t(\rho)$ and using the embedding scalar $w(\rho) \equiv w_5(\rho)$, the zero temperature D7-brane Lagrangian reads

$$\mathcal{L} = -\mathcal{N}_{\rm D7}\rho^3 \sqrt{1 + \dot{w}^2 - (2\pi\alpha')^2\, \dot{A}_t^2} \tag{1.74}$$

where all coordinates are rescaled by $1/L$ to make them dimensionless, such that an overall factor L^8 enters $\mathcal{N}_{\rm D7}$. For simplicity, we divide both sides of (1.73) by the volume of $\mathbb{R}^{3,1}$ and work with the action density $\mathcal{S}_{\rm D7} = \int \mathrm{d}\rho \mathcal{L}$

Only derivatives of $w(\rho)$ and $A_t(\rho)$ appear in the Lagrangian, therefore there are two conserved charges c and d

$$\begin{aligned} \tfrac{\delta\mathcal{L}}{\delta\dot{w}} &= -\mathcal{N}_{\rm D7}\rho^3 \tfrac{\dot{w}}{\sqrt{1+\dot{w}^2-(2\pi\alpha')^2\dot{A}_t^2}} \equiv -c \\ \tfrac{\delta\mathcal{L}}{\delta\dot{A}_t} &= \mathcal{N}_{\rm D7}\rho^3 \tfrac{(2\pi\alpha')^2\dot{A}_t}{\sqrt{1+\dot{w}^2-(2\pi\alpha')^2\dot{A}_t^2}} \equiv d \end{aligned} \tag{1.75}$$

c is related to the quark condensate as discussed previously, while d is related to the quark density. The ratio of the two charges implies

$$\dot{A}_t^2 = \frac{d^2}{(2\pi\alpha')^4\, c^2}\dot{w}^2 \tag{1.76}$$

solving the algebraic system of equations for $\dot{w}(\rho)$ and $\dot{A}_t(\rho)$ in terms of c and d we get

$$\dot{w} = \frac{c}{\sqrt{\mathcal{N}_{\rm D7}^2\rho^6 + \frac{d^2}{(2\pi\alpha')^2} - c^2}}, \qquad \dot{A}_t = \frac{d/(2\pi\alpha')^2}{\sqrt{\mathcal{N}_{\rm D7}^2\rho^6 + \frac{d^2}{(2\pi\alpha')^2} - c^2}} \tag{1.77}$$

which can be integrated using incomplete Beta functions. The result depends on the sign of $d^2/(2\pi\alpha')^2 - c^2$. When $c = d = 0$, we obtain the solution with $\dot{w}(\rho) = 0$ and $\dot{A}_t(\rho) = 0$ so $w(\rho)$ and $A_t(\rho)$ are constants. Solutions with $d^2/(2\pi\alpha')^2 - c^2 > 0$ correspond to D7-brane embeddings which bend to reach the D3-branes. When $\frac{d^2}{(2\pi\alpha')^2} - c^2 < 0$, the D7-branes bend in such a way that they turn away from the D3-branes The action

evaluated on these solutions is

$$\mathcal{S}_{\rm D7} = -\mathcal{N}_{\rm D7}\int^{\Lambda} {\rm d}\rho\rho^3\sqrt{\frac{\mathcal{N}_{\rm D7}^2\rho^6}{\mathcal{N}_{\rm D7}^2\rho^6+\frac{d^2}{(2\pi\alpha')^2}-c^2}} \tag{1.78}$$

The lower endpoint of the integration depends on the sign of $\frac{d^2}{(2\pi\alpha')^2}-c^2$. Moreover, the integral diverges if we integrate to $\rho=\infty$. We therefore regulate the integral with a cut-off at $\rho=\Lambda$. For $d=c=0$, the divergent term takes the form

$$\mathcal{S}_{\rm ct} = \mathcal{N}_{\rm D7}\int_0^{\Lambda} {\rm d}\rho\rho^3 = \frac{1}{4}\mathcal{N}_{\rm D7}\Lambda^4 \tag{1.79}$$

Then we obtain the renormalized on-shell action $\mathcal{S}_{\rm ren}$, by adding the relevant counterterm,

$$\mathcal{S}_{\rm ren} = \lim_{\Lambda\to\infty}\left(\mathcal{S}_{\rm D7}+\mathcal{S}_{\rm ct}\right) \tag{1.80}$$

In the QFT, the thermodynamic grand potential Ω is given by $\Omega=-S_{ren}$. One can Legendre transform to obtain the free energy density in the canonical ensemble, $F=\Omega+\mu d$. At zero temperature, free energy and energy are the same, so at zero temperature F is also the energy density. The conserved charges c and d determine the vevs $\langle\mathcal{O}\rangle$ and $\langle J^t\rangle$ as follows,

$$\langle\mathcal{O}\rangle = \frac{\delta\Omega}{\delta m_q} = -\left(2\pi\alpha'\right)\frac{\delta\mathcal{S}_{\rm ren}}{\delta w(\infty)}, \quad \langle J^t\rangle = -\frac{\delta\Omega}{\delta\mu} = \frac{\delta\mathcal{S}_{\rm ren}}{\delta A_t(\infty)} \tag{1.81}$$

where in each case one field is varied while holding the other fixed. We then have that

$$\delta\mathcal{S}_{\rm D7} = \int {\rm d}\rho\left(\frac{\delta\mathcal{L}}{\delta\dot{A}_t(\rho)}\partial_\rho\delta A_t(\rho)+\frac{\delta\mathcal{L}}{\delta\dot{w}(\rho)}\partial_\rho\delta w(\rho)\right) = d\delta A_t(\infty)-c\delta w(\infty) \tag{1.82}$$

where we impose that $\delta A_t(\rho)$ and $\delta w(\rho)$ are always zero at the lower endpoint of the ρ integration. If we vary $A_t(\rho)$ while holding $w(\rho)$ fixed, $\delta w(\rho)=0$, we find

$$\langle J^t\rangle = -\left(2\pi\alpha'\right)^2\mu_7 d, \quad \langle\mathcal{O}\rangle = -2\pi\alpha'^3\mu_7 c \tag{1.83}$$

This implies that the sub-leading term in (1.71) is indeed the charge density since $J^\mu=(\rho,\vec{J})$.

Inspired by the results with finite temperature and chemical potential, a phenomenological approach has been proposed. These models which attempt to describe QCD are generically called AdS/QCD [42]. These bottom-up[3] models consist of a gauge theory in AdS with the field content picked to match to certain QCD bound states and operators

[3]In contrast with the top-down approach in which one tries to obtain results from the complete String Theory, the bottom-up approach to build models is to first aim for the correct fundamental particle content, and then incrementally adjust to add more ingredients.

via the holographic dictionary. Additionally the large N limit is not always used, instead a value $N = 3$ is more generally adopted.

This is the approach that will be followed in the remaining chapters of this thesis. We use an AdS space to phenomenologically describe the conformal symmetries of the free fermions in the QFT, which are then broken by the operators and sources of the theory that appear in the bulk, such as temperature and chemical potential.

One should worry that at low N the bulk modes might become strongly coupled and stringy, but the AdS/QCD philosophy is to carry on and measure the success of the models by their results. The goals of these models are to study the quark gluon plasma at high densities and to develop a sensible description of the phases found in the QCD phase diagram.

1.4 Compact Stars

In this section we provide an introduction to the advances in the study of the composition of the interior of neutron stars. For more details we refer to the books [43, 44]. We will review aspects of General Relativity that are used to model compact stars, as well as how to use the current models for matter inside the star to obtain observable quantities such as the mass and radius of the star. All of which will be needed for understanding later chapters of this thesis. Finally we introduce gravitational wave detection as a possible way to constrain our models for the composition of a neutron star.

Compact stars, which broadly refers to neutron stars as well as white dwarfs, are the fate of many luminous stars once the nuclear fusion reactions in their core are not able to support the gravitational attraction of its own mass. In this thesis we will particularly focus in the study of the densest of the two: neutron stars. A broader introduction to neutron stars can be found in [43, 44].

As all stars, neutron stars rotate, thus they experience a centrifugal force that must be counterbalanced by its own gravitational field otherwise the star would tear apart. The balance of the two forces can give us a lower bound for the compact star density. Neutron stars are around $7 \times 10^{14}\ g/cm^3$. As some neutron stars are in a binary orbit with another compact star, the application of orbital mechanics allows us to estimate the mass in some cases. The mass of a neutron star is typically 1.5 solar masses. With this we can infer their radii: about ten kilometers. This give us an image of the kind of astronomical objects we are treating, in which the entire mass of our sun is compressed in a very small region.

The existence of neutron stars have been inferred from supernova explosions, which are the violent release of the outer layers of the progenitor massive star in the moment where its nucleus suffers gravitational collapse. Neutron stars have also been observed

by their periodic emission of electromagnetic radiation. Originally discovered as pulsars in 1967 [45], they are now known to be neutron stars. Pulsars acquire high angular velocities through conservation of angular momentum and they acquire strong magnetic fields through conservation of magnetic flux during the collapse of the progenitor stars. So these two features mean neutron stars can be detected by the beamed periodic signal they emit.

Neutron stars are unique systems in which we can find matter at low temperatures and very high densities. The range of values that the density can reach in compact stars is high enough to consider the existence of a deconfined quark phase, although it is not high enough to allows us to apply perturbative techniques in QCD. In compact stars it is believed that matter can be in a plethora of different phases: from nuclei embedded in a sea of electrons at low densities in the crust, to the extremely neutron-rich uniform matter in the outer core, and possibly exotic states such as deconfined matter in the inner core.

1.4.1 Composition of Neutron Stars

The name "neutron star" can be misleading. Although inside neutron stars we can find baryons such as nucleons and hyperons, there is also the possibility to find quark matter in some cases. This last possibility will be examined in chapter 3 of this thesis. The notion of a neutron star as the remnant of a normal, luminous star at the end point of its evolution originates in the study of supernova explosions. During the lifespan of the luminous progenitor star, part of the hydrogen from which they are formed is converted, by fusion reactions, into heavier elements. When the majority of the hydrogen is converted into iron, which is the last product that exothermic fusion can obtain, nuclear fusion becomes unable to sustain the core against its own gravity and then it collapses releasing an enormous energy. Baade and Zwicky [46], argued that the source of such enormous energy must be gravitational potential energy. The star collapses to densities high enough to tear all nuclei apart into their constituents.

Following the discovery of the quantum theory and Fermi-Dirac statistics, very dense, degenerate Fermi systems were conceived. Prior to that the high density inferred for white dwarfs seemed to present a dilemma. High densities could be explained from the ionization of the atoms in the hot star making possible their compaction by gravity. However, it was not known what would happen ultimately when it had consumed all its nuclear fuel as cold matter was known only in the form it is on earth, where densities are very low. The solution was that matter was in a state of Fermi-Dirac degeneracy.

The constituents of neutron stars, originally leptons and baryons, and possibly quarks are degenerate to the lowest energy state available to them. As fusion reactions in the progenitor star can't contribute any more with energy release the star has no remaining

source of energy to excite the fermions. Only the Fermi pressure and the short-range repulsion of the nuclear force sustain the neutron star against further gravitational collapse. If the progenitor star is very massive the gravitational collapse continues into a black hole. The maximum mass a neutron star can have in order to be sustained against gravitational collapse and not become a black hole is called the Tolman-Oppenheimer-Volkoff limit [47] and is in the range from approximately 1.5 to 3 solar masses.

In the past, the models of dense matter most commonly used have been based on phenomenological nuclear interactions [48]. Two-nucleon and three-nucleon interactions are usually constructed to fit scattering data at low energies. Nevertheless the many-body problem based on those interactions is not easy to solve due to strongly repulsive forces at small relative distances.

More recently the development of Chiral effective theories (EFT), has provided the framework for a systematic expansion for nuclear forces at low momenta in which nucleons interact by pion exchanges and by short-range contact interactions,. EFT has been able to provide a method to constrain the properties of neutron-rich matter up to the nuclear saturation density to a high degree.

The current knowledge of the behaviour of the matter at densities greater than 1 or 2 times the saturation density is very limited. Descriptions of the higher density region can be found by extending the microscopic results at low densities. The high-density extensions used by authors in [49] were only constrained by causality and by the heaviest observed neutron star at that time which has a mass of 1.65 solar masses. These kind of extensions are called polytropic extensions.

1.4.2 Equation of State

The equation of state (EoS) relates state variables of the system. In the present case of neutron stars, the state variables are the pressure P and the energy density $\mathcal{E}$. The EoS is the manner in which matter is taken into account in the relativistic equations of stellar structure. It is a key ingredient to fully model a neutron star; with this equation we can obtain properties of the star such as its mass and radius using the central pressure as a parameter.

A complete EoS would also be very important in the light of the recent measurement of gravitational wave signals from mergers of binary neutron stars [50], since the model of the wave signal is sensitive to the specific form of the EoS. Nevertheless, there has been a struggle to find a complete EoS; the difficulty of the task resides in the need to solve QCD in the non-perturbative regime at finite baryon chemical potential.

At the moment the EoS of strongly interacting matter at low temperatures is relatively well described at baryon densities below the nuclear saturation limit $n_B \leq n_s \approx 0.16$

fm^{-3}, where Chiral Effective Theory (CET) works, as well as at very high baryon chemical potential where the perturbative techniques can be applied. However this excludes the values of density where a phase transition to quark matter would be expected to occur.

1.4.3 Tolman-Oppenheimer-Volkov Equations

The equations that describe the structure of relativistic stars are the so-called Tolman-Oppenheimer-Volkoff (TOV) equations, which are the form that Einstein's equations take for the case of isotropic, spherical static stars. They can be interpreted as equations of hydrostatic equilibrium in general relativity. The equations for stellar structure lead us to the equation for hydrostatic equilibrium because they were built in by the condition that each fluid element is at rest in the star.

No form of matter whatsoever can support a relativistic star above a certain mass called the limiting mass or the Chandrasekhar limit. Its value depends on the nature of matter but the existence of the limit does not. The implied fate of stars more massive than the limit is that either mass is lost in great quantity during the evolution of the star or it collapses to form a black hole.

The EoS of strongly interacting matter is crucial to determine a relation between the mass and the radius of neutron stars. The TOV equations (1.84) provide this link.

$$\begin{aligned} \frac{dP}{dr} &= -G\left(\mathcal{E}+P\right)\frac{m+4\pi r^3 P}{r(r-2Gm)}, \\ \frac{dm}{dr} &= 4\pi r^2 \mathcal{E} \end{aligned} \tag{1.84}$$

To integrate the equations we need to input the EoS: $\mathcal{E}(P)$, as well as the central pressure $P_c = p(r=0)$ as initial condition, and its outcome are the mass M and Pressure P of the corresponding star. To solve the TOV equations we work in its dimensionless form:

$$\begin{aligned} \frac{dp}{d\xi} &= -B\frac{ye\left(1+\frac{p_0}{\epsilon_0}\frac{p}{e}\right)}{\xi^2(1-2B\frac{p_0}{\epsilon_0}\frac{y}{\xi})}\left(1+A\frac{p_0}{\epsilon_0}\xi^3\frac{p}{y}\right), \\ \frac{dy}{d\xi} &= A\xi^2 e(\xi) \end{aligned} \tag{1.85}$$

Where $r = r_0\xi$, $m = m_0 y(\xi)$, $P = p_0 p(\xi)$, $\mathcal{E} = \epsilon_0 e(\xi)$, $A = \frac{4\pi r_0^3 \epsilon_0}{m_0}$ and $B = \frac{G m_0 \epsilon_0}{p_0 r_0}$. We fixed the scale with the value of $p_0 = \epsilon_0 = \frac{(308.55MeV)^4}{\pi^2}$; this choice also fixes the rest of our scale parameters.

As we mentioned previously, from the solution of (1.84) we obtain the pressure $P(r)$ and the mass $m(r)$ of the neutron star as a function of the radial distance r. The radius R of the star will be the value of r in which the pressure vanishes as we expect outside of

the star. Then varying the initial condition P_c as a parameter we can construct a curve for the mass of the star $m(r = R) = M$ against R.

The solutions in hydrostatic equilibrium found with the TOV equations do not guarantee that the star in question is stable. There can be an instability to radial oscillations. It can be proved that as one moves along the sequence of equilibrium configurations of the TOV equations, perfect fluid stars can pass from stability to instability if the equilibrium mass, m is stationary with respect to the central energy density, $\mathcal{E}_c$ [43]. Therefore, a condition for stability is that

$$\frac{\partial m\left(\mathcal{E}_c\right)}{\partial \mathcal{E}_c} > 0 \tag{1.86}$$

This is seen as follows: one can make a radial perturbation of a solution. In terms of the mass vs radius curve one increases the value of the central density $\mathcal{E}_c$ whilst keeping the same mass. If $\frac{\partial m(\mathcal{E}_c)}{\partial \mathcal{E}_c} > 0$ then the corresponding equilibrium solution for this new configuration has a higher mass and therefore there is a deficit of mass. The gravitational force thus needs to be balanced by increasing the central pressure. The forces acting on the matter in the star will therefore act to return the new configuration toward its original unperturbed place. However for the case in which $\frac{\partial m(\mathcal{E}_c)}{\partial \mathcal{E}_c)} \leq 0$ we arrive at the conclusion that, if the star is perturbed, the forces acting on the perturbed star will act to drive it further from its original point in the mass vs radius curve. Therefore the condition for stability is given by (1.86).

Furthermore, in [51], the authors discuss methods for determining the stability of a star in terms of the Bardeen, Thorne, and Meltzer (BTM) criteria [52]. Stability of a star can be determined from the mass vs radius curve using BTM which established a simple formulation to know if all its radial modes are stable:

1. At each extremum where the $M(R)$ curve rotates counter-clockwise with increasing central pressure, one radial stable mode becomes unstable.

2. At each extremum where the $M(R)$ curve rotates clockwise with increasing central pressure, one unstable radial stable mode becomes stable.

1.4.4 Gravitational Wave detection and Model Constraint

Gravitational waves are wave-like perturbations of space-time. Assuming the background space to be flat, with metric $g_{ij}^{(0)} = \text{diag}(1, -1, -1, -1)$. Then the metric representing weak gravitational waves is

$$g_{ij} = g_{ij}^{(0)} + h_{ij}, \quad |h_{ij}| \sim h \ll 1, \tag{1.87}$$

Then we can think of the linearized version of general relativity, where effects of higher than first order in $h_{\mu\nu}$ are neglected, as describing a theory of a symmetric tensor field

propagating on a flat background space-time. Thus h corresponds to the amplitude of the gravitational wave. Gravitational waves are transverse waves.

Consider two test particles which are at rest in the absence of gravitational waves. Let ξ determine the relative position of these particles. Then a gravitational wave induces their relative acceleration $\ddot{\xi}$. A variation $\delta\xi$ of ξ under the action of the gravitational wave is similar to the one produced by a tidal force,

$$\delta\xi_j = h_{jk}^{TT}\xi_k/2 \tag{1.88}$$

where h_{jk}^{TT} is the traceless and transverse part of h_{jk}. This equation leads to an estimate

$$\delta\xi/\xi \simeq h \tag{1.89}$$

It is natural to call h the relative gravitational wave strain. This is the major quantity which characterises the detectability of gravitational waves [44] and is typically of the order of $\sim 10^{-21}$.

LIGO and Virgo collaboration detected gravitational waves for the first time using a Michelson interferometer in 2015 [53], with a strain of the order of $\sim 10^{-21}$.

Michelson interferometers use the interference of the waves. If two waves superpose their amplitudes adds up. If they are in phase the amplitude increases and it is called constructive interference and if they are out of phase, the amplitude diminishes until they are in anti-phase. This is called destructive interference.

The basic principle of the Michelson interferometer is that a wave of known wavelength from a source fall on a beam splitter which allow 50% the light to pass through and 50% reflected at 90 degree. The transmitted and reflected waves travel through two arms of the interferometer to the mirrors M_1 and M_2 to get reflected back and merge at the splitter. The splitter then reflects the merged beam to a detector. In merging, light waves of two beams superpose on each other. Depending on the path lengths travelled by the two beams, interference patter will be formed at the detector. A mismatch in the travel length will result in a fringe pattern. The separation of the fringes depends on the wavelength and path length difference of the beams. For a known wavelength, the fringe separation gives the difference in length traversed by the two beams.

Now consider a Michelson interferometer in the x-y plane with the same length from the splitter to both mirrors M_1 and M_2 and a gravitational wave propagate along the Z-axis. The gravitational wave will set the mirrors to some oscillation and the lengths will change from L to $L + \Delta L$ and $L - \Delta L$. The change of length ΔL will result in an interference pattern and the induced change ΔL, which is the gravitational wave strength h, can be measured.

Compact binaries containing neutron stars are sources of gravitational radiation especially at the final inspiral stage during a merger. Gravitational radiation of double neutron star binaries and neutron star - white dwarf binaries has already been observed indirectly, by detecting relativistic decay of pulsar orbits. In 2017 the Advanced LIGO and Advanced Virgo gravitational-wave detectors made their first observation of a binary neutron star inspiral. The inferred component masses of the binary are between 0.86 and 2.26 solar masses, in agreement with masses of known neutron stars [54].

One of the key goals of detecting neutron star binaries is to obtain information about the EoS, which is at present fairly unconstrained.

The tidal deformation between neutron stars in a binary system connects the EoS that describe the matter inside neutron stars to the gravitational wave emission during the inspiral. It has been showed that a small tidal signature arises in the inspiral below 400 Hz [55]. This signature amounts to a phase correction which can be described in terms of a single EoS dependent tidal deformability parameter $\bar{\lambda}^{(\mathrm{tid})}$, which is the ratio of each star's induced quadrupole moment to the tidal field of its companion in the binary system. The parameter $\bar{\lambda}^{(\mathrm{tid})}$ depends on the EoS via both the Neutron Star radius R and mass M, and a dimensionless quantity $k_2^{(\mathrm{tid})}$ called the Love number:

$$\bar{\lambda}^{(\mathrm{tid})} = \frac{2}{3}\left(\frac{M}{R}\right)^{-5} k_2^{(\mathrm{tid})} \tag{1.90}$$

This expression is obtained if we consider a static, spherically symmetric star of mass M placed in a time-independent external quadrupolar tidal field $\mathcal{E}_{ij}$. In response, the star will develop a quadrupole moment Q_{ij}. In the star's local rest frame, for large values of the radial coordinate r, the metric coefficient g_{tt} is given by [56]:

$$\frac{(1-g_{tt})}{2} = -\frac{m}{r} - \frac{3Q_{ij}}{2r^3}\left(n^i n^j - \frac{\delta^{ij}}{3}\right) + \frac{\mathcal{E}_{ij}}{2}x^i x^j + \ldots \tag{1.91}$$

where $n^i = x^i/r$. This expansion defines the traceless tensors $\mathcal{E}_{ij}$ and Q_{ij}. To linear order, the induced quadrupole will be of the form

$$Q_{ij} = -\bar{\lambda}^{(\mathrm{tid})}\mathcal{E}_{ij} \tag{1.92}$$

Thus Q_{ij} and E_{ij} are defined as the coefficients in an asymptotic expansion of the metric at large distances from the star. This perturbation to the metric is expanded in spherical harmonics. A first degree differential equation is obtained for the radial function of the spherical harmonics and when solved together with the TOV equations can give us the value of the tidal deformability λ from the following expression for the Love number $k_2^{(\mathrm{tid})}$:

$$
\begin{aligned}
k_2^{(\mathrm{tid})} &= \frac{8}{5}\beta^5(1-2\beta)^2[2+2\beta(z_R-1)-z_R] \\
&\quad \times\{2\beta[6-3z_R+3\beta(5z_R-8)] \\
&\quad +4\beta^3\left[13-11z_R+\beta(3z_R-2)+2\beta^2(1+z_R)\right] \\
&\quad +3(1-2\beta)^2[2-z_R+2\beta(z_R-1)]\ln(1-2\beta)\}^{-1}
\end{aligned}
\tag{1.93}
$$

where $\beta = M/R$ is the compactness parameter, and $z_R = RH'(R)/H(R)$ is evaluated using the surface value of the radial function $H(r)$ determined by the system of differential equations (1.94) that comes from the expansion of the metric in spherical harmonics:

$$
\begin{aligned}
\frac{dH}{dr} &= Y \\
\frac{dY}{dr} &= 2\left(1-2\frac{m(r)}{r}\right)^{-1} H\Big\{-2\pi[5\mathcal{E}+9p+\frac{(\mathcal{E}+p)}{c_s^2}] \\
&\quad +\frac{3}{r^2}+2\left(1-2\frac{m(r)}{r}\right)^{-1}\left(\frac{m(r)}{r^2}+4\pi rp\right)^2\Big\} \\
&\quad +\frac{2Y}{r}\left(1-2\frac{m(r)}{r}\right)^{-1}\left[-1+\frac{m(r)}{r}+2\pi r^2(\mathcal{E}-p)\right]
\end{aligned}
\tag{1.94}
$$

with a boundary condition $H(r) = a_0 r^2$, $Y(r) = 2a_0 r$ for $r \ll 1$ and a_0 is a constant that determines how much the star is deformed and can be fixed arbitrarily as it cancels in the expression for the Love number (1.93). The functions $m(r)$, $p(r)$ and $\mathcal{E}(r)$ are the enclosed mass, pressure and energy density at the radial distance r, respectively, obtained using the TOV equations. Here we also have the appearance of the sound speed $c_s = \sqrt{\partial p/\partial \mathcal{E}}$.

Since a change in the central pressure P_c would change the mass and the radius of the star and then would change the value z_R, varying P_c we can obtain the dimensionless tidal defomability of the star $\bar{\lambda}^{(\mathrm{tid})}$ as a function of the mass of the star.

LIGO and Virgo have provided a constraint for the values of the tidal deformability for a star of a mass $M = 1.4M_\odot$ [54], for the case of slowly rotating stars at a 90% Bayesian probability level. In addition to this, Fig. 5 of this reference gives both 90% and 50% probability contours for the independent tidal deformabilities of the two stars on a $\lambda_1 - \lambda_2$ plane.

Thus one can compare the results of a mode with these values, and show how exotic phases relate to these contours. The curves are generated by independently determining the tidal deformabilities for each of the stars involved in the merger, obtaining the possible mass pairs using the chirp mass of the event, $M = 1.188M_\odot$.

Chapter 2

Color Superconductivity

2.1 Introduction

It has been proposed that QCD at high density and low temperature could be a colour superconductor. In this chapter, we will try to build a holographic model of this phase and obtain a better picture of the phase diagram of QCD at low temperatures.

In this chapter we study a D3/D7 holographic bottom-up model in which we use an AdS-space to phenomenologically describe the conformal symmetries of the free fermions below a Debye gap scale. These symmetries are then broken by the operators and sources of the theory that appear in the bulk. In particular we will use a scalar field in the gravity side of the duality to model the Cooper pair formation in QCD at small temperatures and high chemical potential. This allows us to study the colour superconductivity phase in QCD.

As we mentioned in the previous chapter in subsection 1.2.4, a fermionic system at finite chemical potential is expected to develop a Fermi surface, then an attractive interaction between the fermions will form a Cooper pair, causing superconductivity or superfluidity. This was made clear to the particle physics community by the renormalization group flow analysis in [18, 57, 19, 20] and updated to a relativistic system in [21]. This fact leads to the natural expectation that quarks will condense in high density QCD and there has been considerable work over the year on understanding the phase structure (see for example [22]). Typically the preferred condensation channel is expected to break the colour gauge group so the phenomena is referred to as colour superconductivity (CSC).

At very large chemical potentials QCD is believed to become weakly coupled due to asymptotic freedom and an exact computation of the quark condensation pattern is possible [58]. The more experimentally interesting case to study though is when the density and temperature of the quark gluon plasma are of order the strong coupling scale Λ_c, however at this regime the strongly coupled nature of the problem makes

precise computation difficult. Gap equation and renormalization group analysis has been done and there is a large literature on the possible phase structure as a function of N_f and the quark masses [22].

As we stated in Chapter 1 the Gauge/Gravity duality has provide us with a framework to rigorously compute in theories close to large N, $\mathcal{N} = 4$ super Yang-Mills theory. The framework has been expanded phenomenologically to a wider space of theories [42] in which one tries to obtain a field theory more closely related to QCD. This approach has been called AdS/QCD. It has been natural since the beginning of this kind of approach, to attempt to study the CSC phase of QCD with the AdS/QCD framework. However there are big obstacles: the colour superconductivity effect is subleading in the large number of colours N limit; in the context of finite density QCD in [59, 60] is noticed that colour superconductivity is suppressed at large N due to the fact that the Cooper pair is not a colour singlet, thus the diagrams responsible for colour superconductivity are non-planar, then since the quark condensate depends on N there is no clear large N limit. Another issue is that the condensate that breaks the gauge group has conformal dimension $\Delta = 3$, but on the gravitational side only gauge invariant operators are manifest; the field dual to the quark condensate qq gets a vev which is dimension 3 but the square of the operator is a gauge invariant of dimension 6. In the gravity dual there are only gauge invariant operators and only up to dimension 4, everything else is either an irrelevant operator or a string mode which is infinitely massive [31]. Nevertheless there has been some promising leads, for example an instability to pair condensation of gauginos, which can form a colour singlet pair, in the presence of a chemical potential was observed in [39]. This idea was phenomenologically used to develop AdS descriptions of superconducting condensed matter systems [61] leading to the AdS/CM field of study. Holographic studies of related instabilities in theories with scalar quarks have also been studied in [62, 63, 64].

In this chapter we will side step the problems mentioned above to achieve a consistent holographic description of colour superconductivity. We consider the intermediate density phase of QCD where the quark gluon plasma is strongly coupled and full of free electrically charged quarks and presumably composite, magnetically charged scalars [65]. These latter condense below the chiral phase transition to cause confinement. The expectation is that these fields, through loop diagrams, will generate a mass of order $g\sqrt{T^2+\mu^2}$ for both the electric and magnetic gluons[1] (the latter are not gapped at weak coupling where there are no magnetic charges present [66]), where g is the running coupling of QCD, T the temperature and μ the chemical potential. We propose that, because g is large, since we are in the strongly coupled regime, there can be an order of magnitude gap between the gluon mass and the chemical potential/temperature scale. Then we will squeeze a holographic description into this energy scale. Since the gluons

[1] Electric gluons are in analogy with an $U(1)$ electric field E so it is associated with the component A_t of the gauge field. The magnetic ones are like a field B associated with $\vec{A}$. Naively an E field photon has a loop diagram with an electron in it but a B field doesn't.

are gapped we avoid the issue of treating the $SU(3)$ colour symmetry of the quarks as a gauge symmetry and instead impose it as just a flavour symmetry, if the gauge bosons become massive then the colour charges become global charges; to illustrate this take for example the electron and the neutrino in the weak force description, they exist as separate particles even though from an $SU(2)$ point of view they are not gauge invariant. When we say gluons are massive we are allowed to start talking about red quarks and green quarks in a low energy theory, colour becomes a global (not gauge) quantum number and now the condensate qq can be treated as a scalar in AdS. Although the bi-quark condensate will further gap the gluons we presume this to be a small effect relative to the Debye screening. These assumptions will save us from the problems encountered holographically to date.

Our model is based on the simplest AdS/superconductor model given in [61]. To correctly describe the broken QCD interactions that generate the Cooper pair condensation we will discuss reintroducing the interactions as four fermion terms using Witten's double trace prescription [67] (Recent work on developing the holography of four fermion operators can be found in [68, 69]). There are subtleties in this analysis including excited states of the vacuum and it turns out that an infinitely repulsive force is needed to switch off the inherent attractive channel of the base AdS/superconductivity model. Thus we conclude we should just choose to tune the intrinsic pairing interaction of the holographic model to represent the broken QCD interactions on the global colour degrees of freedom. The goal of this chapter is to study such broken gauge interactions in the quark gluon plasma to develop a sensible description of the CSC phase in the QCD phase diagram.

Let us quickly review the CSC condensation patterns that will interest us here. The superconducting condensation is triggered by a chemical potential for $\mathrm{U}(1)_B$ and the associated quark number density. We are interested in the condensation of a bi-quark operator with quark number 2 or baryon number 2/3. We assume that at strong coupling the $\bar{3}$ colour channel remains attractive as at the weak coupling regime whilst the 6 is repulsive so the condensation is the usual anti-symmetric $\bar{3}$ state. As mentioned in the previous chapter (1.2.4) a spin 0 condensate is formed from an anti-symmetric combination of spins. The flavour wave function of the condensate must also therefore be anti-symmetric. First with three massless quark flavours, this implies the condensate is an anti-symmetric flavour $\bar{3}$ also. We can represent this state by the following matrix (we show the make up of the $\bar{3}$s of colour and flavour in terms of the constituents)

$$\begin{array}{cc|ccc|} & & \bar{R} & \bar{G} & \bar{B} \\ & & BG-GB & BR-RB & RG-GR \\ \bar{u} & sd-ds & \Delta_1 & & \\ \bar{d} & su-us & & \Delta_2 & \\ \bar{s} & ud-du & & & \Delta_3 \end{array} \tag{2.1}$$

In the three flavour massless limit the expectation is that the condensate will be the diagonal as shown with all Δ_i equal, this is the CFL phase mentioned in last chapter. As the strange quark becomes massive the condensates of the top two rows (Δ_1, Δ_2) switch off and we expect to find a vev for the triplet, $SU(2)$ flavour singlet of the bottom row (Δ_3), this is the 2SC phase of the massless two flavour case. Note all of these states carry net colour charge although we have argued the main source of gluon mass is the Debye screening rather than the Meissner induced mass. In the holographic model we will describe an AdS-scalar ψ that is dual to an element Δ_i of this matrix which acquires a vev. We will seek the phase boundary where the condensate switches on in the $T-\mu$ plane. We will briefly discuss including a quark mass in our final section to display a transition between the colour-flavour locked and the 2SC phases although as we will stress the analysis is very naive and challenges remain to find a complete holographic picture.

This chapter is organized as follows: in Section 2.2 we will review the origin of the electric and magnetic Debye gluon masses that generate a gap. In Section 2.3 we review the AdS superconductor model that we will use including fields for each of the biquark gaps we consider. In Section 2.4 we look at the role of four quark operators in the superconductor model including the role of unstable minima of the model. In Section 2.5 we match the superconductor model's coupling to the QCD coupling in the $T-\mu$ plane to predict the gap size. In sub-section 2.5.1 we discuss how quark mass would enter the holographic model to suppress the bi-quark condensates. Finally in Section 2.6 we conclude.

2.2 Electric and Magnetic Debye Masses

Our arguments about the gapping of the gluonic degrees of freedom are important to our approach so we will review the ideas, already in the literature, in more detail. At high density QCD is believed to become weakly coupled and one can explicitly compute using perturbation theory [70, 71, 66]. It is then known that the electric A_0 component of the gluon field acquire a Debye mass[2] of order $g\mu$. The magnetic A_i degrees of freedom though are not fully screened but instead Landau damped. Their self energy behaves as $\Sigma^2 \sim g^2\mu^2|p_0|/|p|$ with p the gluonic four momentum. In such weakly coupled theories if colour superconductivity sets in then the charged gap is the only source of mass for the magnetic gluonic degrees of freedom. Indeed a central point of the analysis in [58] was to include the effects of the Landau damping in the estimate for the gap scale.

We argue here that at low chemical potential, which is relevant for neutron star and heavy ion collisions, the behaviour is probably rather different. In particular we expect

[2]The Debye screening mass parameterizes the dynamically generated screening of fields with electric and colour charge, due to the strong interactions of QCD at high temperature.

the QCD plasma to contain magnetically charged scalars (see [65] for a recent discussion) because of their role in the confinement of quarks below the chiral/deconfinement transition. If such composite states do exist then they will simply, through one loop diagrams, generate a Debye like mass for the magnetic A_i gluonic degrees of freedom too. Now all the gluons are gapped at the scale $g\mu$ which for chemical potentials in the hundreds of MeV and for $g \sim 4\pi$ are much higher than the superconductor gap scale which is typically estimated in the 10's of MeV. This separation of scales motivates a description of colour superconductivity in which the quarks exist as the sole degrees of freedom in the low energy theory below $g\mu$ interacting only by four fermion operators generated by the gluons. In such a description the colour quantum numbers of the quarks will appear as global quantum numbers (although a full description of all higher dimension operators would secretly include gauge invariance). Since holographic colour superconductor models describe the breaking of global symmetries we can now hope to apply that framework to this energy regime in high density QCD. Note that we assume that the contribution of the gluon gap from the low scale superconducting condensate is small relative to the Debye masses generated by the plasma so that the cut-off scale and gap can be considered disconnected.

2.3 AdS Superconductors

As a first start, we will just address the CSC phase which is the novel physics of interest. We will assume the chiral transition, where the $\bar{q}q$ condensation occurs, is at the scale where the QCD coupling diverges Λ_c. Thus consider T, μ scales above this energy scale only. One finds the phase diagram in Figure 2.5.

Let us begin by setting up a very simple AdS description of superconductivity following the start up model of [61]. We place our description in a black hole geometry (which we will not backreact)

$$ds^2 = r^2(-f dt^2 + d\vec{x}^2) + \frac{1}{r^2 f} dr^2, \qquad f = 1 - \frac{r_H^4}{r^4}. \tag{2.2}$$

Here $\vec{x} = x, y, z$ are the boundary coordinates and the radial distance is r so that the boundary is located at infinity. The usual relation between temperature and the horizon position is $r_H = \pi T$ (we have set the AdS radius to 1).

The key ingredients we need are a scalar field, ψ_i, to represent the quark bilinear Δ_i from (2.1) (here a component of the quark bilinear in the $\bar{3}$ of colour), with baryon number $B = 2/3$ and dimension 3, and a gauge field associated with $\mathrm{U}(1)_B$ whose A_t component will describe the chemical potential. We use an action

$$\mathcal{L} = -\frac{1}{4} F^{\mu\nu} F_{\mu\nu} - |\partial\psi_i - iBA\psi_i|^2 + 3\psi_i^2, \tag{2.3}$$

the mass is picked to be minus three in units of the AdS radius since this corresponds holographically via $M^2 = \Delta(\Delta - 4)$ to a dimension 3 operator. We have neglected any order ψ^4 interaction terms between different ψ_i.

The equations of motion are

$$\psi_i'' + \left(\frac{f'}{f} + \frac{5}{r}\right)\psi_i' + \frac{B^2}{r^4 f^2}A_t^2\psi_i + \frac{3}{r^2 f}\psi_i = 0, \tag{2.4}$$

and

$$A_t'' + \frac{3}{r}A_t' - \sum_i \frac{2B^2}{r^2 f}\psi_i^2 A_t = 0. \tag{2.5}$$

As usual for regularity one requires $A_t = 0$ at the horizon which implies from the first equation of motion that

$$\psi_i' = -\frac{3}{4r_H}\psi_i. \tag{2.6}$$

Note that strictly at $T = 0$ we can not assume this boundary condition and the model is not complete. We will use the model to work out the edge of the phase boundary at finite T and not address the T=0 state.

There is always a solution

$$\psi_i = 0, \qquad A_t = \mu - \frac{\mu r_H^2}{r^2}. \tag{2.7}$$

There are more complex solutions that we can find numerically by shooting out from the horizon. In the UV they take the form

$$\psi_i = \frac{J_c}{r} + \frac{c}{r^3} + ... \qquad A_t = \mu + \frac{d}{r^2} + ... \tag{2.8}$$

c is interpreted as the Cooper pair condensate, $\mathcal{O} = \psi\psi$, J_c the source for that operator (which carries both colour and flavour indices generically), μ is the chemical potential and d the density. Since there are two constraints on ψ, ψ', A_t, A_t' at the horizon we get a two parameter family of solutions (set in the IR by $\psi(r_H)$ and $A_t'(r_H)$ which we label by the values of J_c and μ, predicting c and d).

For example, let us consider the case with a single ψ_i field which might describe Δ_3 in the two flavour case. Note that if there is more than one identical ψ_i then there is an effective factor of N_i in the interaction term in (2.5). This can be removed by rescaling the ψ_i by $1/\sqrt{N_i}$ leaving the same equations to be solved. In practice this means the CFL condensates will be a factor of $\sqrt{3}$ smaller than the 2SC computations we make. Crucially though the phase boundaries remain at the same coupling values. For this reason we will focus on the $N_i = 1$ case.

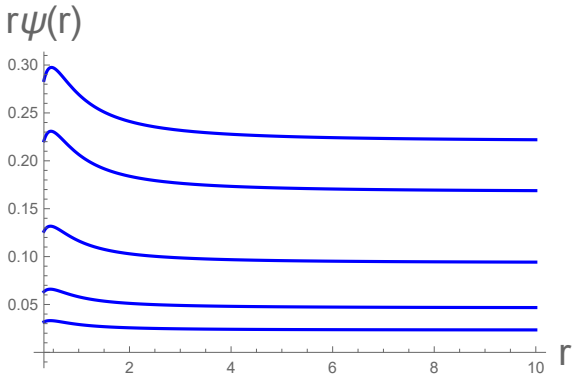

(a)

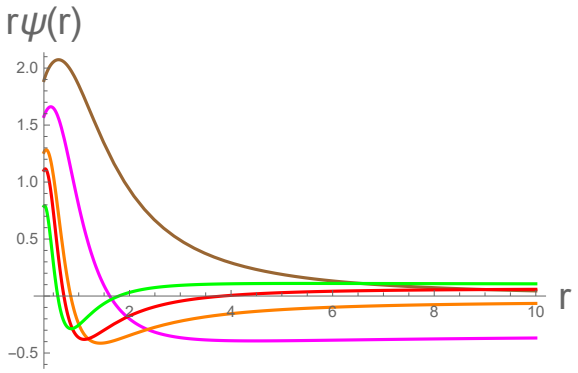

(b)

Figure 2.1: *(a) The ψ functions in the unbroken phase at $T = 0.1, \mu = 1.0$. (b) The ψ functions in the broken phase at $T = 0.1, \mu = 5.0$.*

Now we can solve (2.4) and (2.5) numerically: in Figure 2.1 (a) for $T = 0.1$ we plot the solutions of ψ (we plot $r\psi$ which asymptotes to J_c in the UV) where in each case $A_t'(r_H)$ has been adjusted to set $\mu = 1.0$. In Figure 2.1 (b) we show solutions for $\mu = 5.0$. At low μ there is no symmetry breaking, the only solution with $J_c = 0$ is that with $\psi = 0$ so that $c = 0$. For the higher value of μ, the solution that asymptotes to $J_c = 0$ is symmetry breaking (the curve shown with the highest IR value), this solution has a non-zero condensate c. the physics here in AdS is that the chemical potential generates an effective negative mass squared for the scalar ψ and when it violates The Breitenlohner-Freedman (BF) bound of $M^2 = -4$ an instability to ψ condensation results.

In Figure 2.2 we plot the value of the condensate against μ for the $J_c = 0$ embeddings at fixed $T = 0.1$ and show there is a second order transition. Note that the presence of this transition means the model has an intrinsic attractive interaction built into it, condensation would not occur otherwise. Below we will investigate switching off this intrinsic attraction by switching on a repulsive four fermion interaction but also move to adjusting its strength to play the role of the QCD interactions.

The model has interesting structure beyond the basic transition. If in the broken phase we allow $\psi(r_H)$ to fall below the value that generates the $J_c = 0, c \neq 0$ solution there are solutions, shown in Figure 2.1b, that asymptote to negative J_c. A minimum J_c is

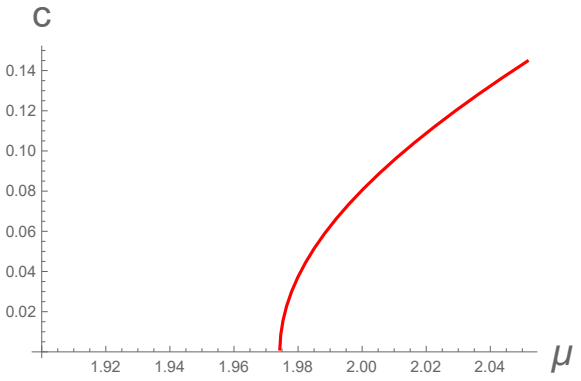

Figure 2.2: *The condensation vs μ in the broken phase at $T = 0.1$.*

encountered as one lowers $\psi(r_H)$ and the UV value of J_c then rises again. There is a further solution with $J_c = 0, c \neq 0$ where the ψ function dips once below the axis. This is an excited state of the vacuum where the first radially excited state of the bound states associated with ψ has condensed rather than the ground state. As $\psi(r_H)$ falls further excited states can occur, with condensation of higher and higher excitation modes. We demonstrate this by plotting the solutions in the J_c, c plane for $\mu = 5, 10$ in Figure 2.3 where a spiral structure is revealed. As the spiral moves between quadrants of the plane the solutions for ψ change: first there are solutions for which ψ is always positive, then when the solution falls below the axis in the UV we switch to negative J_c and so on. This is typical in holographic models of symmetry breaking having first been identified in the D3/D7 system with a magnetic field [72]. These extra vacua will play an interesting role in the discussions to come.

We will next turn to introducing NJL interactions into the model.

2.4 NJL Operators

A natural step is to include the QCD interactions into our model of CSC as four fermion operators since the gluons are assumed to have acquired a large mass. Four fermion operators are an example of a "double trace" operator and can be incorporated using Witten's prescription [67]. Previous work on NJL operators in holographic superconductors can be found in [68] and recent work understanding the holographic description of the relativistic Nambu-Jona-Lasinio model is in [69].

Consider the holographic description of an operator/source pair $\mathcal{O}, J$ by a holographic field ψ in AdS

$$ds^2 = r^2 dx^2_{3+1} + \frac{dr^2}{r^2}, \tag{2.9}$$

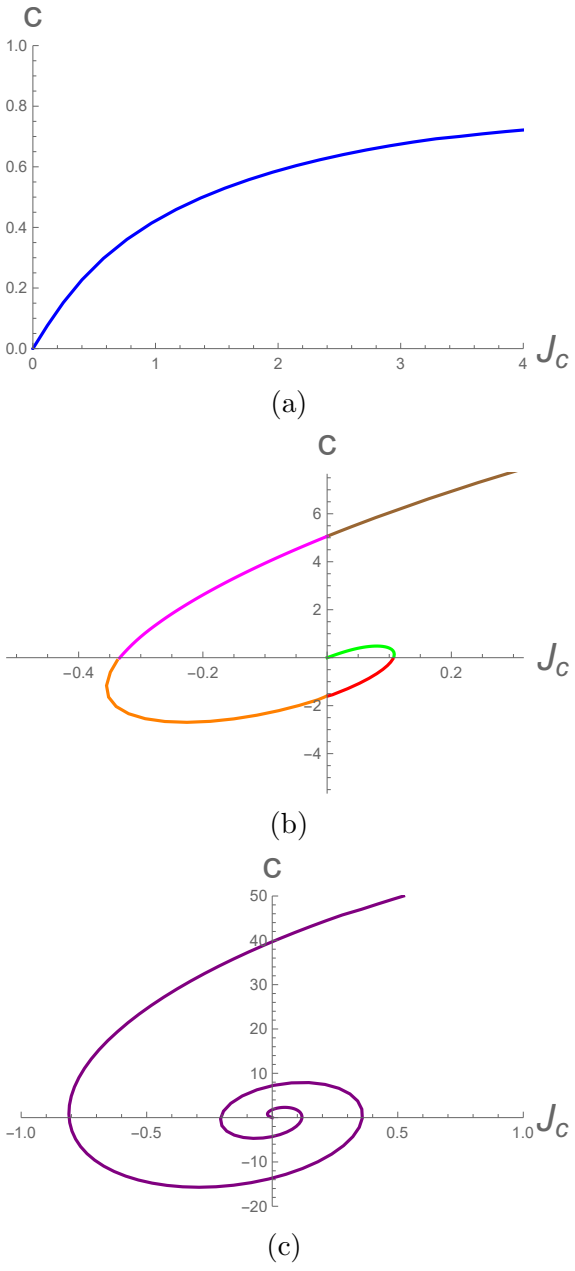

Figure 2.3: *c vs J_c where $T = 0.1$. (a) Unbroken phase where $\mu = 1.0$. (b): Broken phase where $\mu = 5.0$. (c) Broken phase where $\mu = 10.0$.*

with action (here we pick $M^2 = -3$ since all our operators are dimension 3)

$$S = -\int dr \frac{1}{2}\left(r^5(\partial_r\psi)^2 - 3r^2\psi^2\right). \tag{2.10}$$

The solutions take the form

$$\psi = J/r + \mathcal{O}/r^3. \tag{2.11}$$

Evaluating the action there is a UV divergence so we must include the counter term at the UV boundary (Λ)

$$\mathcal{L}_{UV} = -\frac{1}{2}\Lambda^4\psi^2|_\Lambda. \tag{2.12}$$

This term is crucial for the analysis below.

(Note that in the reference [69] the authors worked with a rescaled field $L = r\psi$. This is natural from the point of view of the D3/probe D7 system where the UV action takes precisely this form. If one substitutes this rescaled field into the action above and integrates by part then the surface term vanishes and the action takes the form

$$\mathcal{L} = -\int dr \frac{1}{2} r^3 (\partial_r L)^2, \tag{2.13}$$

which, since $L \sim J + ..$, has no UV divergence and hence no counter term. The IR boundary condition $\partial_r L = 0$ forces $\mathcal{O} = 0$ which is appropriate for supersymmetric gauge theory configurations where, for example, the quark condensate is forbidden. Here, the action also vanishes with $L =$ constant corresponding to the vacuum energy of the gauge theory vanishing.)

We now wish to include in the field theory a term of the form

$$\Delta\mathcal{L} = -\frac{g^2}{\Lambda^2}\mathcal{O}\mathcal{O}, \tag{2.14}$$

where $\mathcal{O} \neq 0$ then this term generates a source $J = \frac{g^2}{\Lambda^2}\mathcal{O}$. If we substitute this relation back into the Lagrangian term we uncover

$$\Delta\mathcal{L} = -\frac{\Lambda^2 J^2}{g^2}. \tag{2.15}$$

In analogy to this term Witten's prescription in the holographic description is to add a UV surface term evaluated at the cut off Λ

$$\Delta\mathcal{L} = -\frac{\Lambda^4 \psi^2}{g^2}, \tag{2.16}$$

since $\psi \sim J/\Lambda + ..$ in the UV these match.

The simplest way to include this extra term in the analysis is by considering the result of the change to the UV boundary condition on the solutions. Varying the action gives

$$\delta S = 0 = -\int dr \left(\partial_r \frac{\partial\mathcal{L}}{\partial\psi'} - \frac{\partial}{\partial\psi}\right)\delta\psi + \left.\frac{\partial\mathcal{L}}{\partial\psi'}\delta\psi\right|_{UV,IR}. \tag{2.17}$$

There is also the variation of the surface counter term

$$\delta S = -2\Lambda^4 \psi \delta\psi|_{UV}. \tag{2.18}$$

Normally in the UV one would require the source to be fixed and $\delta\psi = 0$ to satisfy the boundary condition. We do this by fixing the source J to specify a particular theory.

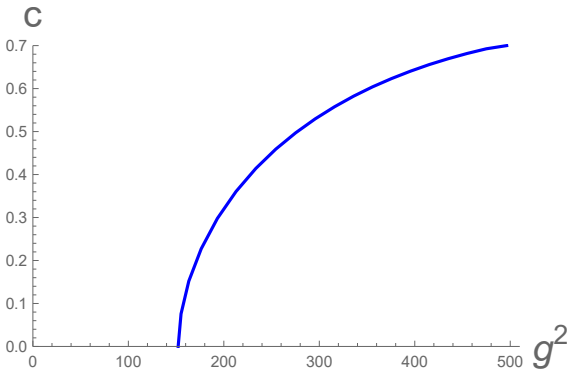

(a)

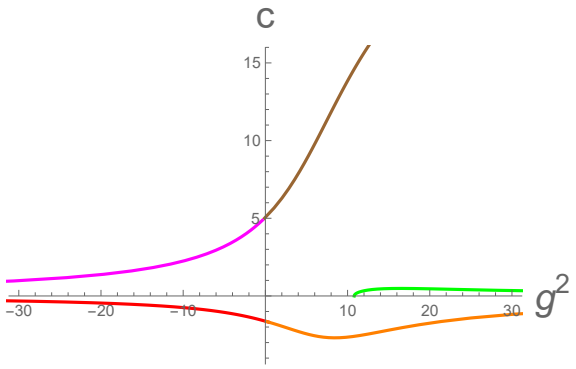

(b)

Figure 2.4: *(a) Plot of c against g^2 ($\Lambda = 10$) in the unbroken phase for embeddings in Fig. 2.1a. (T=0.1, $\mu = 0.1$) (b) Plot of c against g^2 ($\Lambda = 10$) in the broken phase (T=0.1, $\mu = 5$) for solutions in Fig. 2.1b.*

To describe the double trace operator though we allow ψ (J) to change at the UV boundary and instead impose the vanishing at that boundary of

$$0 = \frac{\partial \mathcal{L}}{\partial \psi'} + \psi \Lambda_{UV}^4 + \frac{2\psi \Lambda_{UV}^4}{g^2}\,, \tag{2.19}$$

where we have included the variation of the new surface term. For our action $\frac{\partial \mathcal{L}}{\partial \psi'} = -r^5 \psi'$. Assuming (2.11) we find that we need

$$J \simeq \frac{g^2}{\Lambda^2} \mathcal{O}. \tag{2.20}$$

This condition (which matches the expectation under (2.14)) is simple to apply to the solutions of the (unchanged) equation of motion we already have.

2.4.1 NJL Operators in the Superconductor

Let us now return to the holographic superconductor model of the previous section. We can apply our analysis to the ψ functions of Fig. 2.1. We can interpret each function,

including those with $J_c \neq 0$ as describing the model with zero intrinsic J_c but a four fermion operator present. The four fermion operator in the presence of the condensate c generates the UV source J_c. For example we can translate the functions of Fig. 2.1a, where μ lies below the critical value, through Fig. 2.3a, to a plot of c against g^2 which we show in Fig. 2.4a. Here we have taken $\Lambda = 10$ numerically. We observe a critical value of the NJL coupling that triggers symmetry breaking at a second order transition. Note here there are no solutions where in the UV J_c and c have opposite signs, this means that putting in a repulsive four fermion term (negative g^2) produces no solutions other than $J_c = 0, c = 0$ as one might expect.

Similarly we can translate the functions of Fig. 2.1b through Fig. 2.3b to the plot in Fig. 2.4b which again shows c vs g^2 but here at $g^2 = 0$ there is already symmetry breaking. There are two interesting additional features here. Firstly there are solutions at negative, repulsive, g^2. This is not surprising because at $g^2 = 0$ there is symmetry breaking, so switching on a repulsive four fermion term would be expected to reduce the condensation, and so it does. The surprising feature is that the condensation does not switch off completely except at infinite repulsive interaction strength (there are solutions with zero c but non-zero J_c that generate infinite g^2 values). The intrinsic attractive interaction in the AdS/superconductor model is presumably more subtle in structure than the NJL operator which is only switching parts of the interaction off. Remember in superconductor theory any attractive interaction will result in condensation. The remaining structure in the $c - g^2$ plane is the translation of the spiral in the $c - J_c$ plane seen previously.

Our initial intention to describe QCD had been to take the basic holographic superconductor model and introduce a critically tuned repulsive NJL operator to switch off condensation at each T, μ value. On this interaction free description of the quark gluon plasma we would then add back the QCD interactions as further positive shifts in the NJL coupling strengths. We have now shown that this is not achievable because the intrinsic interactions are more subtle than the NJL interaction so an infinitely repulsive interaction is needed to switch off the base condensation. However, an equally sensible approach is to simply modify the strength of the interaction between ψ and A_t to reflect the QCD interaction strength. Our assumption is still that the gluons are massive in this strongly coupled phase so that we can describe the colour of quarks by a global symmetry but now the interactions will be introduced through the action

$$\mathcal{L} = -\frac{1}{4}F^{\mu\nu}F_{\mu\nu} - |\partial\psi - iGBA\psi|^2 + 3/L^2\psi^2. \tag{2.21}$$

We interpret the $A\psi$ interaction term as the holographic model's knowledge of the broken gauge interactions. Note the inclusion of the new coupling G which we will shortly relate to the QCD running coupling.

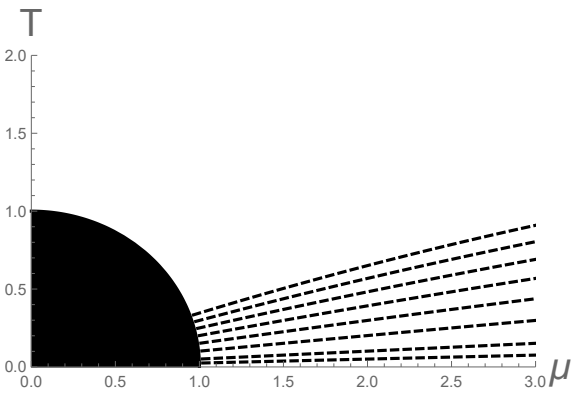

Figure 2.5: *Plot of the superconducting phase boundary at different* $G = 0.5, 1, 2, 3, 4, 5, 6, 7$ *from bottom to top in the* T *-* μ *plane. The black region is expected to be the chirally symmetric phase below a scale of* $\mu^2 + T^2 = 1$.

First though we can find the phase boundary for the superconducting phase as a function of G. For each T and G we make plots as in Figure 2.2 and then plot $\mu_c(T)$ in the plane. This is shown in Figure 2.5. Note that given the solutions for $G = 1$ one can move to another G by scaling $\psi \to G\psi$ and $A_t \to GA_t$ in (2.4), (2.5) so the critical μ just scales with G.

2.5 The QCD Phase Diagram

Let us now attempt to describe the colour superconducting phase of QCD using these tools. We will assume that the chiral phase transition occurs at $T^2 + \mu^2 = \Lambda_c^2$ and numerically set $\Lambda_c = 1$ with a UV cut off on the holographic model of $\Lambda = 10\Lambda_c$ where we read off c, J_c. We will assume a phase with a $\bar{q}q$ condensate lives below Λ_c.

In the quark gluon plasma phase we will use the action of (2.21) but we must set the value of G at the cut off scale to a sensible ansatz in QCD. A natural choice based on the one loop running is

$$G^2 = \frac{\kappa}{b \ln(T^2 + \mu^2)/\Lambda_c^2}, \qquad b = 11N/3 - 2N_f/3, \tag{2.22}$$

which blows up at Λ_c. We need to fix κ so it is appropriate for the strength of attraction that generates the $\bar{3}$ of colour condensate.

Perturbatively, the strength of tree level t-channel one gluon exchange interaction for the four different colour channels for $\bar{q}q$ and qq is

$$1_{\bar{q}q} : 8_{\bar{q}q} : 6_{qq} : \bar{3}_{qq} = -\frac{8}{3} : \frac{1}{3} : \frac{1}{6} : -\frac{1}{3} \tag{2.23}$$

The attraction might be as little as $1/8$ the attraction for the chiral condensate. Of course at strong coupling the relative strength of these interactions is not known. The intrinsic

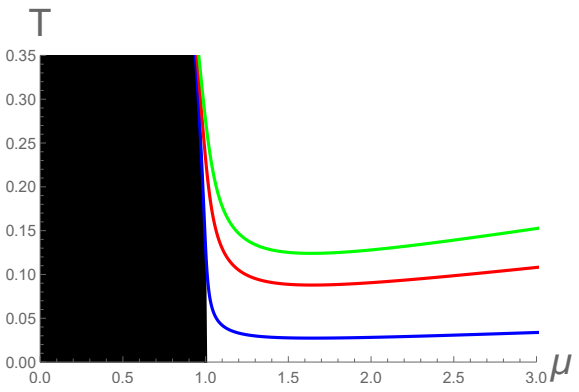

Figure 2.6: *QCD phase diagram: the blacked out area is below Λ_c where chiral symmetry breaking is expected. The remaining phase edges shows where the CFL phase is present for the choices of $\kappa = 1, 10, 20$ from bottom to top.*

interaction between the fields ψ and A_t in the holographic model should be controlled by the strength of the QCD interactions that presumably lie between $\kappa = 1 - (4\pi)^2$. Given the 1/8th suppression we will study the range of κ between 1 and 20 to estimate the area of the phase diagram where superconductivity is likely.

It is now simple to construct the phase diagram from the analysis of Figure 2.5. We overlay circles in the T, μ plane for each value of G from (2.22) taking $N_f = 3$ and identify the points where they cross the same G value transition curve. We find the phase diagram in Figure 2.6. Very close to Λ_c the coupling gets very strong and the superconducting phase then hugs the phase boundary up to high values of T. Most likely the chiral phase will extend a little above Λ_c though and this feature will be greatly reduced. Typically we see the superconducting phase is predicted to exist below T of 0.15 Λ_c (for $\kappa \simeq 10$), which we might estimate as 20 MeV or so if $\Lambda_c \simeq 175$ MeV, the expected temperature of the chiral transition. This value might rise sharply just before the chiral transition. Usual estimates place the gap in the 10-100 MeV range [22] so this seems a sensible model.

2.5.1 Quark Mass

Our phase diagram so far has been plotted for the massless theory and the expected condensation has the colour flavour locked form for $N_f = 3$ and 2SC for $N_f = 2$. One might expect there to be a transition as the strange quark mass grows from CFL to a two flavour 2SC phase at lower μ. The presence of the mass leads to a lower value of the Fermi momentum which will reduce the condensate but also relative differences in the Fermi surface levels for different quark flavours is expected to frustrate the formation of the colour flavour locked condensate.

Holographically modelling this transition is not straightforward. Each component of (2.1) is of mixed flavour and should see the different chemical potentials and masses

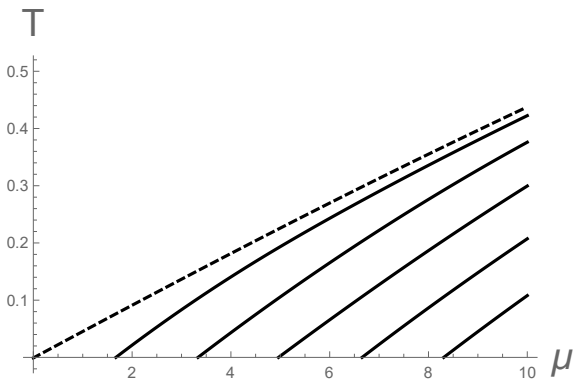

Figure 2.7: *Phase diagram for the model at fixed* $G = 0.9$ *and for quark mass* $m = 0, 1.3, 2, 3, 4, 5$ *from left to right.*

associated with each of the two constituents. Presumably this should be described by a non-abelian Dirac-Born-Infeld type action (assuming one could neglect the stringy nature of the states stretched between different flavour branes). Here though we will try something very naive to show a mechanism by which mass could switch off the condensation.

The quark mass, m should be described by a new holographic field χ with asymptotic behaviour $\chi = m/r + ...$ (the solution for a scalar of mass -3 in pure AdS) and IR dynamics that should be connected to the formation of the chiral condensate which is the sub-leading operator part of the solution. One would need a full model of the chiral transition to write down a potential for the χ scalar so to avoid getting bogged down in that dynamics we will just set $\chi = m/r$ and look at its effects on the ψ Cooper pair formation (of course really one should solve linked equations but our simplistic approach will show how the mass could suppress the Cooper pair condensation). We imagine a simple Lagrangian coupling of the form $|\chi|^2|\psi|^2$ so that the equation of motion for ψ becomes

$$\psi'' + \left(\frac{f'}{f} + \frac{5}{r}\right)\psi' + \frac{G^2B^2}{r^4 f^2}A_t^2\psi + \frac{1}{r^2 f}\left(3 - \frac{m^2}{r^2}\right)\psi = 0. \tag{2.24}$$

Clearly the m^2 term acts to oppose the instability induced by μ, which is the main mechanism we wish to flag here.

We first plot the phase boundary for $G = 0.9$ at different values of m in Figure 2.7. As the quark mass rises the boundary line tilts in the plane until for masses of order the chemical potential the phase is excluded at low μ. The positive contribution to the scalar ψ's mass squared is greater than the BF bound violating negative contribution from A_t. The mass therefore discourages the condensation.

We plot the phase structure of the theory with the running coupling (2.22) for $\kappa = 10$ and $m = 0., 0.5, 1.0, 1.3$ in Figure 2.8. For small quark masses the phase boundary simply moves to lower values of T at a given μ. If the mass becomes larger though then for a range of μ there is no condensation present. At large μ the mass is overwhelmed

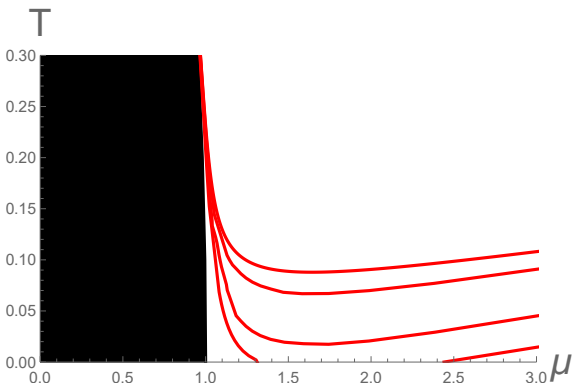

Figure 2.8: *QCD phase diagram with a quark mass m: in the blacked out area chiral symmetry breaking is expected. The remaining phase edges shows where the CFL phase is present for the choices of $\kappa = 10$ and $m = 0, 0.5, 1.0, 1.3$ from top to bottom.*

and the condensation returns. Note at $\mu \simeq 1$ where the coupling becomes arbitrarily strong the phase briefly returns however large m is, but this region is likely inside the chirally broken phase since the quark anti-quark attraction is also getting very strong.

In the case of QCD one can interpret the above description as that for Δ_1 and Δ_2 with the interaction with χ describing the interplay with the strange quark mass. The phase boundaries in Figure 2.8 for different m represent our estimate of where the CFL phase (Δ_1 and Δ_2) will switch off, although it is only a naive estimate since we have not include the effect of different Fermi surface levels. The 2SC phase would be expected to exist between the edge of the CFL phase and boundary for $m = 0$ since Δ_1 is oblivious to the strange mass. If we take $\kappa = 10$ and assume $\Lambda_c = 10$MeV then the physical strange mass corresponds roughly to the $m = 0.5$ curve and the CFL phase exist down to the chiral boundary although with a transition to the 2SC phase at higher T. For lower κ values the CFL phase might cease completely at lower μ.

This discussion has been very naive, although it reveals a mechanism by which the CFL phase will be shut down by the strange quark mass, and we leave to future work including the correct dynamics for χ, including the chiral transition, as well as incorporating the non-abelian nature of the discussion.

2.6 Discussion

The goal of this chapter has been to push through the block in thinking as to how to describe the colour superconducting phase of QCD holographically. For a long while the colour charged nature of the bi-quark condensate has stopped progress. We have attempted to side step this issue by arguing that at strong coupling and intermediate temperatures and chemical potentials the gluons are likely gapped by the plasma. If we treat the colour symmetry of the quarks as a global index then holographic models

can progress. Indeed here we have demonstrated that by recycling the simplest holographic superconductor model adjusted to this setting. The key question was how to then include the QCD interactions. We investigated NJL operators as one possibility and we have included the discussion here because there is an interesting story connected to the spiral structure in the operator-source plane in the superconductor model reflecting excited states of the vacuum (note that this structure is also present in the AdS_4 superconductor but we are not aware of any discussion of it in the literature). This leads to the conclusion that only an infinitely repulsive four fermion operator suffices to switch off the intrinsic attractive interaction of the holographic superconductor model. That attractive interaction is presumably more complex in structure than the four fermion operator and any residual attraction would lead to superconductivity. In fact we moved to simply adjusting the strength of that intrinsic interaction to reflect the QCD couplings value as a function of μ, T. As a result we can plot the phase diagram of the superconducting phase (see Fig. 2.6). The transition temperature lies near 20MeV, which we obtain by multiplying the temperature by Λ_c as we were working in units where $\Lambda_c \to 1$, which matches the usually quoted range of 10-100MeV obtained by weak coupling regime calculations.

The model we have used is somewhat like an NJL model of colour superconductivity but the holographic setting would allow one to easily compute equations of state and transport properties of the phases. In chapter 4 we shall investigate such equations of state and the consequences for neutron star structure. There is also plenty of scope to make a more sophisticated model of the phase structure including back reaction on the metric, describing the chiral transition of QCD and the interplay between the quark mass and the condensation pattern. We made a first attempt at understanding that mass dependence by a very simple model of an interaction between a quark mass and the Cooper pair which revealed a transition between a colour flavour locked phase and a 2SC phase, shown in Figure 2.8. Again this matches the form of the usually expected phase structure.

In the next chapter we discuss a holographic phenomenological model of chiral symmetry breaking. The equation of state this model provides will allows us to obtain stable solutions of quark matter neutron stars.

Chapter 3

Deconfined, Massive Quark Phase at High Density and Compact Stars

3.1 Introduction

In this chapter, we turn to the study of neutron stars. We study the possibility of these kind of astrophysical objects of having a core made of deconfined quarks. Thus we will describe the deconfined phase of matter using holography, and see whether we obtain sensible results according to recent astronomical measurements.

In Hoyos *et al.* [73] a holographic D3/D7 system was used to describe a deconfined yet massive quark phase of QCD at finite density, concluding that the equation of state of such a phase was not stiff enough to support exotic dense stars. A stiff equation of state of the matter is such that the pressure increases quickly for a given increase in density. Such a material would be harder to compress and offers more support against gravity. Conversely, a soft equation of state produces a smaller increase of pressure for a change in density and is easy to compress. The analysis in [73] used a hard quark mass to represent the dynamical mass and assumed a conformal gauge background. In this chapter we phenomenologically adjust the D3/D7 system to include a running anomalous dimension for the quark condensate that occurs in this holographic system. This introduces a dynamical mechanism for chiral symmetry breaking in which the model still has a deconfined massive phase at intermediate densities.

Here we show that these systems, dependent on the running profile in the deep IR, generate much stiffer equations of state and non-monotonic behaviour in the speed of sound. As a result there are the first hints that the holographic equation of state may be closer to supporting hybrid stars with quark cores.

The equation of state (EoS) of the dense matter, which relates state variables of the system, is a key ingredient to fully model a neutron star. A complete EoS would also be very important in the light of the recent measurement of gravitational wave signals from mergers of binary neutron stars [54], since the model of the wave signal is sensitive to the specific form of the EoS. Nevertheless, there has been a struggle to find a complete EoS; the difficulty of the task resides in the need to solve QCD in the non-perturbative regime at finite baryon chemical potential. At the moment the EoS of strongly interacting matter at low temperatures is relatively well described at baryon densities below the nuclear saturation limit $n_B \leq n_s \approx 0.16$ fm^{-3}, where Chiral Effective Theory (CET) works [74, 75], as well as at baryon chemical potential above ~ 2.5 GeV where the perturbative techniques can be applied [66, 76, 77]. However this excludes the values of density where a phase transition to quark matter would be expected to occur [78].

In the context of the Gauge/Gravity duality, which has emerged as a new tool to study strongly coupled gauge theories, it is natural then to ask if a holographic model of the high density phase of QCD can be constructed and the corresponding EoS obtained. Holographic EoS at finite density have also been studied in [73, 79, 80, 81, 82].

Our goal in the present chapter is to investigate whether a deconfined phase in the core of neutron stars could be stable. In [73] the authors made a first attempt at such a description using the D3/D7 system that describes quarks with a hard mass of order 308 MeV in $\mathcal{N} = 4$ super-Yang Mills (SYM) background at finite density. Exact analytic results for the free energy are known in this case [41]. The glue fields are deconfined, and conformal so the theory describes a putative massive, deconfined quark phase. They concluded that the equation of state was too soft to support exotic stars. However, one can critique the model since there is no chiral symmetry breaking mechanism and the hard mass is only an approximation to chiral symmetry breaking which should switch off at yet higher densities. Also since they match the conformal theory's free energy at large density to the UV of QCD they, in a sense, match the dynamics to perturbative gluons whilst one might expect a running coupling from weak to strong to have significant impact.

Here we will take a phenomenological approach to improving the D3/D7 systems predictions. We will include an effective dilaton (although it is not backreacted on the geometry) that controls by hand the running of the anomalous dimension, γ, of the quark bilinear [83]. We pick a simple ansatz that has $\gamma = 0$ in the UV but then runs to a dial-able fixed point value in the IR. At zero density such theories have a BKT transition as γ in the IR is changed through one [84, 83] (the Breitenlohner-Freedman bound [33] is violated in the model for $\gamma > 1$) from a chiral symmetric phase ($\gamma < 1$) to a chiral symmetry broken phase ($\gamma > 1$). When density is included in a theory that runs to a fixed IR γ we show that there are two second order transitions: first density switches on, then at a distinct transition chiral symmetry breaking switches off. This phase structure has been seen previously in the D3/D7 system with a magnetic field

[72, 85] and phenomenologically related models [86]. Similar structures have also been seen recently [87] in the Witten Sakai Sugimoto model [88]. The intermediate phase is an example of a massive yet deconfined quark phase. Our model though contains a description of a dynamical quark mass and a running anomalous dimension. We show how the EoS in these systems depends on the IR fixed point value for γ and show that runnings that might plausibly describe QCD have a considerable stiffer EoS than the pure D3/D7 system. The speed of sound in units of the speed of light equal to one, can reach as high as $c_s^2 = 0.55$.

Once the EoS is obtained, solutions of the Tolman-Oppenheimer-Volkoff (TOV) equations which correspond to spherically symmetric stellar configurations that are in hydrostatic equilibrium can be found. Nevertheless, the equilibrium of the solution does not guarantee that it is stable.

We explore the effect of the holographic EoS we find in the TOV equation solutions. Even the stiffer possible descriptions of the deconfined quark phase we generate are not quite sufficient to construct a convincing description of both the heaviest neutron stars and new stable hybrid stars with quark matter cores. However, the situation is closer than [73] reported and in some cases there are hints that lighter hybrid stars may exist supported by the deconfined quark matter. We report on this picture since it strongly suggests that the changes we have made are steps towards a description with interesting phenomenology and it will hopefully trigger further refinement of the holographic set up. We briefly and rather crudely discuss an example of such a refinement, adding the confinement transition as an additional shift in the pressure between the high and low density phases which may further stabilise hybrid stars although obtaining both hybrids and very heavy neutron stars remains an issue.

The chapter is organized in the following way: in Section 3.2 we will review the different possible phases relevant to neutron stars: a confined phase of neutron stars which is modelled with an EoS that comes from considering a chiral effective field theory and a piece-wise polytropic extension towards higher values of density; the previous work [73] implementing a deconfined phase in the neutron stars using a top-down approach to AdS/CFT and a hard mass to the quarks; and a bottom-up D3/D7 brane intersection model with a chiral symmetry breaking mechanism. In Section 3.3 we solve the TOV equations and analyse the mass-radius relations of neutron stars using the models of the previous section. We mention how to compute the tidal deformabilities of a binary neutron star system in Section 3.4. We summarise in Section 3.5.

3.2 The Finite Density Phase Structure of QCD

In this section we will review our model of the low temperature QCD phase structure and the models that we use to study each phase. In Figure 3.1 we sketch the phase structures

that we will see below as a function of quark chemical potential at low temperature. In fact in this chapter we will only compute at strictly $T = 0$ although holography would straightforwardly allow computation at finite T also.

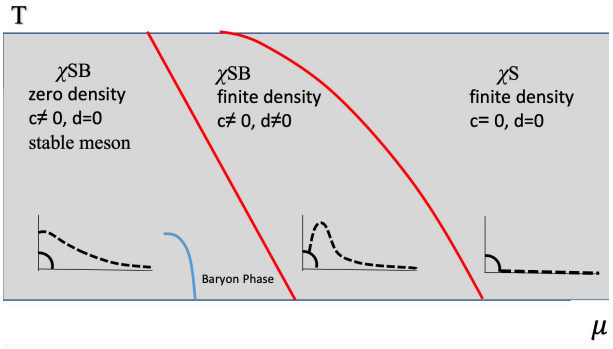

Figure 3.1: *A sketch of the low temperature phase structures we observe in the holographic models we explore. At low chemical potential the theory has chiral symmetry breaking (χSB), a non-zero chiral condensate (c) and zero density (d); in an intermediate regime there is a deconfined massive quark phase with non-zero density; at high μ there is chiral symmetry restoration. The D7 embedding function (field χ) is also sketched in each phase. These transitions are all second or higher order in the holographic models. Note we have also sketched the position of the baryon phase with non-zero neutron density which is not present in the holographic models (we include it phenomenologically from low energy analysis). We expect the transition to the high density phases from the baryon phase to be first order.*

3.2.1 Nuclear phase

At small chemical potentials QCD is well understood. The confined, chirally broken vacuum is empty until a chemical potential of $\mu = 308.55$ MeV when there is a first order phase transition to nuclear matter. This transition is already well studied and the nuclear matter equation of state has been explored in [48]. In this reference, the authors combined observations of a 1.97 solar mass neutron star with effective field theory (EFT), thereafter extrapolating it with a constrained piecewise polytropic form. Here holography is probably least able to help, given its origin at infinite N baryons are naturally very heavy and far from the QCD limit so, following several other authors [73, 89, 81], we will simply use the results of [48] to model the nuclear phase. Note there have been attempts to study the QCD nuclear phase holographically, for example in [90, 91, 92], but this will not be our focus in this chapter.

Three ansatz for the EoS (soft, medium and stiff) are presented in Table 5 of [48]. The energy density and pressure for different densities is given. We have encoded their data as a numerical fitting polynomial for the analysis below and we plot these in Figure 3.2. We will see (Figure 3.10) that this is sufficient to reproduce the neutron star mass radius plots in [48].

For each EoS there is a maximum central pressure/energy density for which data is provided in [48]. Above this maximum pressure either the speed of sound (which is

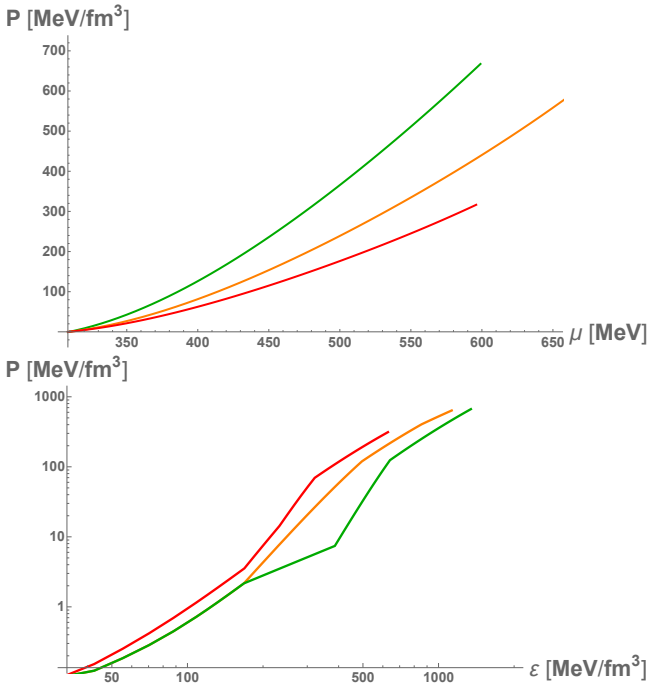

Figure 3.2: *Data for the nuclear phase taken from [48]: we show both the pressure versus chemical potential and energy density. The Green line represents a soft EoS, the orange a medium EoS and the red line a stiff EoS.*

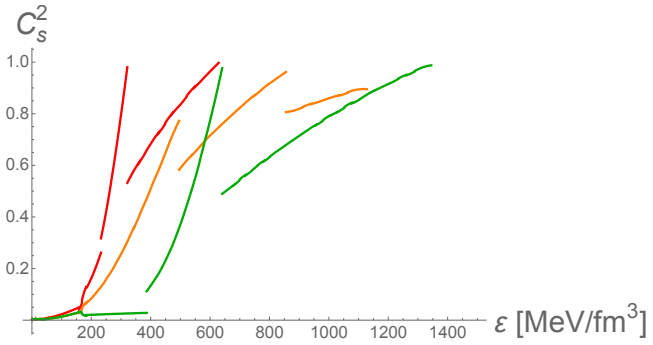

Figure 3.3: *Speed of Sound squared (Setting $c = 1$) as a function of the energy density for nuclear matter [48]. The different coloured lines represent nuclear matter from EFT EoS; (Green) soft EoS, (orange) medium EoS and (red) stiff EoS.*

simply $\frac{\partial P}{\partial \mathcal{E}}$) grows greater than the speed of light, or the EoS has been sufficient to model the most massive neutron stars observed. In figure 3.3 we plot the speed of sound against $\mathcal{E}$ to show this behaviour (note the discontinuities reflect moves between different polytropes in the piece-wise construction of the equation of state in [48]); the equivalent maximum pressures for the three possible EoS are 312.6 MeV fm^{-3} (stiff) 637.2 MeV fm^{-3} (medium) 666.5 MeV fm^{-3} (soft).

3.2.2 Holography of a Deconfined Massive Quark Phase

The next expected transition beyond the nuclear phase as the chemical potential is raised is normally presented as a transition to a deconfined, chirally symmetric quark phase. The transition from the nuclear matter phase is normally assumed to be first order although since this regime lies outside the region of controlled computation this is fundamentally a guess.

Holography can potentially inform us about the transition from the empty low μ vacuum to the higher μ vacuum with non-zero quark density. The first reference studying neutron stars using holographic equations of state was [73]. There, the authors used the equation of state of the massive D3/D7 system at finite density [41] to describe the quark matter phase. The D3/D7 model at finite density is always deconfined in the large N limit and further has no chiral symmetry breaking mechanism. This phase naively therefore has deconfined massless quarks. The authors then included a bare (hard) quark mass of order Λ_{QCD} as an approximation to a chirally broken state. This is a simplistic approximation to a phase of deconfined yet massive quarks. Inherently there is an assumption here that confinement and chiral symmetry breaking transitions are separated in the high density phase structure and we will further consider such a possibility in this chapter.

There is evidence for such a phase in more refined D3/D7 systems with explicit chiral symmetry breaking dynamics (see [28] for examples of adding chiral symmetry breaking to the D3/D7 system). The most controlled case is where a magnetic field is introduced [72]; the phase diagram was generated in [85]. It has the structure shown in Figure 3.1, we can see that there is a low μ phase with chiral symmetry breaking and no density. A second order transition then takes the model to a phase with non-zero density but chiral symmetry breaking which is precisely such a massive deconfined phase. Then another second order transition moves the system to a dense but chirally symmetric phase. Other examples of these transitions have been explored in [86]. The phenomenological model we use below is motivated by this example but allows one to control the running of the quark bilinear anomalous dimension γ by hand. The key role of this running for chiral symmetry breaking was highlighted in [84] and adapted to the D3/D7 system in [83]. Our model has the advantages of an explicit chiral symmetry breaking mechanism, a running γ and a very high μ phase with chirally symmetric quarks. Note though none of these models naively include confinement of the gluon degrees of freedom. We will discuss this issue more in subsection 3.3.2.

In this subsection we will review the original D3/D7 model and then provide a more sophisticated D3/D7 inspired phenomenological model that has a chiral symmetry breaking mechanism built in and naturally generates this massive deconfined phase.

The Basic D3/D7 Model

Let us quickly review the model of [73]. Their base model is $\mathcal{N} = 2$ SYM with the matter content of $\mathcal{N} = 4$ $SU(N)$ SYM in the adjoint sector and N_f matter hypermultiplet in the fundamental representation. The DBI action for a probe $D7$-brane in pure AdS, with a constant dilaton, is

$$S = -\frac{N_f N}{\lambda} T_{D7} V_3 \int d\rho \rho^3 \sqrt{1 + (\partial_\rho \chi)^2 - 2\pi\alpha'(\partial_\rho A_t)^2} \tag{3.1}$$

Here λ is the 'tHooft coupling, $T_{D7} = (2\pi)^{-7}\alpha'^{-4}$ is the $D7$-brane tension, $V_3 = 2\pi^2$ is the volume of the S^3 on the $D7$-brane and ρ the radial direction in AdS_5. $\chi(\rho)$, the brane embedding function, is holographically dual to the quark mass and condensate and A_t is a gauge field dual to the quark number chemical potential and density. In practice one works with the action

$$S = -\int d\rho \ \rho^3 \sqrt{1 + (\partial_\rho \chi)^2 - (\partial_\rho A_t)^2} \tag{3.2}$$

then an analytic form for the free energy can be found [41]

$$\mathcal{F} = \frac{\eta}{4}(\mu^2 - m^2)^2 + \mathcal{O}(\mu^3 T, T^4) \qquad \eta = \left(\frac{1}{6} B\left(\frac{1}{6}, \frac{1}{3}\right)\right)^{-3} \approx 0.363 \tag{3.3}$$

where $B(a, b)$ is the beta function, and m and μ are the UV asymptotic values of χ and A_t respectively. The field theory mass and chemical potential are given by $(2\pi\alpha')^{-1}$ times these quantities. Note that α' (which is formally infinite in the supergravity limit) then cancels from the resulting free energy for the field theory, as usual in the AdS/CFT correspondence.

To match the asymptotic UV form known from QCD one can pick $\lambda = 2^4\pi^2/3\eta$ so that:

$$\mathcal{F} = \frac{N N_f}{12\pi^2}\mu^4. \tag{3.4}$$

In practice one computes with (3.2) and rescales by $\frac{4NN_f}{\eta 12\pi^2}$. We will use $N_f = N = 3$.

Note that at any non-zero T this theory is deconfined. The phase therefore describes a vacuum with a density of quarks of mass m.

The EoS, which relates the pressure P to the energy density $\mathcal{E}$ is found from

$$P = -\mathcal{F}, \qquad \mathcal{E} = \mu\frac{\partial P}{\partial \mu} - P. \tag{3.5}$$

The authors of [73] match this quark matter description with the nuclear EoS from the previous section to model a transition between confined and deconfined matter inside a neutron star. They equated the zero μ phases in the nuclear model of QCD and in the

D3/D7 system. This allows comparison of the nuclear phase's free energy, with the free energy of the holographic model at finite μ and then determines the dominant phase at each quark chemical potential. The hard mass of the quarks is a free parameter and, as can be seen from (3.3), the phase transition occurs at $\mu = m$ when the free energy rises from zero (the phase with density does not exist for $\mu < m$).

In [73] the authors set, somewhat arbitrarily, $m = 308.55$MeV which places the transition to the nuclear phase in one model and that to the deconfined massive quark phase in the other at the same critical μ. We reproduce the plots for this case in Figure 3.4. The transition between the nuclear and deconfined massive phases occurs at the value of μ where the pressure of the deconfined quarks is greater than the chosen nuclear phase. The nuclear phase is preferred at μ just above 308.55 MeV but then there is a transition to the deconfined massive phase (note in each case before the nuclear phase reaches the pressure at which the speed of sounds becomes too large). We also display the pressure versus energy density plot which shows a jump at the first order transition.

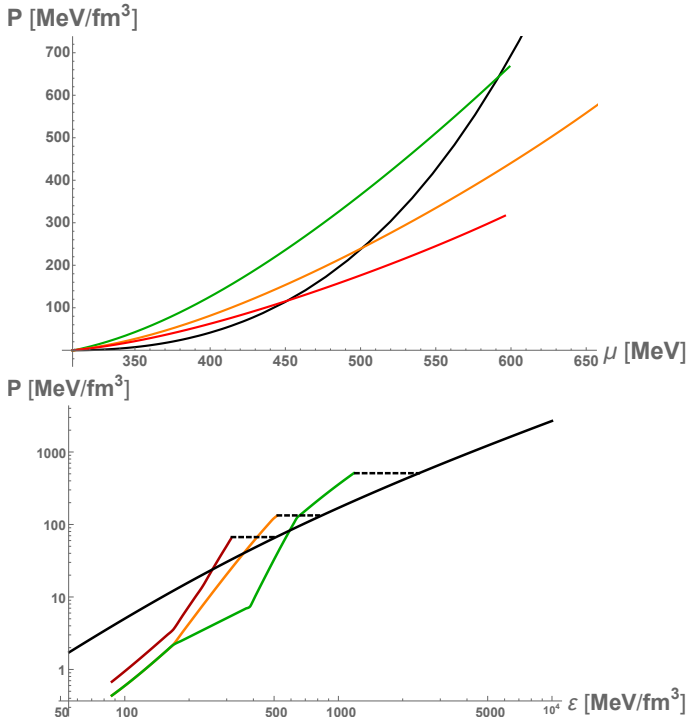

Figure 3.4: *Pressure versus μ and energy density for the basic D3/D7 model of [73] in solid black. Coloured lines represent the nuclear matter from the EFT EoS. The horizontal black dotted lines shows the change of phase.*

In the later paper [80] the authors allowed the critical μ of the massive deconfined phase to vary by simply dialling the quark mass m. If it is pushed higher than 308.55MeV the transitions occur at higher μ. The authors also proposed moving the critical μ less than 308.55MeV. Now the massive deconfined phase is favoured at μ less than 308.55MeV but they showed that in intermediate regions the nuclear phase could be favoured. This leads to compact stars with a variety of quark and neutron layers. This is quite a radical view of the phase structure although not obviously impossible. We will not consider such

cases further here though. Here we will always assume any quark phase lies at μ above where the nuclear phase exists.

Bottom-Up D3/D7 model with chiral symmetry breaking mechanism

The first new question we wish to ask is how robust the simple D3/D7 model's predictions are? In particular it is a very rough and ready description of a massive deconfined quark phase with chiral symmetry breaking since the quark mass is put in by hand as a hard mass. In particular since the gauge coupling of $\mathcal{N} = 4$ SYM is conformal one would expect the IR action to not reflect the growth of the gauge coupling. It is quite simple to construct a D3/D7 inspired bottom-up model with an explicit chiral symmetry breaking mechanism that realizes the deconfined yet massive quark phase. Here we will follow this path to cross check the results with those of the simpler model.

Our simple model is a small variation of the DBI action for a probe D7 brane in AdS_5

$$\mathcal{L} = -\int d\rho\ h[\rho^2+\chi^2]\ \rho^3\sqrt{1+(\partial_\rho\chi)^2-(\partial_\rho A_t)^2} \tag{3.6}$$

The function h which is crucially a function of $(\rho^2+\chi^2)$ is the key extra ingredient beyond (3.2), an effective dilaton term. In top down models the dilaton will be constant for $\mathcal{N} = 4$ SYM or for more complicated cases backreact on the metric. Here in a bottom-up approach we will allow h to be non-trivial yet neglect any backreaction in the metric. h will trigger chiral symmetry breaking. Note an explicit top-down example of precisely this action and a non-trivial, yet not backreacted, $h[\rho^2+\chi^2]$ that causes breaking of the symmetry is obtained for the example of magnetic field B induced chiral symmetry breaking in [72]. We will restrict ourselves to functions for h that return in the UV to a constant so that the UV normalization follows that of the discussion around (3.4).

Naively one might think to use the running coupling from QCD as the ansatz for the dilaton h. However, in [84, 83] it was shown that the mapping of the dilaton to the running anomalous dimension of the $\bar{q}q$ operator, that determines the chiral symmetry breaking dynamics, is more subtle. In particular chiral symmetry breaking is triggered when the chirally symmetric embedding $\chi = 0$ becomes unstable. One can expand the action for small χ [83] to give

$$S \simeq \int d\rho\ \left[\frac{1}{2}h|_{\chi=0}\ \rho^3(\partial_\rho\chi)^2+\rho^3\ \frac{\partial h}{\partial\chi^2}\bigg|_{\chi=0}\chi^2\right] \tag{3.7}$$

The first term can be made the kinetic term of a canonical scale in AdS_5 by writing $\chi = \tilde{\rho}\phi$ with the coordinate change

$$\tilde{\rho} = \frac{1}{\sqrt{2}} \left(\int_{\rho}^{\infty} h^{-1} \rho^{-3} d\rho \right)^{-1/2} \tag{3.8}$$

leaving

$$S \simeq \int d\tilde{\rho} \frac{1}{2} \left(\tilde{\rho}^5 (\partial_{\tilde{\rho}} \phi)^2 - m^2 \phi^2 \right) \tag{3.9}$$

with

$$m^2 = -3 + h \frac{\rho^5}{\tilde{\rho}^4} \frac{dh}{d\rho} \tag{3.10}$$

As expected the field χ maps to a field ϕ with $m^2 = -3$ in the case where $h =$ constant; it holographically describes the mass and quark condensate of dimensions 1 and 3 (satisfying the required $m^2 = \Delta(\Delta - 4)$). When h is ρ dependent in the IR though there is an additional contribution to m^2, a running of Δ. If m^2 passes through -4 then the BF bound in AdS_5 is violated, there is an instability and the D7 embedding function moves away from $\chi = 0$ - chiral symmetry is then broken.

Thus $h =$ constant describes a theory with no anomalous dimension. In [83] it was shown that $h = 1/\rho^q$ describes a theory with

$$m^2 = -3 - \delta m^2, \ \delta m^2 = \frac{4q}{(2-q)^2} \tag{3.11}$$

$m^2 = -4$ is achieved when $q = 0.536$ and it becomes infinite at $q = 2$. In terms of the anomalous dimension of the IR phase we have

$$\gamma = 1 - \sqrt{1 - \frac{4q}{(2-q)^2}}. \tag{3.12}$$

It's worth stressing that this analysis in a sense legitimises not backreacting the dilaton factor in our model. If one did have a fully backreacted geometry then the expansion to (3.7) would be more complicated but the additional pieces from expanding metric terms and so forth would simply be an additional contribution to the running mass in (3.10). At the level of studying the instability to chiral symmetry breaking putting in a hand chosen dilaton is as good as including a more elaborate bottom up geometry (of course if one had an honest full description of the particular chiral symmetry breaking system then the subtleties would be important!).

A natural choice to describe the running in a QCD like theory is

$$h = 1 + \frac{1}{(\rho^2 + \chi^2)^{\frac{q}{2}}} \tag{3.13}$$

which has zero anomalous dimension in the UV whilst moving to an IR regime below $(\rho^2+\chi^2)^{\frac{1}{2}}=1$ with a fixed point for the anomalous dimension. Note we include χ here in the spirit of the D3/D7 models we have discussed. Importantly if it were not present the BF bound would be violated in the model no matter how large χ became so there would be no stable solutions for χ.

There is intrinsically a single scale in this ansatz (the numerator of the fraction), which we have set to 1, and it loosely sets units where Λ_{QCD}=1. In fact this scale represents where the model moves from weak coupling to strong coupling. For the walking theories this scale may be quite separated from the IR scale where the BF bound is violated and chiral symmetry breaking occurs. We find it more intuitive therefore below to write all physical observables in units of the IR quark mass $\chi_0=\chi(0)$ which for comparison to QCD should be taken to be 330 MeV or so. There is still though only the single scale in the model.

By varying q one can pick very walking theories [93] where the anomalous dimension asymptotes to the BF bound at $q=0.536$ or theories that run quickly to large IR fixed points $q\simeq 2$. There are also theories that have a divergent anomalous dimension at some finite value of $(\rho^2+\chi^2)^{\frac{1}{2}}$ by picking $q>2$. It is interesting in this latter case that the anomalous dimension diverges at some finite energy scale (as it would at one or two loop level in QCD) yet the gravity dual provides a smooth description below that scale. It is a matter of speculation as to the IR behaviour of the QCD running and we will explore a range of possible IR divergent and fixed point behaviours below. The theory is known not to be very walking though so values of q towards 2 are most likely appropriate. In [83] it was shown that the zero density chiral transition as one varies q shows BKT or Miransky scaling [94, 95] because the IR mass is smoothly tuned through the BF bound.

The reader might wonder how generic our ansatz for h is. In the UV it must be a constant (so $\gamma=0$). In the IR it must go as $1/\rho^q$ at $\chi=0$ (so γ has the desired fixed point value). Writing the AdS radial direction r as $(\rho^2+\chi^2)^{\frac{1}{2}}$ is correct in the probe D7 model and dimensionally correct, so it seems as sensible choice. The question then is about the transition region between the IR and UV regimes - here we have picked something generically monotonic. In fact in [96] the authors argued that in these chiral symmetry breaking models the physics is determined by the derivative of gamma at the scale of the BF bound violation. Here our function simply raises this derivative as q and the fixed point value of γ rises. Of course, one could imagine doing some wilder things where there are, for example, multiple plateaus in the running but given nothing like that is well motivated we believe our ansatz is in fact reasonably generic.

Our theory then is (3.6) with (3.13). Note that in the large ρ limit these theories return to the description of [73] since $h\to 1$ so we fix the coefficient of the Lagrangian as in

[73] to match to the asymptotic perturbative prediction of the free energy from QCD - that is we enforce (3.4) in the UV.

Since the Lagrangian does not depend on the field A_t we have a conserved constant, the density, $d = \frac{\delta\mathcal{L}}{\delta A_t'}$, from here we can find an equation for A_t. Then we can perform a Legendre transformation $\mathcal{L}' = \mathcal{L} - A_t' \frac{\delta\mathcal{L}}{\delta A_t'}$ to replace A_t by d in the Lagrangian and find an equation for χ. The equations of motion are

$$(\partial_\rho A_t)^2 = \frac{d^2(1+(\partial_\rho\chi)^2)}{\rho^6+d^2}, \tag{3.14}$$

$$\begin{aligned}&\partial_\rho\left(\frac{(h^2\rho^6+d^2)\partial_\rho\chi}{\sqrt{(1+(\partial_\rho\chi)^2)(h^2\rho^6+d^2)}}\right)\\&-\frac{(1+(\partial_\rho\chi)^2)\rho^6 h\frac{\partial h}{\partial\chi}}{\sqrt{(1+(\partial_\rho\chi)^2)(h^2\rho^6+d^2)(\rho^2+\chi^2)^3}}=0\end{aligned} \tag{3.15}$$

which we then numerically solve.

First consider the case where $d = 0$, the low chemical potential phase, we fix the initial condition $\chi'(0) = 0$ and tune $\chi(0) = \chi_0$ (these are the standard IR boundary conditions in such models) in order that the UV mass obtained from the large ρ behaviour of $\chi(\rho)$ is zero. We display the solution in red in Figure 3.5 for the case $q = 1.8$: the function $\chi(\rho)$ can be viewed as the dynamical mass function of the quarks. In the UV (large ρ) limit the bare mass is zero, but as one runs to the IR (low ρ) a dynamical mass switches on.

In the large chemical potential phase we vary the value of d which is in correspondence to the chemical potential through (3.14). We set $A_t(0) = \chi(0) = 0$ and vary $\chi'(0)$ (again standard D3/D7 boundary conditions with density [40]) for each value of d in order to obtain solutions that have a UV mass equal to zero, see the blue curves in Fig 3.5 in the case of $q = 1.8$. We also obtain the value of the chemical potential as the UV value of A_t, i.e $\mu = A_t(\rho \to \infty)$ from integrating (3.14). We find that there is a critical value d_c above which there is not a symmetry breaking process and then the only solutions with a zero UV mass are the solutions that have $\chi = 0$ for every value of ρ (green in Fig 3.5). There are two second order transitions here, from the red $d = 0$ solution to the blue chiral symmetry breaking solutions, which is the massive deconfined phase we discuss, to the green very large d chirally symmetric phase. In Figure 3.6 we show the density as a function of μ for several different values of q. It displays the two transitions: one where d switches on, and the second is where one can observe kinks, corresponding to the point where the condensate switches off. At each transition d is continuous but there is a discontinuity in the derivative showing the transitions are second order. d seems to be the best variable to see both these discontinuities. Other variables we will display show it less clearly but the discontinuity is still expected to be present.

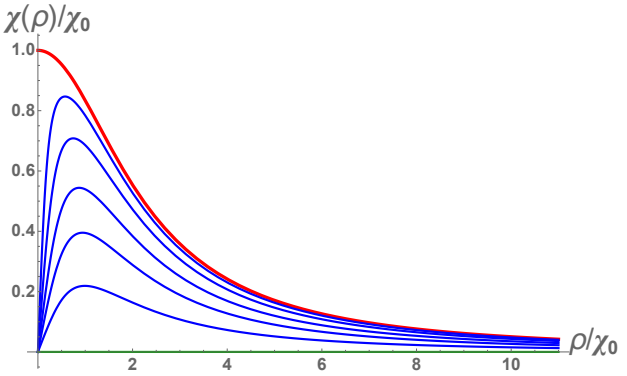

Figure 3.5: *Solutions for $\chi(\rho)$ for the case $q = 1.8$ in equation (3.13) for $d = 0$ (Red), $d = 0.005, 0.015, 0.075, 0.15, 0.29$ (from top to bottom in Blue) and $d = 0.501$ (Green).*

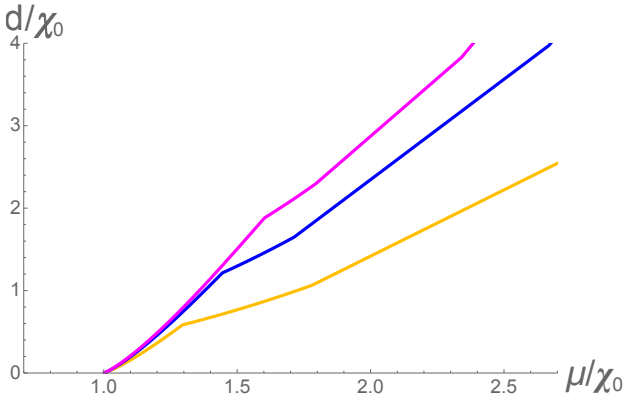

Figure 3.6: *d vs μ for different values of q. The different coloured lines represent different values of q; (yellow) q=1.6, (dark blue) q=1.99, (magenta) q=2.3*

We obtain the free energy of the vacuum for each value of d by integrating the action using the solutions of (3.15). The integrals all share the same divergence which can be removed by subtracting the counter term $\int d\rho\rho^3$. We further subtract the $d = 0$ free energy from the $d \neq 0$ solutions free energies so that the vacuum at low μ has $\mathcal{F} = 0$ as assumed in the previous nuclear equation of state analysis. Since d is related to μ we can obtain results as a function of the chemical potential.

Now we can study the behaviour of the model as a function of q. To make this comparison fair we write all dimensionful parameters in units of $\chi_0 = \chi(0)$ at $\mu = 0$. This can be thought of as the constituent quark mass (naively $\simeq 330$ MeV, a third the proton mass) which we are then using to fix the comparison. First of all we can look at the phase structure with chemical potential; in Fig. 3.7 we display the peak value of the embedding $\chi(\rho)$ against μ for different q. The larger q values represent high IR fixed point theories with strong running as the BF bound is violated and they more strongly support the embedding χ as μ rises but then rather rapidly switch to the $\chi = 0$ phase. Lower q theories that have smaller IR fixed point values support the peak of $\chi(\rho)$ less well but the chirally broken phase persists to higher μ - this supports the idea that the $\chi(\rho)$ functions have support in the more walking theories to higher energy scales.

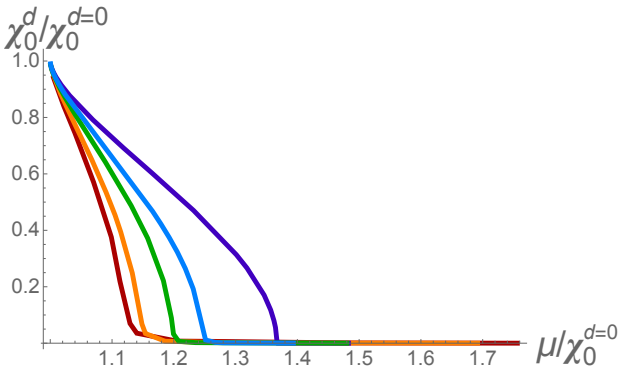

Figure 3.7: *Maximum of $\chi(\rho)$ in the IR vs μ for different q. The different coloured lines represent different values of q; (Red) q=1, (orange) q=1.1, (green) q=1.3, (blue) q=1.45, (purple) q=1.8.*

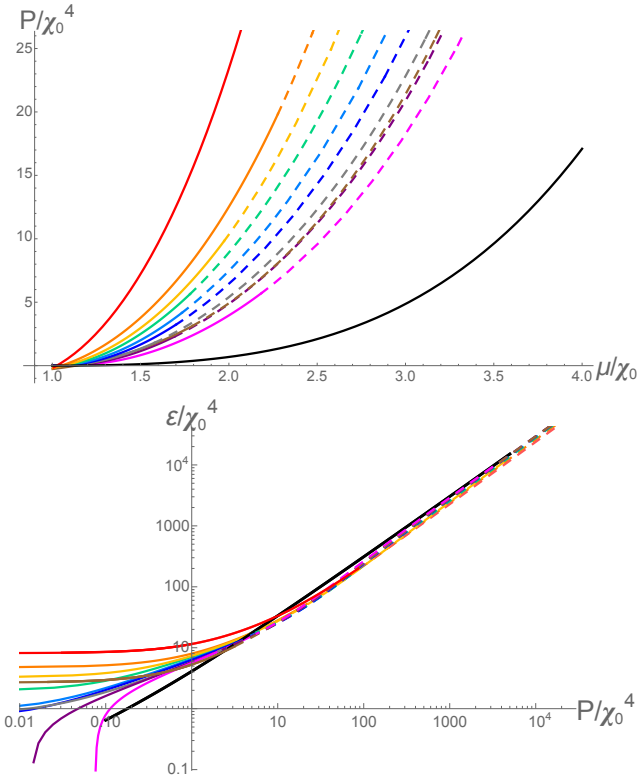

Figure 3.8: *Plots of pressure versus μ and energy density vs pressure for the holographic model with running anomalous dimension. The coloured lines represent different values of q; (Red) q=1, (orange) q=1.3, (yellow) q=1.45, (green) q=1.6, (light blue) q=1.8, (blue) q=1.99, (gray) q=2.2, (brown) q=2.3, (purple) q=2.4, (magenta) q=2.8 Solid lines are the massive quark phase, dotted lines the chirally symmetric phase. The black lines are the case of a constant dilaton.*

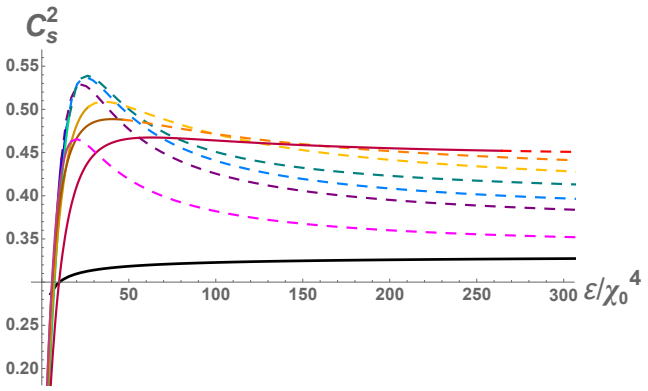

Figure 3.9: *The speed of sound (with $c = 1$) plotted against energy density in units of χ_0 for theories with different q. The coloured lines represent different values of q; (Red) q=1, (orange) q=1.3, (yellow) q=1.45, (green) q=1.6, (blue) q=1.8, (purple) q=1.99, (magenta) q=2.8. Solid lines are the massive quark phase, dotted lines the chirally symmetric phase. The black line is the case of a constant dilaton.*

Next in Fig 3.8 we plot the pressure (minus the free energy) against μ for these theories. For each q we mark the lines to show where the novel deconfined yet massive phase and the massless phase are present. Note that in a natural theory, with one scale, in the deep IR we would expect the energy density over χ_0 to lie around one and it does for $q \simeq 2$ - here the theory has the scale where the BF bound is violated very close to one and the derivative of γ in the ρ direction at the BF bound violating point is also close to one. Theories with q either much greater than 2, or that are walking, have an extra parameter (the gradient of γ) that changes the IR behaviour. We include the basic conformal D3/D7 model prediction also (here the phase is massive for all μ). We see that the inclusion of a running anomalous dimension raises the free energy in all cases relative to the basic D3/D7 model - this is to be expected since the dilaton profiles we use increase the action in the IR. We also show the energy density against pressure to show the theories are all converging in their predictions in the UV whilst distinct in the IR.

The theories with the running anomalous dimension clearly have stiffer equations of state than the basic D3/D7 model and a useful check of how much stiffer is to compute the speed of sound - we show the speed of sound against energy density in Fig 3.9. The non-monotonicity of the speed of sound is a notable feature. Here the peak is caused around the scale at which the coupling runs from the UV $\gamma = 0$ regime to the IR fixed point regime. This point is also close to the scale where the massive deconfined phase transitions to the chirally symmetric phase. The highest peak seems to occur where in the running of γ both the gradient to leave the UV regime and to enter the IR regime are largest. The higher IR fixed point theories with q just below 2, which naively one would have chosen to represent QCD, have the highest speed of sound and it rises briefly above 0.5 which is a rough guide to where interesting neutron star physics may occur [97]- we will investigate this below. Note all the theories asymptote to the speed of sound being a third at high μ.

3.3 Neutron Star Phenomenology

We have developed a holographic model of the high density regime of QCD with a parameter q that describes a variety of running anomalous dimension profiles. The models include a deconfined yet chirally broken phase and suggest that quite stiff EoS can exist. It's now interesting to see what these models predict for neutron star phenomenology. We convert our equations of state to a relation between the mass and radius of a neutron stars by using the TOV equations mentioned in subsection 1.4.3 of chapter 1 .

To integrate the equations we need to input the EoS $\mathcal{E}(P)$, as well as the central pressure $P_c = P(r = 0)$ as initial condition, and the output are the mass $m(r)$ and Pressure $P(r)$ of the corresponding star at a radial distance r. The radius R of the star will be the value of r at which the pressure vanishes as we expect outside of the star. Then varying the initial condition P_c as a parameter we can construct a curve for the mass of the star $M = m(r = R)$ against R.

We will fix the scale with the value of $p_0 = \epsilon_0 = \frac{(308.55MeV)^4}{\pi^2}$ as is sensible in the context of the nuclear equation of state discussed above; this choice then fixes the rest of our scale parameters.

As mentioned in subsection 1.4.3 we can also determine the stability of a star from the mass vs radius curve using the Bardeen, Thorne and Meltzer (BTM) criteria.

3.3.1 Mass Radius Relations

Nuclear phase

In subsection 3.2.1 we included three equations of state from [48] for the nuclear phase above 308.55 MeV.

To obtain the mass vs radius curve we solve the TOV equations starting from the highest density region (centre of the star), using the numerical equation of state. The maximum density the equations of state are consistent for (see subsection 3.2.1) set a maximum neutron star mass in each case. The result of the computations, confirming previous analysis is shown in Figure 3.10. The observation of neutron stars in the 2-2.5 solar mass range suggest that the stiffer EoS are more physical.

Basic D3/D7

As a further cross check of our methods we reproduce the mass radius plot for neutron stars with the equation of state from subsection 3.2.2 in "The Basic D3/D7 Model" part. That is the basic, constant dilaton D3/D7 model of [41] with the mass scale set so that

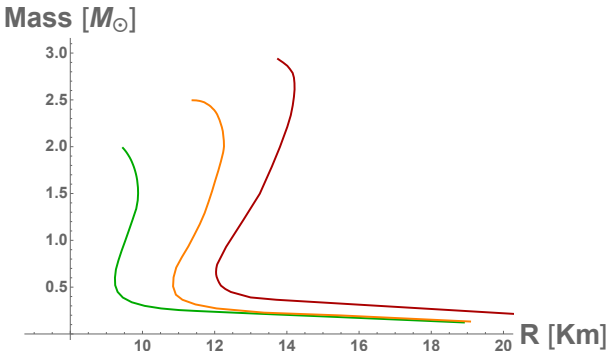

Figure 3.10: *Mass of the Neutron Star (in units of solar mass $M_\odot$) as a function of its radius (in kilometres) for nuclear matter from EFT EoS. The Green line represents a soft EoS, the orange a medium EoS and the red line a stiff EoS.*

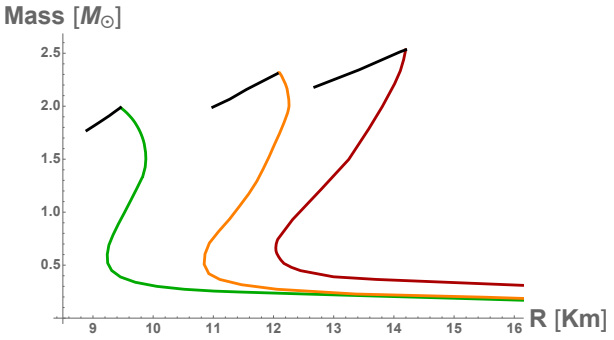

Figure 3.11: *Mass of the Neutron Star (in units of solar mass $M_\odot$) as a function of its radius (in kilometres). Colour lines represent Nuclear matter star from EFT EoS, the black lines represent the change of phase towards a hybrid star with a quark core using the constant dilaton D3/D7 model.*

the transition for the on-set of density occurs at $\mu = 308.55$ MeV. The transitions to the high density phase are those shown in Figure 3.11. As in [73] we find only unstable stars with a core of this material.

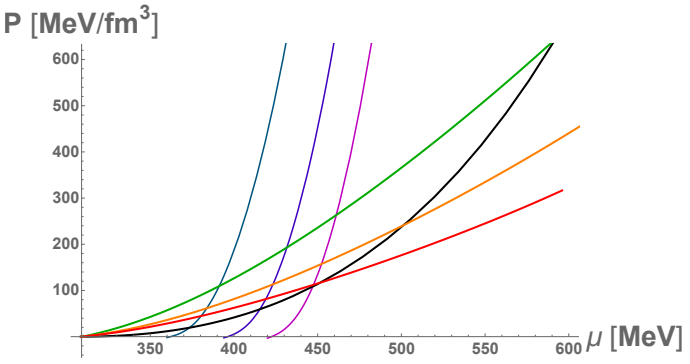

Figure 3.12: *Transition from nuclear to quark matter for the case of q=1.8. The Black line correspond to the case of a constant dilaton and the green, orange and red curves represent nuclear matter as in Fig 3.4. The dark teal curve corresponds to $\chi_0 = 360$ MeV, the purple curve corresponds to $\chi_0 = 395$ and the magenta curve corresponds to $\chi_0 = 420$.*

Bottom-Up D3/D7 with Running γ

We have seen that our bottom up models have a stiffer equation of state when the running anomalous dimension of the quarks is included. In fact, as we will see, only the stiffest models with $c_s^2 > 0.5$ are of any interest phenomenologically for neutron stars. Let us therefore begin by studying the case $q = 1.8$ which has the stiffest equation of state.

For $q = 1.8$ we must also pick the scale χ_0. Naively this is roughly 330 MeV (a third the proton mass) but if we make such a low choice the nuclear phase barely exists before the quark phase takes over. The naive relation to the proton mass though is only an estimate so we will allow ourselves to consider a range of test cases: $\chi_0 = 360, 395$ and 420 MeV. In Fig. 3.12 we show the pressure against chemical potential plots for these cases. The nuclear curves are also displayed so the position of the phase transitions can be read off. Note the transition to the quark phase are typically at lower scales than in the basic D3/D7 model since the pressure is larger.

It is instructive to see how stiff the quark matter is at the transition. In Fig. 3.13 we plot c_s^2 against μ separately for each of the nuclear equations of states. The black dotted lines show where the phase transitions occur. Clearly there is a distinct drop in c_s^2 as one moves to the quark phase in all these cases but the stiffness does then grow at higher μ. One might expect that the neutron star stability will decay when the core moves above the transition but that there might be a new class of stars with the denser cores reflecting the stiffness at higher μ.

We solve the TOV equations for these cases and display the mass vs radius curves in Fig 3.14. The results indeed fit our intuition. The stable neutron star branch ends in all cases when the transition to the quark matter occurs. The stiff area of the equation of state does kick in again though hinting at a new branch of smaller, lighter, hybrid stars with quark matter cores. The stable solutions are marked in red. We should also immediately caveat that such a disconnected branch of smaller stable stars might not be possible to produce in astrophysical processes. It is very plausible that in stellar collapses neutron stars would form; then when the mass grows enough to make them unstable, black holes would form with no obvious route to the smaller stable branch. On the other hand in the light of the expected new gravitational wave data it is interesting to find exotic predictions, in case there are surprising signals. Note that in our model in no case are there both quark core hybrid stars and neutron stars as massive as 2 solar masses. Nevertheless the solutions suggest that our EoS are closer than those in [73] to generating interesting phenomenology and perhaps with a further increase in stiffness of the EoS both could be realized.

It is interesting to understand the difference in composition of the traditional neutron stars and the new class of stable stars we are predicting here. In Figure 3.15 we plot the

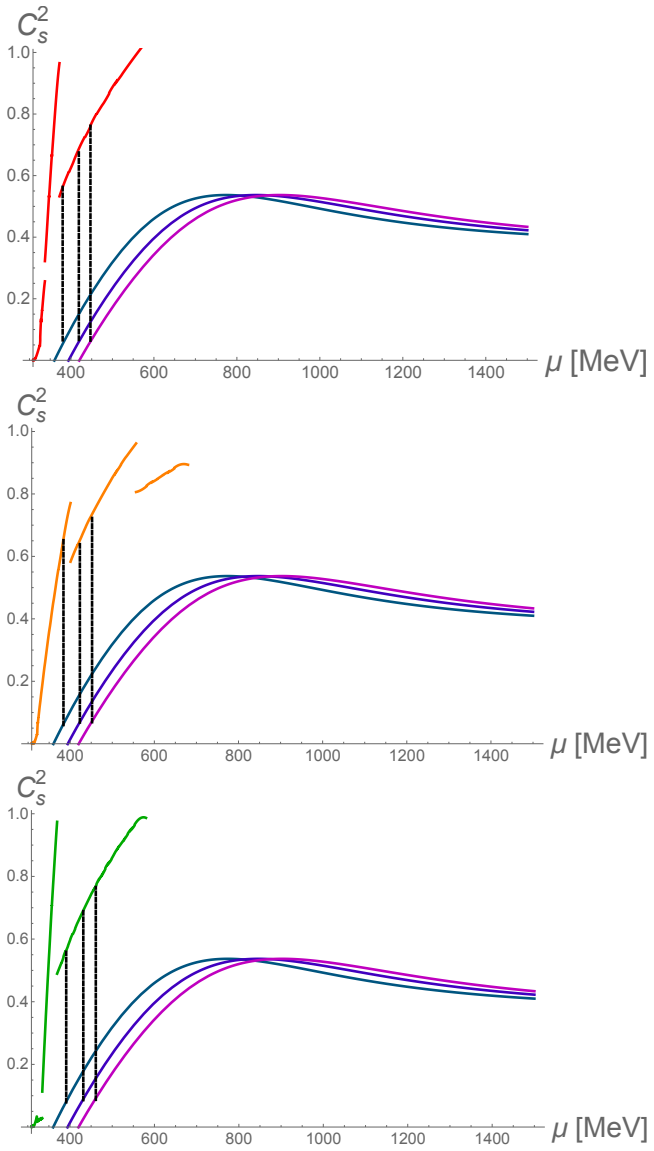

Figure 3.13: *Speed of sound squared (with $c = 1$) as a function of the chemical potential for the case of $q = 1.8$. Green, orange and red curves are those for the three nuclear EoS and the three quark matter curves are in dark teal for $\chi_0 = 360$ MeV, in purple for $\chi_0 = 395$ MeV, and in magenta for $\chi_0 = 420$ MeV. The transition from nuclear to quark matter is indicated with a black dashed line.*

pressure against radius in representative stars with the different phases distinguished. Note the neutron stars have very different central pressures for very similar radii reflecting the sharp rise in speed of sound/stiffness of the neutron equations of state needed to support 2 solar mass neutron stars. The novel hybrid stars are very much quark matter dominated and rely on a broader softer core for stability.

These results have been for the case $q = 1.8$ which has the stiffest EoS and highest peak speed of sound. Lower or higher q values have softer EoS and produce no new conclusions beyond the instability of the hybrid stars. We do not therefore present any analysis of those cases.

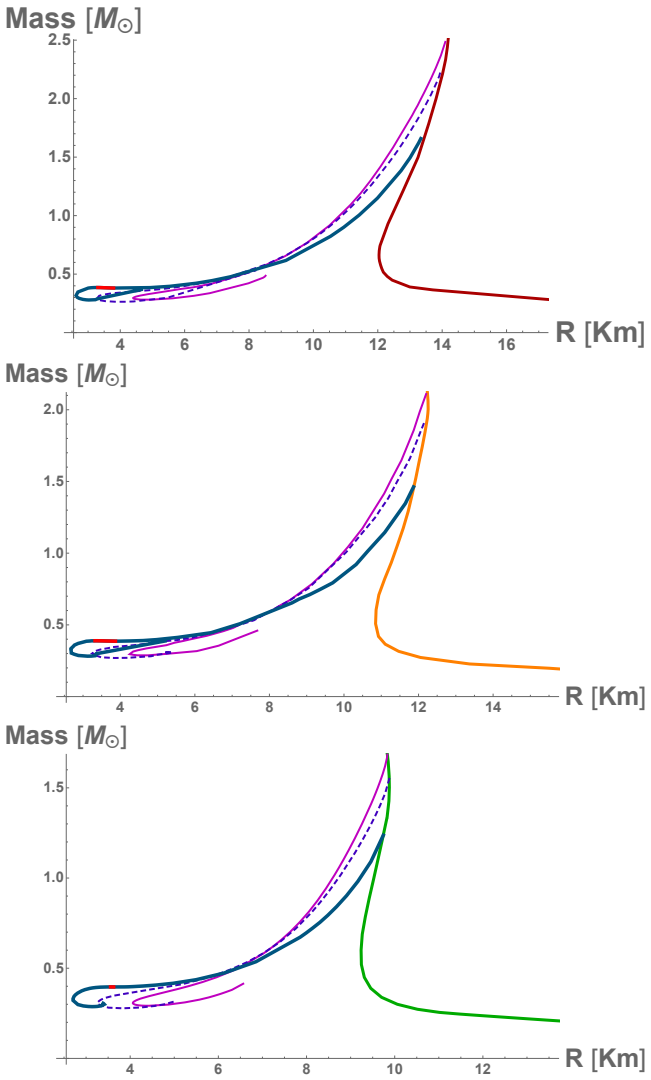

Figure 3.14: *Mass vs radius curves for the case of $q = 1.8$. The three curves leaving the green/red/orange nuclear EoS prediction are the three transitions to a quark phase from Figure 3.13. The small stable branch is indicated in red.*

The EoS in the improved holographic models are still not stiff enough to play a role in compact object phenomenology although the equations hint that they may be closer to a role than those proposed in [73] . This suggests further refinements may lead to interesting predictions.

3.3.2 Restoring Confinement

Our equations of state so far either don't support hybrid stars or are at odds with the 2 solar mass neutron star observations. This need not be the final conclusion though. We have modified the D3/D7 model (which in base form has neither confinement nor chiral symmetry breaking) to include chiral symmetry breaking. We have not though included confinement.

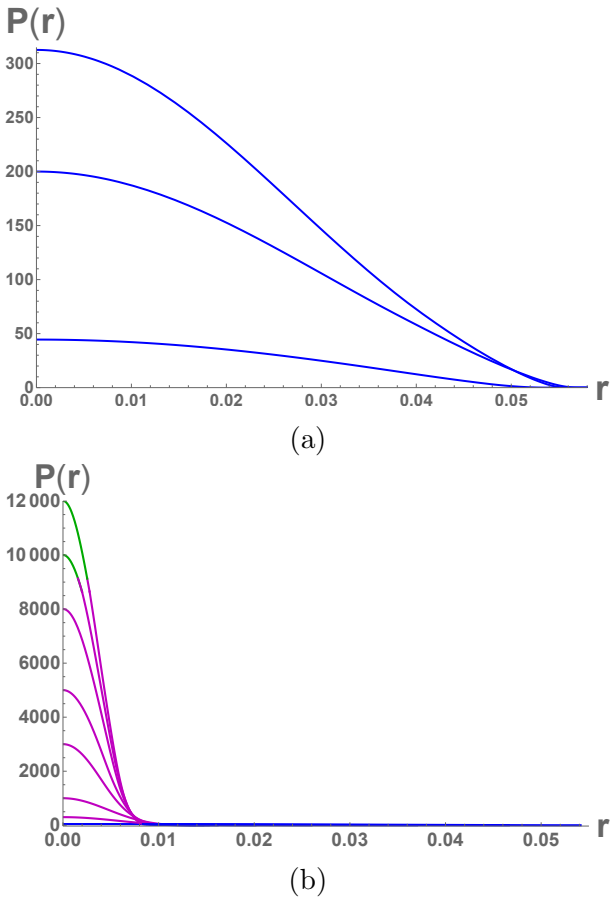

Figure 3.15: *Pressure as a function of the radial variable r. The radius of the Neutron star is the value of r at which P(r) vanishes. (a) Pressure for the case of stiff nuclear matter taken from reference [48] (b) Pressure for a hybrid star where the quark phase (the pink line corresponds to the massive chirally broken phase and the green line corresponds to the massless chirally symmetric phase) correspond to a value of q=1.8 and* $\chi_0 = 360MeV$. *Note the stable cases from Fig 3.14 lie where the chirally symmetric phase just enters at the centre and the speed of sound is highest (see Fig 3.9).*

A justification for this is that chiral symmetry breaking may well set in before confinement. The QCD coupling might run to a critical value for chiral symmetry breaking at which scale the quarks will become massive and decouple from the pure Yang Mills theory running. That running is very fast and starting at rather strong coupling and will very quickly reach any critical value for confinement in the pure glue theory so that confinement and chiral symmetry breaking are intimately linked and lie very close in scale. The D3/D7 system we have does not include this change in phase to confined though and so only describes the phases above the deconfinement transition fully.

The main impact of this omission is that we may be wrongly computing the vacuum energy of the $\mu = 0$ phase of QCD by a constant factor. Then we are placing the phase transitions in the wrong place. We have explored adding such a "bag constant" factor.

The subtraction of such a constant from the high energy phase free energy allows us to set χ_0 smaller than previously whilst maintaining a low density nuclear phase. We

can then move the region of μ where the high density phase has a large speed of sound closer to the transition point. Generically though we have not been able to maintain the neutron star branch of stable stars with ones with quark cores. The quark matter transition always leads to the neutron star branch being unstable (before a 2 solar mass neutron star is achieved). We can though make the novel hybrid stars we have seen more stable in this way. In Figure 3.16 we show an example of the most sympathetic case with a substantial hybrid star region.

3.4 Tidal Deformabilities

As we mentioned in subsection 1.4.4 of chapter 1, it is expected that in a colliding binary system of two neutron stars, the tidal forces between the two objects would have a measurable effect in the gravitational wave signal that could be observed using gravitational wave detectors. In [54] the measurement of this effect was reported as a limit given for the tidal deformabilities of the two stars involved in the merger.

The tidal deformability is related to the Love numbers of the stars and measures their susceptibility of being deformed by tidal forces. To calculate the tidal deformability for specific solutions of the TOV equations that represent a neutron star, we follow references [98, 99, 100].

We start with the solutions of equations (1.84): $m(r)$ and $p(r)$ for a fixed value of the initial condition for the system, which we call the central pressure P_c, then we can solve the system of equations (1.94) to find the radial function $H(r)$ of the spherical harmonics expansion, and then find $z_R = RH'(R)/H(R)$ which is evaluated at the radius R of the star.

With z_R we then can solve (1.93) and obtain the tidal deformability using equation (1.90). As a fixed value of the central pressure P_c gives a fixed value of the mass of the star we can obtain the tidal deformability as a function of the mass of the neutron star.

In fig. 3.17 we obtained the tidal deformability as a function of the mass for the quark matter phase showed in the bottom image of fig. 3.14, where a transition from soft nuclear matter to quark matter with $q = 1.8$ and $\chi_0 = 360$ MeV is presented. As we increase the central pressure in Fig. 3.17 (a) we see that the tidal deformabilty decreases as the mass increases, this happens as the star goes from larger radius and small mass to smaller radius and large mass in the mass vs radius curve. As we keep increasing the value of the central pressure we then reach a maximum value for the mass at $M = 1.24M_\odot$ where the transition to the quark phase happens. Then as we keep increasing P_c the values of the tidal deformability stars to grow as the mass decreases, as shown in fig. 3.17 (b). For smaller values of the mass, the tidal deformability starts

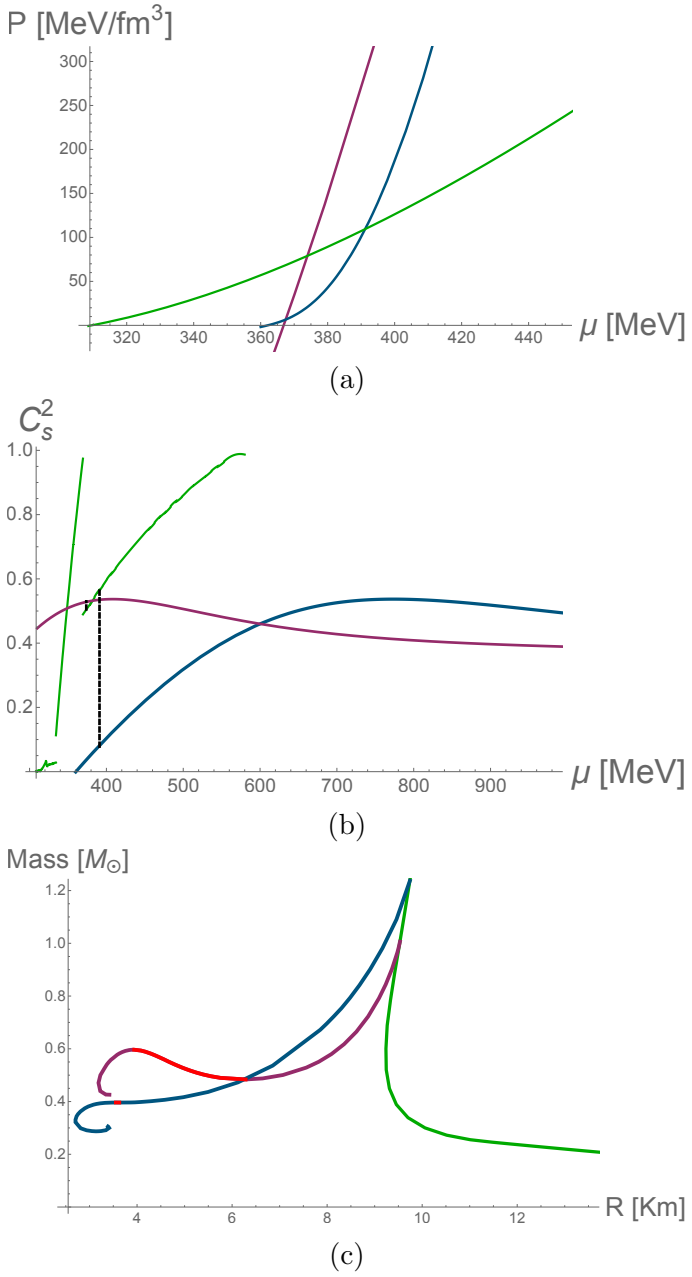

Figure 3.16: *(a) Pressure vs chemical potential for different phases. The nuclear phase (green) correspond to soft nuclear matter; the quark phases: (purple) correspond to a value of $q = 1.8$ and $\chi_0 = 190MeV$ and (dark teal) correspond to a value of q=1.8 and $\chi_0 = 360MeV$. (b) Comparison of the speed of sound squared in units with $c = 1$ as a function of the chemical potential for the same phases. We show with a black dashed line the point of transition between the nuclear phase and the quark phase. (c) Mass vs radius curve showing the same phases as above. The stable branches are indicated in red.*

to oscillate as it shows some points in which $\bar{\lambda}^{(\mathrm{tid})}$ grows unexpectedly and then decrease for a small difference in mass.

Now we would like to compare our results with the constraints in [54]. In order to do that we need to show how our exotic phases relate to the contours showed for the case of low-spin, which means we don't consider rotating stars. The curves are generated

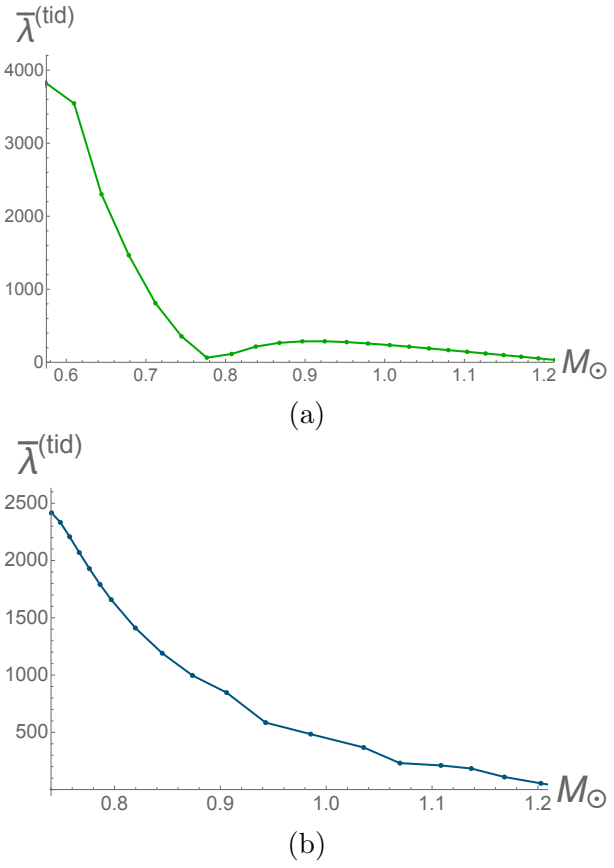

Figure 3.17: *The dimensionless tidal deformability as a function of mass (in units of solar masses) for a holographic quark, and nuclear equations of state (a) The nuclear phase (green) correspond to soft nuclear matter. (b) The quark phases (dark teal) correspond to a value of q=1.8 and* $\chi_0 = 360MeV$.

by independently determining the tidal deformabilities for each of the stars involved in the merger. To describe the binary system we need to consider the chirp mass, which is defined as:

$$\mathcal{M} = \frac{(m_1 m_2)^{3/5}}{(m_1 + m_2)^{1/5}} \tag{3.16}$$

where m_1 and m_2 are the masses of the components of the two body system. We can solve for m_1 in terms of m_2 for a fixed value of $\mathcal{M}$. Then we can vary m_2 as a parameter and use the relation we have of the tidal deformability with the mass of the star to obtain a relation between the tidal deformability of one of the two stars of the binary system with respect to the second one.

Nevertheless we are not able to obtain the tidal deformabilty contour for the event observed by LIGO and Virgo in [54] as the chirp mass of the event is $\mathcal{M} = 1.188 M_\odot$. This means that the the two stars involved in the binary Neutron Star merger correspond to masses $m_1 \in [1.36, 1.60] M_\odot$ and $m_2 \in [1.17, 1.36] M_\odot$ and our model for quark matter neutron stars don't support stable star solutions for such large masses currently.

3.5 Discussion

The existence of neutron stars up to and over 2 solar masses provides a challenge in our understanding of the QCD equation of state even within nuclear matter models. At the cores of these stars it seems the matter must be very stiff with speeds of sound close to the speed of light. Gravitational wave signals from colliding neutron star pairs are also beginning to constrain the EoS through measurements of the tidal deformability. It is therefore interesting to study the deconfined quark matter equations of state to see if they might play a role in the cores of neutron stars or generate other hybrid stars. This requires knowledge of and the ability to calculate in the strongly coupled yet deconfined section of the QCD phase diagram. There are no first principles tools that can be brought to bear, since the lattice can not compute at sizeable chemical potential. This motivates trying to use holography to explore possible descriptions of this regime in QCD.

The first holography paper addressing neutron star structure [73] used the exact results at finite μ for the D3/D7 dual system. That system though has conformal gauge dynamics and no chiral symmetry breaking unless introduced by a hard mass. It predicted a very soft equation of state that could not play a role in neutron star phenomenology. Our goal in the present chapter has been to adjust that model to include a running anomalous dimension for the quark condensate which introduces a dynamical chiral symmetry breaking mechanism. Such theories suggest a massive deconfined phase with deconfined quarks yet chiral symmetry breaking before moving to the chirally restored high density phase. We have shown that this leads to a stiffer equation of state in the relevant intermediate μ phase and that the speed of sound has the required rise and fall (see the non-monotonicity in Figure 3.9) in this regime.

We have used the TOV equations to model compact stars using our EoS varying the IR quark mass. The instability of the neutron star branch remains but in some case we do see the formation of novel hybrid stars with quark matter cores. The models points therefore at twin stars; two classes of 0.4 solar mass object with very different radii. Naively one supposes that these stars will not be produced in astrophysical processes but they are a possible exotic signature in gravitational wave data. Our model does not produce a sufficiently high speed of sound in the material to allow both 2 solar mass neutron stars and hybrids to exist together although the EoS are clearly close to realizing this. They also do not support a branch of solutions beyond the standard neutron star branch that link continuously to neutron stars. Nevertheless, we view the work presented in this chapter as the next step beyond [73] towards a full model.

In the next chapter we change this model by including a mass term for the scalar field by hand that will enable us to include the running anomalous dimension of the quark condensate γ. As we will see, this change will provide us with a more stiff kind of EoS. We will also include a phase of colour superconductivity for larger densities.

Chapter 4

Stiff Holographic Equations of State, Colour Superconductivity and Compact Stars

4.1 Introduction

There is a growing literature [2, 73, 79, 80, 81, 89, 101] attempting to use holography to describe the equation of state of deconfined quark matter to determine whether it can play a role in neutron star cores. In the first such paper [73] the exact results at finite density for the D3/probe D7 system, which is dual to quark multiplets in a supersymmetric theory, were applied in this context. The resulting EoS was not stiff enough to support quark cores in neutron stars. In the previous chapter 3 we adapted this system to a model that included a running anomalous dimension for the quark condensate through an effective dilaton profile, allowing a description of the chiral transition. The transition occurs when the BF bound is violated for a scalar in the bulk dual to the chiral condensate. We parameterized the running of γ so we could control the derivative of the running at the BF bound violation point. For all choices of the derivative the model displayed a second order transition from the chirally broken phase to the chirally symmetric phase as μ increased. Generically the EoS stiffen relative to the pure D3/D7 case with the speed of sound squared in the material peaking, dependent on the chosen derivative, at 0.55 (in units where $c = 1$) for chemical potentials of order the chiral restoration point. Even this was not sufficient to convincingly support large mass neutron stars.

In this chapter we present a related model in which the chirally broken phase resists transition to the chirally restored phase leading to a first order chiral transition. Prior to the transition, the EoS is even stiffer than our previous examples, with a speed of sound rising close to the speed of light. The key extra ingredient relative to the previous

chapter is that we have allowed a discontinuity in the holographic description at the scale of the IR constituent quark mass, where one might expect the quarks to be integrated out of the running dynamics of the gauge fields. This seems rather natural and it is interesting that our first sensible attempt has led to a very different transition and a much stiffer material.

The model is based on the Dirac-Born-Infeld action of a $D7$-brane in AdS_5 with a scalar field describing the chiral condensate and a $U(1)$ gauge field for the chemical potential. In the spirit of the model in [102] we then include a mass term for the scalar by hand that allows us to include the running anomalous dimension of the quark condensate, γ. We input this form from the perturbative QCD running result for γ allowing it to naively extend to the non-perturbative regime. When the scalar mass passes through the Breitenlohner-Freedman bound a chiral condensate is induced. This philosophy has been used before to successfully describe the $T = \mu = 0$ theory and strongly coupled theories beyond the Standard Model. Previously such models have been able to dodge the question of the deep Infra Red physics, below where the quarks become on mass shell as a result of the formation of their constituent mass. Here at finite μ an explicit description is needed for the IR regime. We propose a simple completion where the anomalous dimension is switched off in this regime and sensible physics results.

This model does not explicitly include confinement. The philosophy is that confinement is a property of the pure Yang Mills theory at scales below the IR constituent quark mass and whilst implied in the model is not directly included. We assume that as soon as quark density switches on confinement is lost in the plasma. We find such a phase with quark density and chiral symmetry breaking. We refer to this phase as a massive deconfined quark phase.

Here we do not attempt to describe the nuclear physics phase of QCD, but instead, as in the previous chapter, we take results from the nuclear physics/neutron star literature that provide three possible varying stiffness EoS for the nuclear phase. Above 308 MeV this phase takes over from the vacuum of the holographic theory yet at higher density the chirally broken quark phase returns to be the true vacuum. Then, the first order transition to the chirally symmetric phase occurs and the stiffness of the EoS falls off sharply. Solving the TOV equations for equilibrium neutron stars we do find stable solutions with deconfined yet massive quarks in the core. This is our first successful result.

The second task we undertake is to include a holographic description of a possible colour superconducting state above the first order chiral restoration transition. Traditionally the holography community has declared describing colour superconductivity as very hard because the naive coloured bi-quark condensate qq is not gauge invariant and suppressed at large N [60]. One would need to describe the breaking of the colour group and this remains a tricky issue. However, in Chapter 2 we proposed to be more cavalier at a

phenomenological level and simply allow the inclusion of gauge non-invariant operators and neglect their colour symmetry breaking effects in the dynamics, since the coloured density of quarks and monopoles (associated with confinement) are already likely to have given Debye masses to the gluons before the Cooper pairs form. In this spirit we include a new scalar field dual to the Cooper Pair in analogy to the scalar describing the chiral condensate. Since the Cooper pair carries net baryon charge it couples directly to the $U(1)$ gauge field and the chemical potential itself generates a BF bound violation that can trigger a superconducting phase. We look at the effects for the core of neutron stars including the colour superconducting phase.

This chapter is organized in the following way: in Section 4.2 we will review the different possible phases relevant to neutron stars: a confined phase of neutron starts which is modelled with an EoS that comes from a chiral effective field theory and a piece-wise polytropic extension towards higher values of density; the base D3/D7 work used in [73]; a bottom-up D3/D7 brane intersection model with a chiral symmetry breaking mechanism and a colour superconducting phase. In Section 4.3 we solve the TOV equations and analyse the mass-radius relations of neutron stars using the models of the previous section. We mention the tidal deformabilities of a binary neutron star system, and how the results fit with current observations made by LIGO/Virgo in Section 4.4. We summarise in Section 4.5.

4.2 Descriptions of QCD Phases with μ

In this section we will work through the descriptions we use for the $\mu = 0$ chirally broken vacuum, the nuclear physics phase, a deconfined massive quark phase and a high density chirally restored phase with colour superconductivity. All of these descriptions are holographic except for the nuclear phase. Since our holographic models are inspired by the D3/probe D7 model we review that briefly first.

4.2.1 A review of the base D3/D7 probe model

This is the same model mentioned in subsection 3.2.2, in "The Basic D3/D7 Model" part, where the base model is $\mathcal{N} = 2$ SYM with the matter content of $\mathcal{N} = 4$ $SU(N)$ SYM in the adjoint sector and N_f matter hypermultiplet in the fundamental representation. The DBI action for a probe D7 brane in pure AdS, with a constant dilaton, is given by

$$S = -\frac{N_f N_c}{\lambda} T_{D7} V_3 \int d\rho \rho^3 \sqrt{1 + (\partial_\rho \chi)^2 - 2\pi\alpha'(\partial_\rho A_t)^2} \tag{4.1}$$

where λ is the 'tHooft coupling, $T_{D7} = (2\pi)^{-7}\alpha'^{-4}$ is the D7 brane tension, $V_3 = 2\pi^2$ is the volume of the S^3 on the D7 brane and ρ the radial direction in AdS_5. $\chi(\rho)$, the

brane embedding function, is holographically dual to the quark mass and condensate and A_t is a gauge field dual to the quark number chemical potential and density. In practice we work with the action

$$S = -\int d\rho\ \rho^3 \sqrt{1 + (\partial_\rho \chi)^2 - (\partial_\rho A_t)^2} \tag{4.2}$$

and then we rescale by $\frac{4NN_f}{\eta 12\pi^2}$ choosing $\lambda = 2^4\pi^2/3\eta$ (where $\eta = \left(\frac{1}{6}B\left(\frac{1}{6},\frac{1}{3}\right)\right)^{-3} \approx 0.363$) to match the asymptotic UV form known from QCD (3.4). We will use $N_f = N = 3$.

At any non-zero T this theory is deconfined. Therefore this phase is a description of a vacuum with a density of quarks of mass m. This mass though must be put in by hand and there is no chiral symmetry breaking mechanism.

The EoS, which relates the pressure P to the energy density $\mathcal{E}$ is found from equations (3.5). Here the pressure is too small and the quark interiors of stars can not support neutron stars (see [73]).

4.2.2 The $\mu = 0$ chiral symmetry breaking phase

Our base motivation here is to include the running of the gauge coupling and chiral symmetry breaking to see if the EoS stiffens. In Chapter 3 we added the running as a ρ dependent dilaton prefactor to the action (4.1). As mentioned before the crucial role of the dilaton is that it provides a running anomalous dimension for the quark bilinear operator which displays as a ρ dependent mass for the field L (after expanding the dilaton). In the previous chapter we used a set of functions that ran from $\gamma = 0$ in the UV through the critical $\gamma = 1$ in the IR (with varying derivative at this point) which indeed triggered chiral symmetry breaking. These models all showed a second order transition from the chirally broken to the chirally symmetric phase. We found the EoS stiffened around the transition so that the speed of sound became as large as 0.55 yet this was still not stiff enough to support neutron stars of mass higher than 0.4 solar mass.

Here we will take what appears only a slightly different approach, which is to not introduce running through a dilaton factor but directly through a ρ dependent mass term for χ. This approach has been taken previously in [103]. Our original motivation for this was that we wanted to add a field for a colour superconducting order parameter in sympathy with χ but we didn't want that field to experience the same running as χ which an overall dilaton factor would introduce. We will see that this ansatz can lead to a yet stiffer EoS. Thus we take the Lagrangian

$$\mathcal{L} = -\rho^3 \sqrt{1 + (\partial_\rho \chi)^2} - \rho \Delta m^2\ \chi^2 \tag{4.3}$$

If we write the additional mass term Δm^2 purely as a function of ρ then, were this term lead to a violation of the BF bound in some range of small ρ, the instability would exist however large χ were to grow. Therefore we identify the RG scale in this term with $\sqrt{\rho^2+\chi^2}$ (this naturally happens in the D7 probe action where this quantity is the radial distance in the background space).

When $\Delta m^2 = 0$, near the boundary which corresponds to the UV, the solution is given asymptotically by $\chi(\rho) = m + c/\rho^2$, with $c = \langle \bar{q}q \rangle$ of dimension three and m, the mass, of dimension one (note χ and ρ have dimension one). For non-zero Δm^2, the solution takes the form $L(\rho) = m\rho^{-\gamma} + c\rho^{\gamma-2}$, with

$$\Delta m^2 = \gamma(\gamma - 2) \tag{4.4}$$

Here γ is precisely the anomalous dimension of the quark mass. The BF bound below which an instability occurs is given by $\Delta m^2 = -1$ when $\gamma = 1$. It is simplest to feed in ones desired running of γ at the level of the equation of motion.

We will fix the functional form of Δm^2 using the two loop running of the gauge coupling in QCD with $N_f = 3$ flavours transforming in the fundamental representation. This is found by solving:

$$\begin{aligned} Q\frac{d\alpha}{dQ} &= -b_0\alpha^2 - b_1\alpha^3 \\ b_0 &= \frac{1}{6\pi}\left(11N_c - 2N_F\right) \\ b_1 &= \frac{1}{24\pi^2}\left(34N_c^2 - 10N_cN_f - 3\frac{N_c^2-1}{N_c}N_F\right) \end{aligned} \tag{4.5}$$

The one loop result for the anomalous dimension of the quark mass is

$$\gamma_1 = \frac{3C_2}{2\pi}\alpha, \quad C_2 = \frac{\left(N_c^2-1\right)}{2N_c} \tag{4.6}$$

We stress that using the perturbative result outside the perturbative regime is a sensible but non rigorous, phenomenological parametrization of the running.

We will identify the RG scale, Q with the AdS radial parameter $\sqrt{\rho^2+\chi^2}$ in our model. Working perturbatively from the AdS result $m^2 = \Delta(\Delta - 4)$ we have

$$\Delta m^2 = -2\gamma_1 = -\frac{3\left(N_c^2-1\right)}{2N_c\pi}\alpha \tag{4.7}$$

To find numerical solutions for the vacuum configuration of χ, we need an IR boundary condition. In top down models $\chi'(0) = 0$ is the condition for a regular solution [36]. In previous references using this model this condition has been replaced by the very similar on mass shell condition $\chi\left(\rho = \chi_0\right) = \chi_0$ with $\chi'\left(\chi_0\right) = 0$. Here χ_0 is the IR value of the

quark mass where the on-shell condition $\rho = \chi$ is realized. Thus one shoots out from the identity line in the $\chi - \rho$ plane to find the value of χ_0 that gives the desired quark mass at some UV value; here we will require that the mass vanishes in the UV. The resulting solution for χ is shown in red in Figure 4.1 .

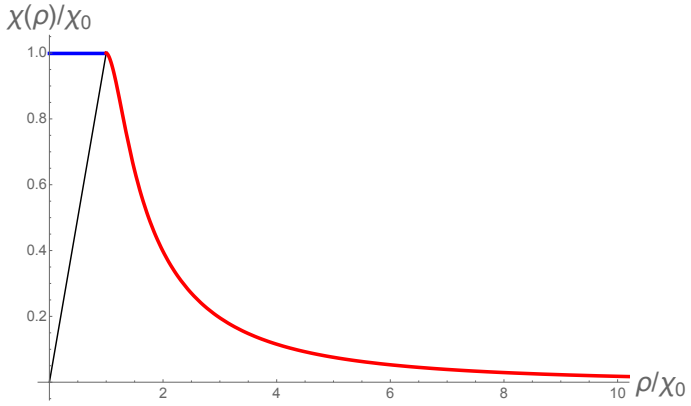

Figure 4.1: *Solution for $d = 0$. The blue curve is the solution in the interior with $\Delta m^2 \equiv 0$, and the red line is the solution in the exterior.*

In previous studies this has been sufficient; bound states masses can be determined by looking at fluctuations of this solution. Now, however, we wish to compute the action of this configuration. There are two complications. First, since we imposed Δm^2 at the level of the equations of motion we have neglected one term dependent on the derivative of Δm^2 in the equation of motion so it is inconsistent to then use Δm^2 directly in the action. Here though, this is considered a small error since Δm^2 only has a large derivative in a very small region of ρ and we will neglect this error.

The second problem is that we have no solution below $\rho = \chi_0$, yet the chirally symmetric solution $\chi = 0$, which we will want to compare the action of our solution to, extends all the way to $\rho = 0$. This problem will become worse below when we allow solutions with density where one expects the solution for χ to "spike" to the origin of the $\chi - \rho$ plane. With the current boundary conditions we will lose all of this part of the solution. Our resolution of this issue here is a little adhoc but based on simply obtaining sensible looking solutions in the region interior to the identity line. We will set $\Delta m^2 = 0$ in the region $\chi^2 + \rho^2 < \chi_0^2$. The solutions of the equations of motion are then just those of the base D3/D7 probe system. Thus for example at $d = 0$ they are the solutions $\chi = m$. We will require the solution to match (χ and χ') to our exterior solution on the $\chi^2 + \rho^2 = \chi_0^2$ circle. Thus we extend the solution in Figure 4.1 with the blue solution shown into the IR region. These solutions are now a sensible approximation to the forms found for χ in complete D3/D7 models with chiral symmetry breaking.

Even now there remains an ambiguity as to the constant prefactor between our UV and IR action pieces. We will keep this ambiguity as a multiplier k_{IR} on the IR action. In the philosophy of this modelling we assume that chiral symmetry breaking occurs at a higher RG scale than confinement. Below χ_0 the quarks should integrate out from the

dynamics leaving the pure glue theory to provide confinement. Since we don't include this dynamics our IR action is likely out by a constant factor. The constant k_{IR} choice is one way to try to include this factor in the dynamics.

Thus the solution for χ in Figure 4.1 is our description of the $\mu = 0$ vacuum of the QCD. We will use the action of this configuration to set our zero of potential energy. In fact this state will persist until quark density switches on at $\mu = \chi_0$ (a scale that is naturally of order 330 MeV in QCD as it is one third of the proton mass). However, before that point we must allow for a density of nucleons to begin.

4.2.3 Nuclear phase

As mentioned in the previous chapter in subsection 3.2.1, at small chemical potentials the nuclear transition in QCD goes as follows: the confined, chirally broken vacuum is empty until a chemical potential of $\mu = 308.55$ MeV when there is a first order phase transition to nuclear matter. The nuclear matter EoS has been explored in [48], where the authors combined observations of a 1.97 solar mass neutron star with effective field theory (EFT) to construct the EoS, extrapolating with a constrained piecewise polytropic form. Here again we will use the results of [48] to model the nuclear phase.

Three ansatz for the EoS (soft, medium and stiff) are presented in Table 5 of [48]; they give the energy density and pressure for different densities. We have encoded their data as a numerical fitting polynomial for the analysis in the following sections and we show these in Fig. 3.2.

4.2.4 The dense quark phase

We next consider the transition to a $d \neq 0$ quark phase in our holographic model. We allow for a quark density by including a $U(1)$ gauge field A in the action

$$\mathcal{L} = -\rho^3\sqrt{1 + (\partial_\rho\chi)^2 - (\partial_\rho A_t)^2} - \rho\Delta m^2\ \chi^2 \tag{4.8}$$

Here A_t has UV asymptotic solution $\mu + d/\rho^2$. where d is the density. We apply a Legendre transformation to obtain the action in terms of the density d

$$\tilde{\mathcal{L}} = -\sqrt{(1 + \chi'^2)\,(\rho^6 + d)} - \rho\chi^2\Delta m^2 \tag{4.9}$$

Then the equations of motion are:

$$\partial_\rho\left[\frac{(\rho^6 + d)\,\partial_\rho\chi}{\sqrt{(1 + \chi'^2)\,(\rho^6 + d)}}\right] - \rho\Delta m^2\chi = 0 \tag{4.10}$$

$$(\partial_\rho A_t)^2 = \frac{d^2\left(1+\chi'^2\right)}{(\rho^6+d)} \tag{4.11}$$

Note in the first equation we have again suppressed the term $\rho\chi^2\frac{\partial}{\partial L}\Delta m^2$.

We solve the equations of motion in two steps at each value of d. We divide the space using the IR value of the quark mass at $d=0$, χ_0. We obtain solutions $\chi(\rho)$ and $A_t(\rho)$ in two intervals: first for $0 \leq \sqrt{\rho^2+\chi^2} \leq \chi_0$, which we call the interior part and the other $\chi_0 \leq \sqrt{\rho^2+\chi^2} \leq \Lambda$, with Λ a large UV cut off, which we call the exterior part.

In the interior part we fixed Δm^2 to zero. For a given d we shoot from the origin of the $\chi-\rho$ plane with different gradients for χ. We solve until we reach the surface $\chi^2+\rho^2=\chi_0^2$ when we read off χ and χ' plus A_t. External to the circle we use the running Δm^2 from the QCD perturbative running and match the initial conditions provided from the interior on the circle. We then seek amongst those solutions the one that shoots to a zero UV quark mass. Then in the UV we can read off the value of the chemical potential from the A_t solution. We repeat this for each value of d.

The results are shown in Figure 4.2. The chirally broken phase exhibits a second order transition where density switches on. This behaviour is controlled by the low ρ phase with $\Delta m^2=0$. It is just the transition of the $\mathcal{N}=2$ model where a spike grows from the origin of the $\rho-\chi$ plane connecting to the flat embedding. The exterior region (in red) plays no role initially. As d increases the model resists returning towards the $\chi=0$ chirally symmetric phase with the maximum value of χ even increasing.

After $d=0.554\chi_0^3$ there are no non-trivial solutions that have a zero UV mass so for values of d higher than this a transformation to the chiral symmetry restored phase must occur (this puts some constraints on the parameter k_{IR} as we will see).

We compute the Free Energy as a function of the chemical potential by obtaining the on-shell action for each value of d. The integration follows the same separation in the interior and exterior regions over the values of ρ. One must be careful when splitting into sub-regions that any counter term is the same for each computation. We normalize so that $F=0$ for the $d=0$ embedding as previously discussed.

We show some examples for various k_{IR} in Figure 4.3. For $k_{IR}=1,2$ the system does not make sense. The chirally broken state ceases to exist before it stops being the true vacuum. On the other hand for $k_{IR}=0.575$ the system is more sensible since the chirally restored vacuum becomes preferred and the chirally broken state becomes metastable before it cease to exist. This provides a sensible description of a first order chiral restoration transition. We also show the case $k_{IR}=0.1$ where the transition occurs at lower μ.

Our expectation is that in the sensible systems the chirally broken phase is rather stiff. It is resisting the transition to the chirally restored phase. A good test of this is to

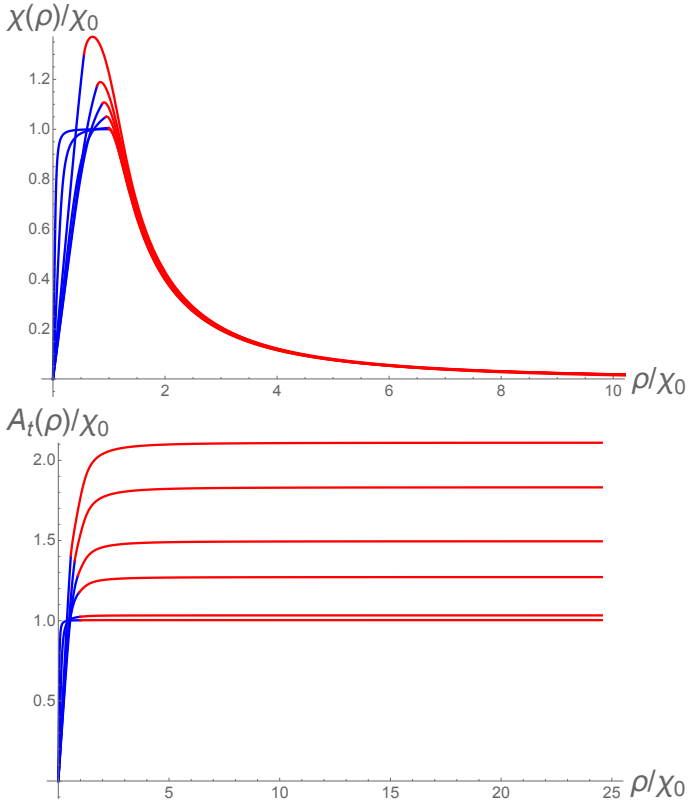

Figure 4.2: *Solutions for equations (4.10) with* $d = 0.00147\chi_0^3$, $0.0147\chi_0^3$, $0.147\chi_0^3$, $0.295\chi_0^3$, $0.488\chi_0^3$ *and* $0.554\chi_0^3$ *from bottom to top. The blue curves are the solutions in the region* $0 \leq \sqrt{\rho^2+\chi^2} \leq \chi_0$*, and the red curves the solutions in the region* $\chi_0 \leq \sqrt{\rho^2+\chi^2} \leq \Lambda$.

determine the speed of sound squared, which we can see in Figure 4.4 in units where $c = 1$. We show the results for the four values of k_{IR} in Figure 4.3 and also for the chirally symmetric phase $\chi = 0$ (dotted line). We plot for values of μ above the transition where density switches on. The speed of sound in the chirally symmetric phase rises to $1/3$ at asymptotically large μ. The speed of sound in the chirally broken phase though rises much higher and even passes through 1. Note that for the cases of $k_{IR} = 1, 2$ again the speed of sound has rather strange behaviour including a turning point; this suggests again that these choices of k_{IR} do not make physical sense.

The cases with $k_{IR} = 0.1 - 0.575$ have a monotonic rising behaviour. For the moment we will not address the issue of the speed of sound being greater than one for some values of μ, but will return to address this issue when we add a colour superconducting condensate to the chirally restored phase.

We can next set $\chi_0 = 330$MeV and compare the free energy of these phases to the nuclear phases' free energy. We do this in Figure 4.5 (top) showing the cases $k_{IR} = 0.1, 0.35$ and 0.575. The transition to the nuclear phase occurs at 308 MeV. At 330 MeV the deconfined massive quark phase's pressure begins to rise. The $k_{IR} = 0.575$ curve rapidly becomes the true vacuum relative to even the least stiff nuclear phase. The case $k_{IR} = 0.1$ only becomes the true vacuum relative to the stiffest nuclear equation of state. For

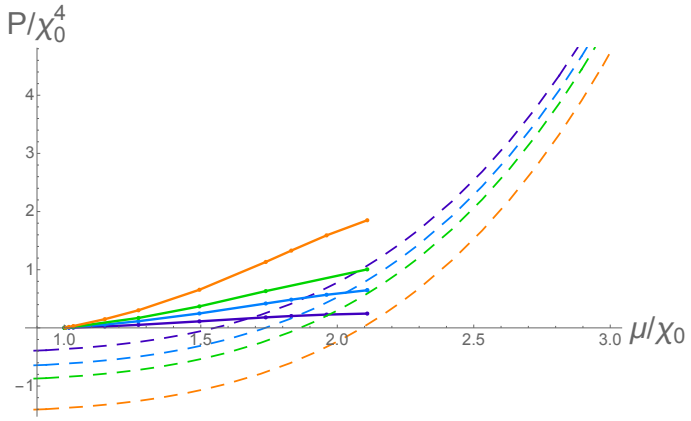

Figure 4.3: *Pressure versus chemical potential. The solid line corresponds to the massive chirally broken phase, and the dashed line represent the chirally restored phase. The different colours represent different values of* k_{IR}*;* $k_{IR} = 0.1$ *(purple),* $k_{IR} = 0.575$ *(blue),* $k_{IR} = 1$ *(green) and* $k_{IR} = 2$ *(orange).*

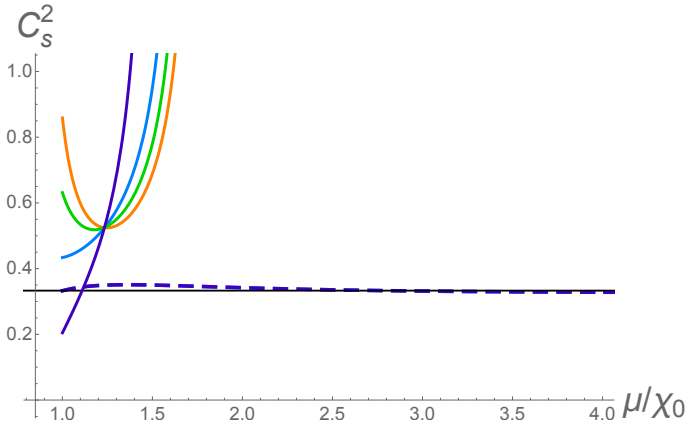

Figure 4.4: *The speed of sound as a function of* μ *for the Figure 4.3 solutions. Solid lines corresponds to the massive chirally broken phase, and the superposed dashed lines represent the chirally restored phase. The different colours represent different values of* k_{IR}*;* $k_{IR} = 0.1$ *(purple),* $k_{IR} = 0.575$ *(blue),* $k_{IR} = 1$ *(green) and* $k_{IR} = 2$ *(orange).*

intermediate k_{IR} one can achieve curves between these limits, for example $k_{IR} = 0.35$ grows to dominate the medium and stiffest nuclear curves but does not replace the soft nuclear curve.

In the bottom plot in Figure 4.5 we show the speed of sound's variation with respect to μ for the case of the soft nuclear EoS (the EoS is piecewise constructed so there are discontinuities, we just quote these from [48]) and the $k_{IR} = 0.575$ case for the chirally broken and chirally symmetric vacua. The vertical dotted lines show where the phase transitions between phases occur. For the moment we allow c_s^2 to rise above one before the final transition to the chirally restored phase. In the next section we will show that by modifying the chirally restored phase by including a colour superconducting condensate the transition away from the deconfined massive quark phase can occur earlier removing the region with $c_s^2 > 1$.

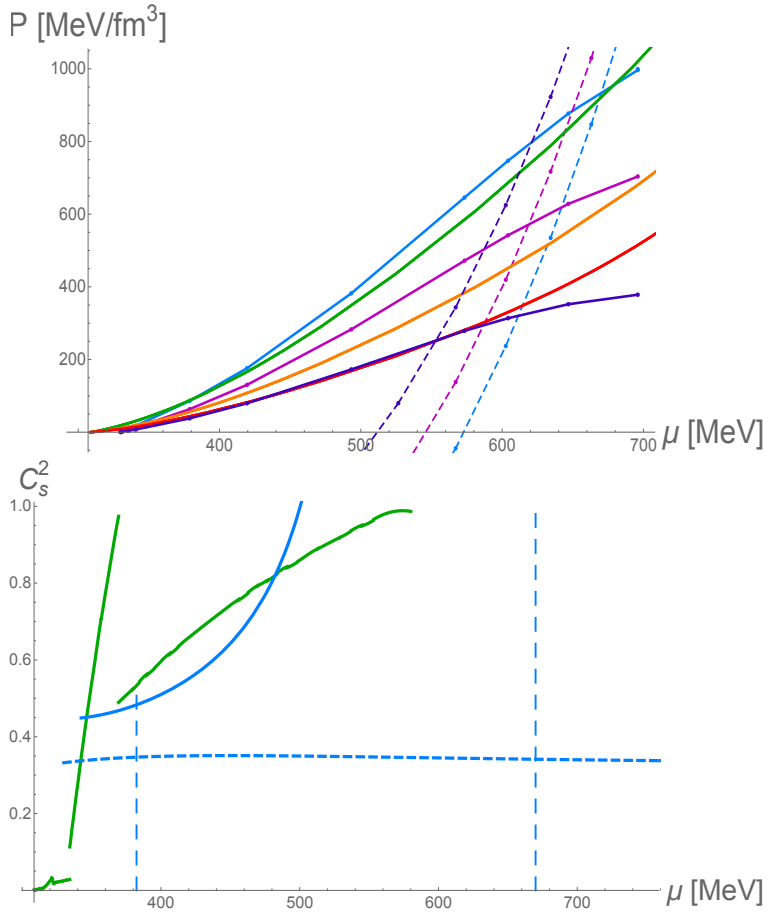

Figure 4.5: *Transitions from the nuclear phase to the deconfined phase. In the top image solid lines corresponds to the massive chirally broken phase and dashed lines represent the chirally restored phase, with $k_{IR} = 0.575$ (blue),$k_{IR} = 0.35$ (magenta) and with $k_{IR} = 0.1$ (purple). In the bottom image we show the speed of sound vs μ (with $c = 1$). The dashed vertical lines represent the transition from nuclear to chirally broken quark matter and from chirally broken quark matter to the chirally restored phase.*

4.2.5 Colour superconducting phases

There has been considerable speculation in recent years that there may be a colour superconducting phase of high density QCD. As we mentioned in Chapter 2, in the presence of a Fermi surface and any attractive interaction the formation of a di-quark condensate is expected. In the two flavour theory the spinless condensate is in the fundamental representation of colour $SU(3)$ and a single coloured qq bilinear condenses. In the three flavour theory a colour flavour locking (CFL) state is expected to form with three qq bilinears non-zero.

Holographically it has been shown that the presence of a chemical potential through a dual gauge field A_t causes a charged scalar's mass to be driven through the BF bound and cause condensation [104, 61]. Thus baryon number charged operators such as the qq bilinears would be expected to condense. The holographic dual is formally a description of gauge invariant operators and so it has proven hard to describe superconducting

operators which are colour charged and should break the gauge group. However, in Chapter 2 we proposed that phenomenologically one can be more relaxed about this constraint.

In a quark gluon plasma near a confining region of the phase diagram one expects a plasma of quarks but also potentially a plasma of charged magnetic monopoles that will play a part in the confinement mechanism. If these are present then the electric and magnetic gluon fields will all already have a Debye mass and the gauged nature of colour will be blurred. We proposed to simple neglect the back reaction of the coloured condensates on the gluons but use holography to describe the condensation mechanism and to compute the vacuum energy. In this spirit we will include the superconducting phase into our holographic model for compact stars.

We will describe each condensing qq operator by a scalar field ψ_i that we introduce into the holographic model in analogy to the chiral condensate field χ (both are dimension 3 scalars). In addition though because the qq operator carries baryon number it will couple directly to the baryon number $U(1)$ gauge field in the bulk. Thus we propose the action

$$\begin{aligned} \mathcal{L} &= -\rho^3\sqrt{1+(\partial_\rho\chi)^2-(\partial_\rho A_t)^2}-\rho^3 g_{\rho\rho}\textstyle\sum_i(D\psi_i)^2-\rho\Delta m^2\chi^2 \\ D_\mu &= \partial_\mu - iG[\rho]BA_\mu \end{aligned} \tag{4.12}$$

We have tested actions where ψ_i enter the square root term, but have not been able to make them give sensible profiles for ψ_i particularly because in the deep IR the square root approaches zero. Here, the action for ψ_i is the kinetic term emerging from the DBI action in the expansion where all fields are small and with the derivative promoted to a covariant derivative. This is intended in the same spirit as Δm^2 is added, in being the leading term for χ when aspects of the metric or dilaton contribute to its running anomalous dimension γ.

B is the baryon number charge of the qq bilinear (which we set to 2). The final issue is that we must match the coupling strength, G,of the $U(1)$ gauge field. In principle one should match this as the coupling runs from the perturbative regime but it may not be appropriate to just use the one loop running for $\alpha(\rho)$. In addition to that running one also expects this coupling to run logarithmically as one approaches the Fermi surface (see [18, 20, 21] for example). This could, at larger μ change the coupling further. We will therefore take G to have the form

$$G^2 = \kappa\ \alpha(\ln\rho) \tag{4.13}$$

where κ is a free parameter we will vary.

We do not expect both χ and ψ to condense together. For example Lagrangian terms we could include such as $|\phi|^2|\psi|^2$ would tend to fight against any BF bound violation for one field if the other field condenses. We will therefore just concentrate on Cooper pair formation in the chirally symmetric $\chi = 0$ phase to see how its presence effects that phase.

The equations of motion are

$$\begin{aligned} \partial_\rho(\rho^3\partial_\rho\psi_i) + \tfrac{G^2B^2}{\rho}A_t^2\psi_i &= 0 \\ \partial_\rho\left(\tfrac{\rho^3\partial_\rho A_t}{\sqrt{1-(\partial_\rho A_t)^2}}\right) - \textstyle\sum_i \tfrac{G^2B^2}{\rho}\psi_i^2 A_t &= 0 \end{aligned} \tag{4.14}$$

We solve the equations between a large UV cut off where $\psi_i \sim J + O/\rho^2$ with J a source and O the Cooper pair vev, and the IR scale $\sqrt{2}\chi_0$ where the running has becomes strong enough to cause χ condensation at $\mu = 0$. Now we need suitable IR boundary conditions. It is not clear what to pick although any none extreme choice give similar behaviour. We pick $\psi_i' = -\psi_i/\chi_0$ which has the same proportionality as the usual holographic superconducting case where the embedding ends on a black hole. Thus we can now set $\psi(\sqrt{2}\chi_0)$ to find solutions that asymptote to $J = 0$.

For A_t, we use the $\mathcal{N} = 2$ theory A_t at $\chi = 0$ for various d and use the values of the solutions at $\rho = \sqrt{2}\chi_0$ to set boundary conditions for A_t externally.

The proof of this construction is in whether we obtain sensible phenomenology for the Cooper pair formation.

In Figure 4.6 we plot some example embeddings for $\kappa = 1$ and varying μ. We indeed find profiles that asymptote to $J = 0$ at each μ and where the gap size grows with μ. We plot O against μ for varying κ in Figure 4.7. Now we can see that there is a second order transition to the colour superconducting phase with respect to μ. For $\kappa = 1$ the condensate only switches on close to $\mu \simeq 1.3\chi_0$. As μ increases in all cases the condensate grows in rough proportion to μ.

We plot the pressure (minus the free energy) of the solutions in Figure 4.8. Here we will consider the case with only one ψ_i corresponding to a two flavour colour superconducting phase. We see that the pressure of the phase is raised depending on the size of κ. We will adjust κ to move the transition to the deconfined phase (now with colour superconductivity) of Figure 4.5 to the left so that the speed of sound in the deconfined massive quark phase never rises above one. We can make the transition occur just before the speed of sound passes through 1 with $\kappa = 0.85$ for the case of $k_{IR} = 0.575$; $\kappa = 0.89$ for $k_{IR} = 0.35$ and finally $\kappa = 0.94$ for the case of $k_{IR} = 0.1$

To display this graphically we again set $\chi_0 = 330$MeV and compare the free energy of these phases to the nuclear phases' free energy and to the massive chirally broken

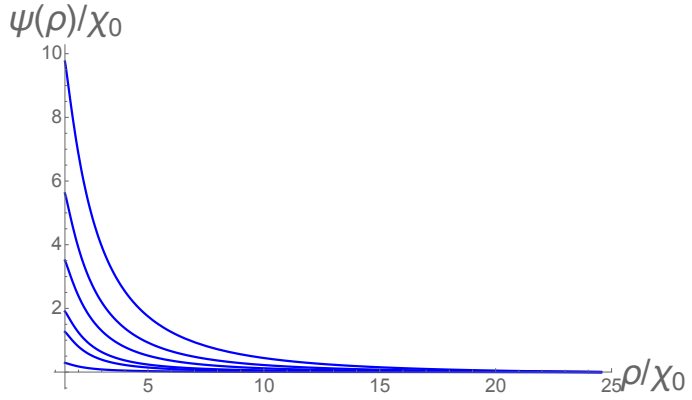

Figure 4.6: *Solutions for equations (4.14) for $\kappa = 1$ and different values of μ after condensation is triggered.*

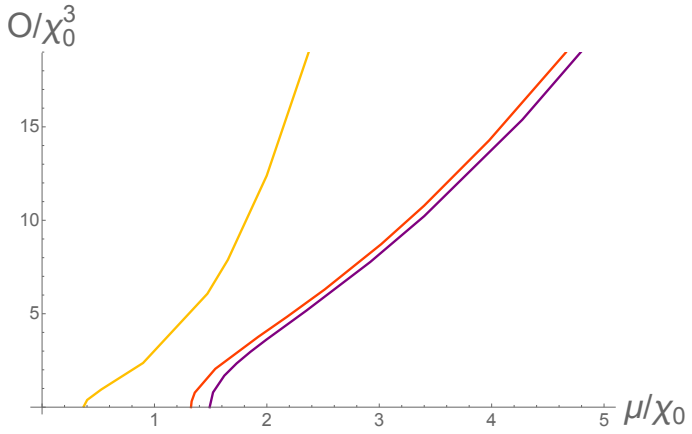

Figure 4.7: *Cooper condensate as a function of the chemical potential for different values of κ; $\kappa = 10$ (yellow), $\kappa = 1$ (red) and $\kappa = 0.85$ (purple).*

phase of the previous sections. We do this in Figure 4.9 (top left) showing the cases $k_{IR} = 0.1, 0.35$ and 0.575.

As seen before the transition to the nuclear phase occurs at 308 MeV. At 330 MeV the deconfined massive quark phase's pressure begins to rise. The $k_{IR} = 0.575$ curve rapidly becomes the true vacuum relative to even the least stiff nuclear phase. The case $k_{IR} = 0.1$ only becomes the true vacuum relative to the stiffest nuclear equation of state. For intermediate k_{IR} one can achieve curves between these limits; for example $k_{IR} = 0.35$ grows to dominate the medium and stiffest nuclear curves but does not replace the soft nuclear curve.

Now though we also include the chirally restored vacuum with colour superconductivity curves for $\kappa = 0.94, 0.89$ and 0.85. It rises sharply in pressure and becomes the true vacuum in the range μ =450-500 MeV.

In the remaining plots in Figure 4.9 we show again the speed of sound's variation with respect to μ in a number of these scenarios. For example, in the upper right we show the c_s^2 for the soft nuclear EoS, for the $k_{IR} = 0.575$ case for the chirally broken, and for

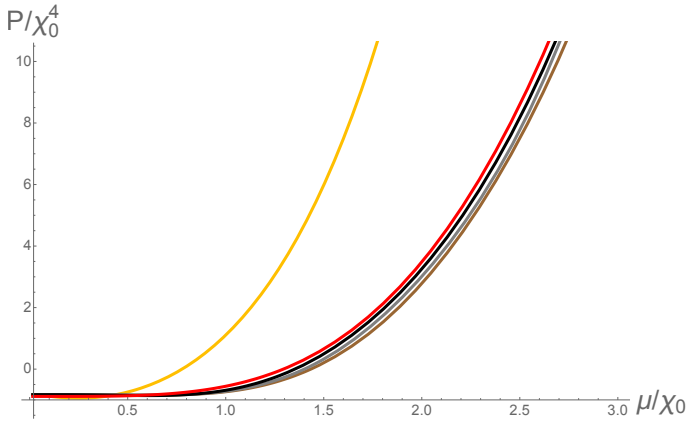

Figure 4.8: *Pressure versus chemical potential for different values of κ; $\kappa = 10$ (yellow), $\kappa = 1$ (red), $\kappa = 0.94$ (black), $\kappa = 0.89$ (gray) and $\kappa = 0.85$ (brown).*

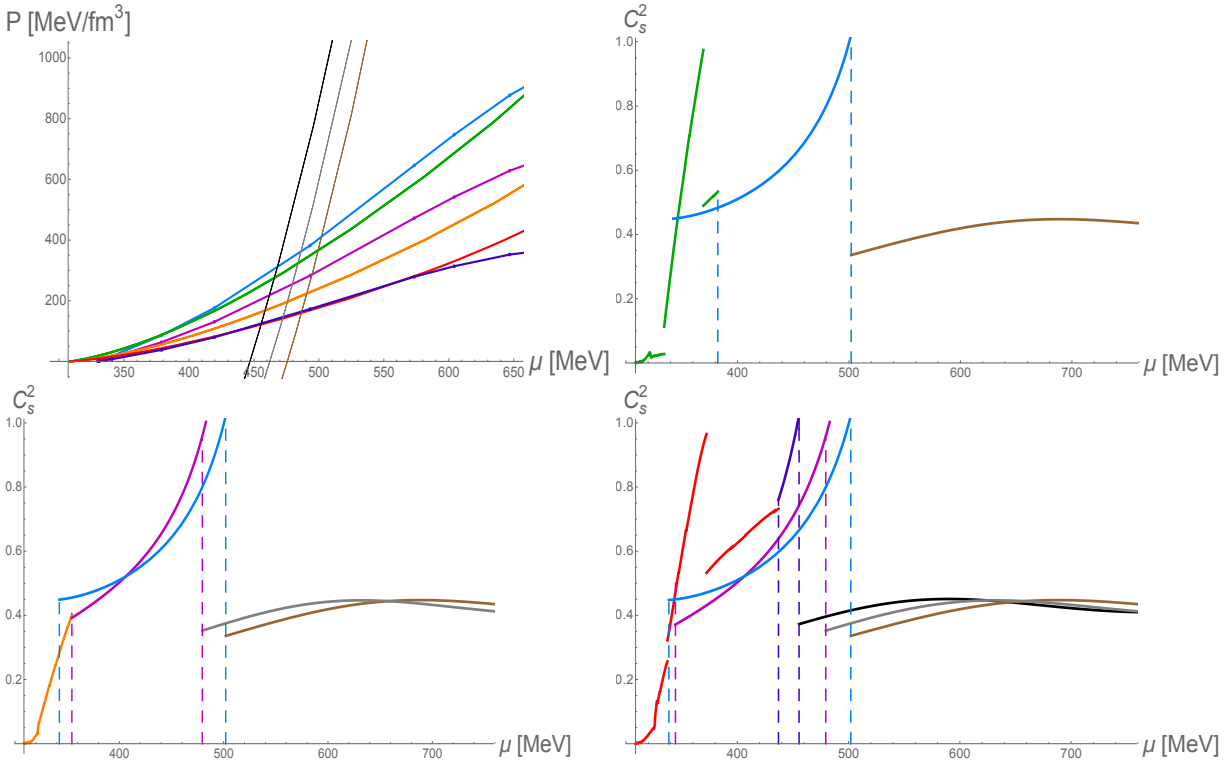

Figure 4.9: *Transitions from the nuclear phase to the deconfined phase and then to csc. The different colours represent the cases of massive chirally broken phase with $k_{IR} = 0.575$ (blue), $k_{IR} = 0.35$ (magenta) and with $k_{IR} = 0.1$ (purple) as in Fig. 4.5, whereas the CSC cases are $\kappa = 0.85$ (brown), $\kappa = 0.89$ (gray) and $\kappa = 0.94$ (black). The dashed vertical lines represent the transition from nuclear to chirally broken quark matter and from chirally broken quark matter to CSC.*

the $\kappa = 0.85$ case of CSC. The vertical dotted lines show where the phase transitions between phases occur. We have tuned κ so that the transition to the CSC phase occurs just before the speed of sound passes through 1 (in order to have the stiffest EoS we can). The inclusion of CSC in the chirally restored phase does raise c_s^2 but only a little to around 0.4. This will not be sufficient to support neutron stars if this material forms the core as we will see in the next section). The crucial role CSC is playing here is to

reduce the critical μ from the deconfined massive quark phase to ensure c_s^2 doesn't rise above 1.

The lower two figures in Fig. 4.9 show a variety of scenarios for the medium and stiff nuclear EoS. In all cases, as μ increases, there are the phases: chiral broken; nuclear; deconfined massive quark; chirally restored with CSC. In each case c_s^2 rises close to 0.7-0.8 in the nuclear phase then to close to 1 in the massive deconfined quark phase.

4.3 Compact star mass radius relations

We now follow the same path as the Section 3.3. We convert our equations of state to a relation between the mass and radius of a neutron stars by using the TOV equations mentioned in subsection 1.4.3 of chapter 1.

We integrate the TOV equations (1.84) by plug in the EoS $\mathcal{E}(P)$ as an input, as well as the central pressure $P_c = P(r = 0)$ as the initial condition, and the output are the mass $m(r)$ and Pressure $P(r)$ of the corresponding star at a radial distance r. The radius R of the star will be the value of r at which the pressure vanishes as we expect outside of the star. Then varying the initial condition P_c as a parameter we can construct a curve for the mass of the star $M = m(r = R)$ against R.

We again fix the scale with the value of $p_0 = \epsilon_0 = \frac{(308.55MeV)^4}{\pi^2}$ as is sensible in the context of the nuclear equation of state discussed above; this choice then fixes the rest of our scale parameters.

We determine the stability of a star from the mass vs radius curve using the Bardeen, Thorne and Meltzer (BTM) criteria detailed in subsection 1.4.3.

We now perform these calculations for the EoS we obtained in Figure 4.9. To summarize, our model has three parameters: χ_0 which is the IR quark mass that we have set to 330MeV; k_{IR} which we have used to ensure there is a sensible transition from the deconfined massive quark phase to the chirally restored phase; and κ which determines the strength of the CSC interaction which we have used to move the chiral restoration phase so that c_s^2 is never greater than one.

We present the mass radius relations for neutron stars that we obtain in Figure 4.10. The top plot shows an example for the softest nuclear EoS. Here we only had the case $k_{IR} = 0.575$, where the deconfined massive quark phase became the vacuum. To invoke a transition to the CSC phase when the c_s^2 has just risen to one, we set $\kappa = 0.85$ (see the top two plots of Figure 4.9). The top plot of Figure 4.10 shows the resulting stars. Where the green curve is the nuclear phase, which only plays a role as the crust of the star. The blue line marks where the star has begun to have a deconfined massive quark phase. If we did not include the CSC phase but instead as in Figure 4.5 transitioned to

the chirally restored $\chi = 0$ phase this branch extends to the highest point. After the core of the star becomes aware of the transition to the chirally restored phase the stars become unstable; this is the sharp transition to the dotted blue line that angles down to the left. The region of these stars which satisfy the stability criteria and have $c_s^2 < 1$ are marked in bright red. Finally if we allow a transition to the CSC phase rather than the $\chi = \psi = 0$ phase then we obtain the brown line. These stars with superconducting cores are again unstable but this transition occurs just before $c_s^2 = 1$ in the deconfined massive quark phase leaving a fully sensible picture of the dynamics at all μ. This EoS does not support neutron stars higher in mass than 1.7 solar masses so is presumably not a good description of QCD.

In the central figure of Figure 4.10 we show example cases using the medium stiffness EoS for the nuclear phase. Here there are deconfined massive quark phases for lower k_{IR} and we show the cases of $k_{IR} = 0.575$ and $k_{IR} = 0.35$. The plots show the same structure and elements as for the top plot as we have described. Again we found stars with quark cores with a maximum mass of 1.9 solar masses.

Finally in the bottom picture we show three cases for the least stiff nuclear EoS, with $k_{IR} = 0.575, 0.35$ and 0.1. Between the last two of these values we find solutions with deconfined massive quark cores and a upper most mass for stable stars between 1.9 and 2.4 solar masses. This is a considerable success. We have taken sensible phenomenological holographic models of the QCD equation of state and shown that such stars do exist within sensible choices of parameters. This lends credence to the idea that quark cores can exist in neutron stars and hopefully encourages study for signals of such cores in gravitational wave signals for neutron star collisions. It is interesting to look at the structure of stars in this range. In Figure 4.11 we plot the pressure vs radius profiles of the stars for the case of the soft nuclear equation of state and $k_{IR} = 0.575$, colouring the radial regions that are nuclear matter, deconfined massive quarks and the CSC phase (stars with CSC cores are unstable).

4.4 LIGO Constraints for Tidal Deformabilites

As we mentioned in subsection 1.4.4 of chapter 1 and in the previous chapter in section 3.4, if we consider a binary system of two neutron stars, the tidal forces between the two objects would have a measurable effect in the gravitational wave signal that could be observed using gravitational wave detectors. In [54] the measurement of this effect was reported as a limit given for the tidal deformabilities of the two stars involved in the merger.

The tidal deformability is related to the Love numbers of the stars and measures their susceptibility of being deformed by tidal forces.

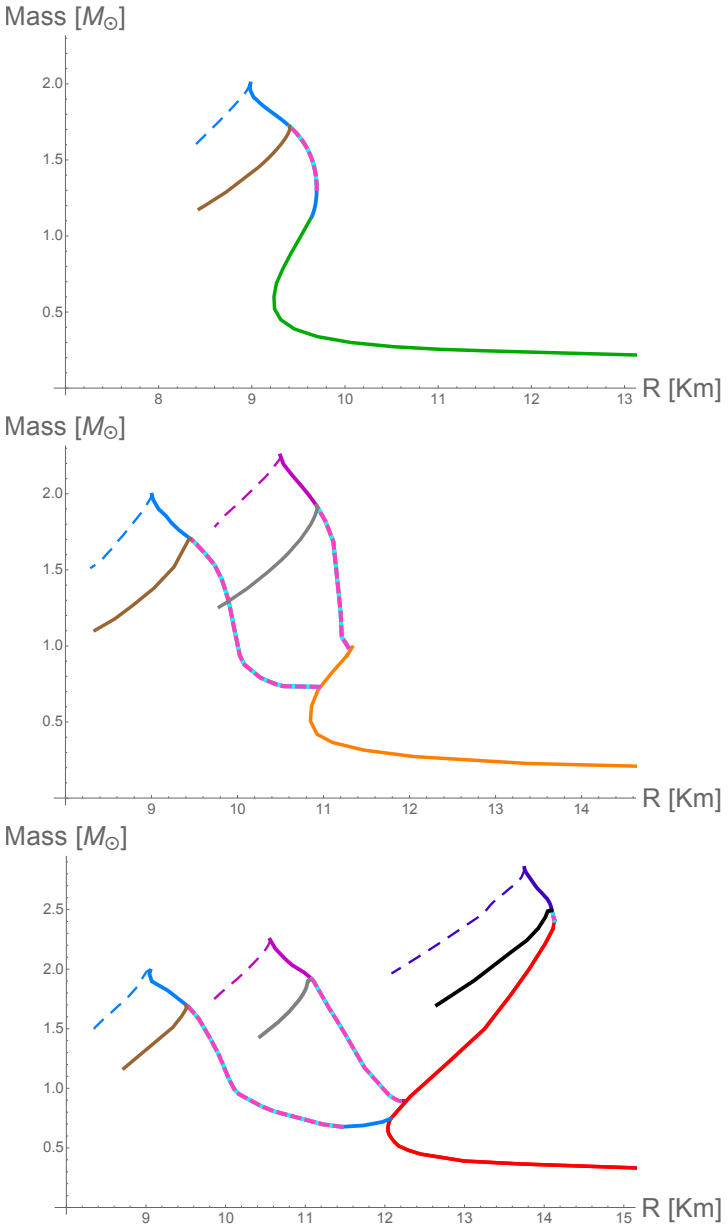

Figure 4.10: *Mass vs radius curves for the case of $k_{IR} = 0.575$ (blue), $k_{IR} = 0.35$ (magenta) and $k_{IR} = 0.1$ (purple). The curves leaving the green/red/orange nuclear EoS prediction is the transition to a quark phase from Figure 3.6. The case with $k_{IR} = 0.35$ only has a transition from medium (orange) and stiff nuclear matter (red) and the case with $k_{IR} = 0.1$ only has a transition from stiff nuclear matter. The stable branch where $c_s^2 \leq 1$ is indicated in dashed cyan/pink . The transition to a superconducting state for $\kappa = 0.85$(brown), $\kappa = 0.89$(gray) and $\kappa = 0.94$(black) just before the speed of sound goes beyond 1 is also shown.*

We calculate the tidal deformability by starting with the solutions of TOV equations (1.84): $m(r)$ and $p(r)$, then we can solve the system of equations (1.94) to find the radial function $H(r)$ of the spherical harmonics expansion, and then find $z_R = RH'(R)/H(R)$ which is evaluated at the radius R of the star.

Then using z_R we then can obtain the Love number with equation (1.93) and then, the tidal deformability with equation (1.90). Thus we obtain the tidal deformability as a

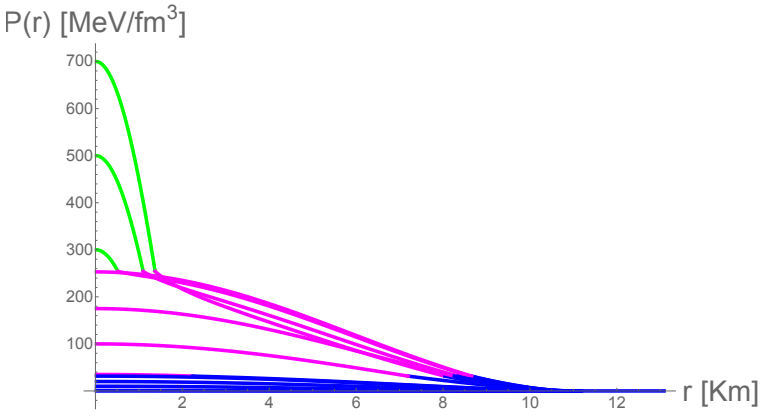

Figure 4.11: *Pressure as a function of the radial distance r in Km for a hybrid star. The blue line corresponds to medium EoS nuclear matter. The pink line corresponds to the massive chirally broken phase with $k_{IR} = 0.35$. The green line corresponds to the superconducting phase with $\kappa = 0.89$ (stars with superconducting cores are unstable).*

function of the mass of one of the neutron stars of the system.

In Figure 4.12 we obtained the tidal deformability as a function of the mass for two of the cases showed in Figure 4.10. The first one corresponds to a transition from soft nuclear matter to the massive deconfined quark matter with $k_{IR} = 0.575$ (blue line); the second one corresponds to a transition from medium nuclear matter to the massive deconfined quark matter with $k_{IR} = 0.35$ (magenta line). We choose this cases since the range of masses they have for stable solutions fit in the range cited for the detected signal from a binary neutron star inspiral in [54].

We can see that as we increase the central pressure for both cases the tidal deformabilty decreases as the mass increases.

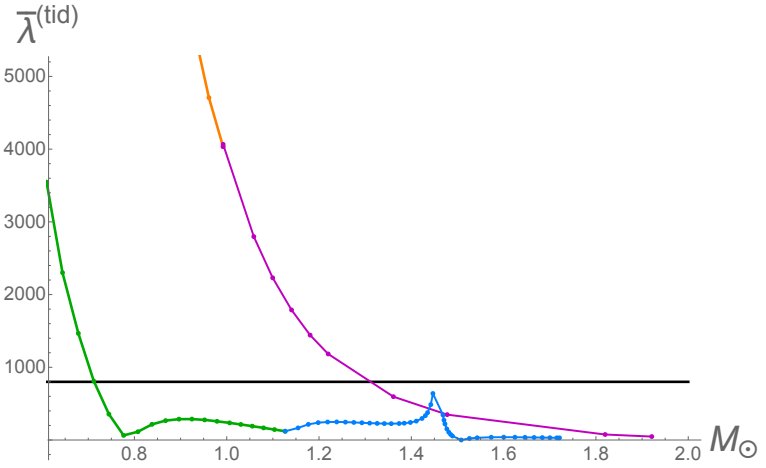

Figure 4.12: *The dimensionless tidal deformability as a function of the mass (in units of solar masses) for a holographic quark, and nuclear equations of state. The soft nuclear phase (green) has a transition to a chirally broken quark matter phase with $k_{IR} = 0.575$ (blue). The medium nuclear phase (orange) has a transition to a chirally broken quark matter phase with $k_{IR} = 0.35$ (magenta). The LIGO/Virgo upper bound of $\bar{\lambda}^{(\mathrm{tid})} = 800$ at $1.4M_\odot$ is indicated by the horizontal black line.*

LIGO and Virgo provide the constraint $\bar{\lambda}(1.4M_\odot) \leq 800$ for the likely case of slowly rotating stars (the low-spin prior) at a 90% Bayesian probability level. Additionally Fig. 5 of [54] gives both 90% and 50% probability contours for the independent tidal deformabilities of the two stars on a $\bar{\lambda}_1 - \bar{\lambda}_2$ plane. To compare our results to these values, we show in Figure 4.4 how our example EoSs relate to these contours. The curves are generated by independently determining the tidal deformabilities for each of the stars involved in the merger. To describe the binary system we take a chirp mass $\mathcal{M} = 1.188$ solar mass. This means that the the two stars involved in the binary neutron star merger correspond to masses $m_1 \in [1.36, 1.60]M_\odot$ and $m_2 \in [1.17, 1.36]M_\odot$. We observe that the two cases considered fit inside the 90% probability contour.

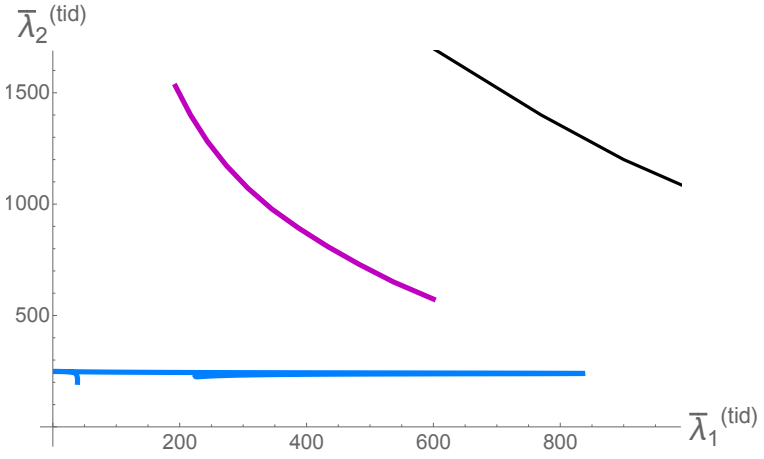

Figure 4.13: *The tidal deformabilities $\bar{\lambda}_i$ obtained for two stars with masses as the ones involved in the binary Neutron Star merger observed by LIGO and Virgo [54], corresponding to masses $m_1 \in [1.36, 1.60]M_\odot$ and $m_2 \in [1.17, 1.36]M_\odot$ (low-spin prior). The curves stand for the corresponding quark matter phases displayed in Fig. 4.12; the chirally broken quark matter phase with $k_{IR} = 0.575$ (blue) and the chirally broken quark matter phase with $k_{IR} = 0.35$ (magenta). The black curve is a sketch of the 90% experimental bound contour given in figure 5 of [54].*

4.5 Discussion

The increase in the number of neutron star radius and mass measurements and the continued reduction of the uncertainties, which recently put the known range between 1.17 up to over 2.14 solar masses and radius between 9.9 and 11.2 km [105, 106], has challenged our understanding of the QCD equation of state even within nuclear matter models. At the cores of these stars it seems the matter must be very stiff with speeds of sound close to the speed of light. Gravitational wave signals from colliding neutron star pairs are also beginning to constrain the EoS through measurements of the tidal deformability. It is therefore interesting to keep studying the possibility of deconfined quark matter in the cores of compact stars or generate other hybrid stars. In order to being able to do this we require the capacity to work and obtain information from the strongly coupled, deconfined section of the QCD phase diagram. As we have stressed

before, at the present time there are no first principles tools that allows us to work in this regime straightforwardly. This is our main motivation to use holography to explore possible descriptions of this regime in QCD.

The first holography paper addressing neutron star structure [73] used the exact results at finite μ for the D3/D7 dual system. That system has conformal gauge dynamics and no chiral symmetry breaking unless introduced by a hard mass. It predicted a very soft equation of state that could not obtain stable solutions for stars with quark matter. Then in the last chapter we adjusted that model to include a running anomalous dimension for the quark condensate which introduces a dynamical chiral symmetry breaking mechanism. The kind of theories obtained suggest a massive deconfined phase with deconfined quarks yet chiral symmetry breaking before moving to the chirally restored high density phase. We have shown that this leads to a stiffer equation of state in the relevant intermediate μ phase and that the speed of sound has the required non-monotonicity in this regime.

In the present chapter we proposed a model based on the DBI action of a $D7$-brane in AdS_5 with a scalar field describing the chiral condensate and a $U(1)$ gauge field for the chemical potential. We included a mass term for the scalar by hand that allows us to include the running anomalous dimension of the condensate, γ. We input the mass term form from the perturbative QCD running result for γ allowing it to naively extend to the non-perturbative regime. The chirally broken phase obtained resists transition to the chirally restored phase leading to a first order chiral transition. This leads to EoS that are even stiffer than our previous examples in Chapter 3, with a speed of sound rising close to the speed of light.

Based in our results in Chapter 2 we included a holographic description of a possible colour superconducting state above the first order chiral restoration transition. We included a new scalar field dual to the Cooper pair in analogy to the scalar describing the chiral condensate. Since the Cooper pair carries net baryon charge it couples directly to the $U(1)$ gauge field and the chemical potential itself generates a BF bound violation that triggers a superconducting phase. This phase allowed us to transition from the chirally broken phase to the CSC phase, just before the speed of sound passes through one. We did this by tuning the strength of the $U(1)$ gauge field interaction.

We have used the TOV equations to model compact stars using our EoS varying the parameters in our model. The instability of the colour superconductivity phase star branch remains but previous to that we do see the formation of novel hybrid stars with quark matter cores. The transition from nuclear matter to quark matter happens at densities of the order of 4 times the nuclear saturation density for the case of soft nuclear matter; of the order of $2n_s$ for the case of medium nuclear matter, and of the order of $1.5n_s$ for the case of stiff nuclear matter. The model allows us to obtain stable

compact stars of masses between 0.74 and 1.93 solar masses with radius in the range of observed neutron stars, and even a star of $2.38 M_{\odot}$ with a radius of 14.1 km.

Chapter 5

Concluding Remarks

In this thesis we have introduced the basic ideas needed to understand the specific approach of the AdS/CFT correspondence made known in [36], in which one adds flavour branes in the quenched approximation (i.e. without backreaction from part of branes to the space-time geometry) in order to introduce matter degrees of freedom in the field theory. Then, in principle, by studying the behaviour of the quantum field side and compare it with known results from QCD where they are available, one can learn more about the family of theories that exhibit some of the key features of QCD. After an introductory Chapter 1, we devoted the following chapters to making an attempt to gain insight into some aspects of high density matter in the low temperature regime and apply this models to astrophysical systems.

In Chapter 2 we were able to obtain an estimate of the phase boundary for the colour superconductivity phase in the temperature-chemical potential phase diagram of QCD. We were also made a conservative estimate of the position of the boundary between the CFL and 2CS phases for the mass dependent case by a very simple model of an interaction between a quark mass and the Cooper pair. This matches the form of the usually expected phase structure.

In Chapter 3 we focused in taking another step in the exploration of the possibility of quark matter inside neutron stars using the holographic correspondence. We adjusted the exact results at finite chemical potential for the D3/D7 dual system that predicts equations of state that are not stiff enough to support stable stars composed of quark matter, by adding a mechanism for the breaking of the chiral symmetry in the field theory side of the correspondence. This mechanism consisted in include a running anomalous dimension for the quark condensate. The kind of theories obtained by this mechanism suggested a massive deconfined phase with deconfined quarks and broken chiral symmetry, before a second order phase transition to a chirally restored high density phase.

We have shown that this leads to stiffer equations of state and that the speed of sound shows a non-monotonic behaviour in this regime, which breaks the conformal bound of $C_s^2 \leq 1/3$. This is in agreement with the existence of more massive neutron stars of around 2 solar masses, since equations of state that hold $C_s^2 \leq 1/3$ are very constrained up to baryon number densities about $2n_s$, so the increase of the pressure with the density is limited by the very assumption $dP/d\mathcal{E} < 1/3$. In those cases, the equation of state with the largest maximum mass is that with the largest pressure above $2n_s$. As a consequence, there is a bound on the largest neutron star mass consistent with the 1/3 bound in the speed of sound. For most of the models the bound is at around 1.9 solar masses, with only a few allowing neutron stars of 2 solar masses and no model allowing a mass $M \geq 2.1 M_\odot$

Nevertheless, the equations of state obtained in this chapter did not provide stable solutions massive enough to compare the tidal deformability of a binary system with observations made by the LIGO-Virgo interferometers.

In Chapter 4 we continued the same line of research as in the previous chapter but we modified the chiral symmetry breaking mechanism introduced in Chapter 3. Motivated by our intention to include a colour superconducting phase, we described the Cooper condensing qq operator with an extra scalar field that we introduced into the holographic model in analogy to the chiral condensate field. Thus for the chiral symmetry breaking mechanism we did not introduce the running of the anomalous dimension through a dilaton factor but directly through a ρ dependent mass term.

This ansatz was successful and led us to very stiff equations of state, stiff enough to support compact stars with quark matter of masses of up to $2.38 M_\odot$. We then compared our stable solutions with observations made by the LIGO and Virgo collaboration of the tidal deformabilities obtained from the detection of gravitational waves from a binary neutron star inspiral. We observed an agreement with the data reported by LIGO and Virgo as the two cases we considered fit inside the 90% probability contour.

Overall we have developed the work presented in this thesis following a phenomenological approach, which means that the work was made in a bottom up fashion in the spirit of AdS/QCD models, where the number of flavours is $N = 3$, or AdS/Condensed Matter, where phonon interactions of electrons are described. Generally speaking we have used an AdS space-time to phenomenologically describe the conformal symmetries of the free fermions, which are then broken by the operators and sources of the theory that appear in the bulk, take for example the chemical potential.

There are clearly a number of limitations in our approach, which encompass for example the fact that the holographic models studied in this thesis are not dual to QCD and that we work in the probe limit of the D3/D7 system, which rigorously can only be applied in the limit $N_f \ll N$. One should also worry that at low N the bulk modes might become

strongly coupled and stringy but the AdS/QCD philosophy in general is to keep going and measure the success of the model by the output obtained.

There is still a long way ahead for these kind of models. There is still work to be done in extending the space of current models. For example, taking holographic models in the Veneziano limit, which would allows us to have gluons and dynamical quarks which are fully backreacted to the glue.

The LIGO and Virgo collaboration has continued observing the cosmos, and even more precise constrains will be put on the equation of state in years to come. In addition, heavy ion collisions experiments, such as the ones taking place in the Relativistic Heavy Ion Collider at Brookhaven National Laboratory, focus on studying the quark-gluon plasma. These experiments may also bring useful data to better understand the QCD phase diagram.

References

[1] Kazem Bitaghsir Fadafan, Jesus Cruz Rojas, and Nick Evans. Holographic description of color superconductivity. *Phys. Rev. D*, 98(6):066010, 2018.

[2] Kazem Bitaghsir Fadafan, Jesus Cruz Rojas, and Nick Evans. Deconfined, Massive Quark Phase at High Density and Compact Stars: A Holographic Study. *Phys. Rev. D*, 101(12):126005, 2020.

[3] S.W. Hawking and G.F.R. Ellis. *The Large Scale Structure of Space-Time*. Cambridge Monographs on Mathematical Physics. Cambridge University Press, 2 2011.

[4] H. Fritzsch, Murray Gell-Mann, and H. Leutwyler. Advantages of the Color Octet Gluon Picture. *Phys. Lett.*, 47B:365–368, 1973.

[5] Christof Gattringer and Kurt Langfeld. Approaches to the sign problem in lattice field theory. *Int. J. Mod. Phys.*, A31(22):1643007, 2016.

[6] Juan Martin Maldacena. The Large N limit of superconformal field theories and supergravity. *Int. J. Theor. Phys.*, 38:1113–1133, 1999. [Adv. Theor. Math. Phys.2,231(1998)].

[7] Michael E. Peskin and Daniel V. Schroeder. *An Introduction to quantum field theory*. Addison-Wesley, Reading, USA, 1995.

[8] John F. Donoghue, Eugene Golowich, and Barry R. Holstein. *Dynamics of the Standard Model*. Cambridge Monographs on Particle Physics, Nuclear Physics and Cosmology. Cambridge University Press, 2 edition, 2014.

[9] Murray Gell-Mann. A Schematic Model of Baryons and Mesons. *Phys. Lett.*, 8:214–215, 1964.

[10] G. Zweig. An SU(3) model for strong interaction symmetry and its breaking. Version 1. 1 1964.

[11] H. Fritzsch. History of QCD. *Subnucl. Ser.*, 50:23–27, 2014.

[12] L.D. Faddeev and V.N. Popov. Feynman Diagrams for the Yang-Mills Field. *Phys. Lett. B*, 25:29–30, 1967.

[13] Kazuo Fujikawa. Path-integral measure for gauge-invariant fermion theories. *Phys. Rev. Lett.*, 42:1195–1198, Apr 1979.

[14] J. Bardeen, L. N. Cooper, and J. R. Schrieffer. Theory of superconductivity. *Phys. Rev.*, 108:1175–1204, Dec 1957.

[15] Jeffrey Goldstone, Abdus Salam, and Steven Weinberg. Broken Symmetries. *Phys. Rev.*, 127:965–970, 1962.

[16] J. C. Collins and M. J. Perry. Superdense matter: Neutrons or asymptotically free quarks? *Phys. Rev. Lett.*, 34:1353–1356, May 1975.

[17] Dirk H. Rischke. The Quark gluon plasma in equilibrium. *Prog. Part. Nucl. Phys.*, 52:197–296, 2004.

[18] G. Benfatto and G. Gallavotti. Renormalization-group approach to the theory of the Fermi surface. *Phys. Rev.*, B42:9967–9972, 1990.

[19] R. Shankar. Renormalization group approach to interacting fermions. *Rev. Mod. Phys.*, 66:129–192, 1994.

[20] Joseph Polchinski. Effective field theory and the Fermi surface. In *Proceedings, Theoretical Advanced Study Institute (TASI 92): From Black Holes and Strings to Particles: Boulder, USA, June 1-26, 1992*, pages 0235–276, 1992.

[21] Nick J. Evans, Stephen D. H. Hsu, and Myckola Schwetz. An Effective field theory approach to color superconductivity at high quark density. *Nucl. Phys.*, B551:275–289, 1999.

[22] Mark G. Alford, Andreas Schmitt, Krishna Rajagopal, and Thomas Schfer. Color superconductivity in dense quark matter. *Rev. Mod. Phys.*, 80:1455–1515, 2008.

[23] Mark G. Alford, Krishna Rajagopal, and Frank Wilczek. Color flavor locking and chiral symmetry breaking in high density QCD. *Nucl. Phys. B*, 537:443–458, 1999.

[24] J. Polchinski. *String theory. Vol. 1: An introduction to the bosonic string.* Cambridge Monographs on Mathematical Physics. Cambridge University Press, 12 2007.

[25] J. Polchinski. *String theory. Vol. 2: Superstring theory and beyond.* Cambridge Monographs on Mathematical Physics. Cambridge University Press, 12 2007.

[26] B. Zwiebach. *A first course in string theory.* Cambridge University Press, 7 2006.

[27] Martin Ammon and Johanna Erdmenger. *Gauge/gravity duality: Foundations and applications.* Cambridge University Press, Cambridge, 4 2015.

[28] Johanna Erdmenger, Nick Evans, Ingo Kirsch, and Ed Threlfall. Mesons in Gauge/Gravity Duals - A Review. *Eur. Phys. J.*, A35:81–133, 2008.

[29] F. Gliozzi, Joel Scherk, and David I. Olive. Supersymmetry, Supergravity Theories and the Dual Spinor Model. *Nucl. Phys. B*, 122:253–290, 1977.

[30] Joseph Polchinski. Dirichlet Branes and Ramond-Ramond charges. *Phys. Rev. Lett.*, 75:4724–4727, 1995.

[31] Edward Witten. Anti-de Sitter space and holography. *Adv. Theor. Math. Phys.*, 2:253–291, 1998.

[32] S.S. Gubser, Igor R. Klebanov, and Alexander M. Polyakov. Gauge theory correlators from noncritical string theory. *Phys. Lett. B*, 428:105–114, 1998.

[33] Peter Breitenlohner and Daniel Z. Freedman. Stability in Gauged Extended Supergravity. *Annals Phys.*, 144:249, 1982.

[34] Sangmin Lee, Shiraz Minwalla, Mukund Rangamani, and Nathan Seiberg. Three point functions of chiral operators in D = 4, N=4 SYM at large N. *Adv. Theor. Math. Phys.*, 2:697–718, 1998.

[35] M. Henningson and K. Skenderis. The Holographic Weyl anomaly. *JHEP*, 07:023, 1998.

[36] Andreas Karch and Emanuel Katz. Adding flavor to AdS / CFT. *JHEP*, 06:043, 2002.

[37] Edward Witten. Anti-de Sitter space, thermal phase transition, and confinement in gauge theories. *Adv. Theor. Math. Phys.*, 2:505–532, 1998.

[38] Andrew Chamblin, Roberto Emparan, Clifford V. Johnson, and Robert C. Myers. Charged AdS black holes and catastrophic holography. *Phys. Rev. D*, 60:064018, 1999.

[39] Nick J. Evans and Michela Petrini. Superfluidity in the AdS / CFT correspondence. *JHEP*, 11:043, 2001.

[40] Shinpei Kobayashi, David Mateos, Shunji Matsuura, Robert C. Myers, and Rowan M. Thomson. Holographic phase transitions at finite baryon density. *JHEP*, 02:016, 2007.

[41] Andreas Karch and Andy O'Bannon. Holographic thermodynamics at finite baryon density: Some exact results. *JHEP*, 11:074, 2007.

[42] Joshua Erlich, Emanuel Katz, Dam T. Son, and Mikhail A. Stephanov. QCD and a holographic model of hadrons. *Phys. Rev. Lett.*, 95:261602, 2005.

[43] Norman K Glendenning. *Compact stars: nuclear physics, particle physics and general relativity.* Astronomy and Astrophysics Library. Springer, New York, 1996.

[44] P. Haensel, A.Y. Potekhin, and D.G. Yakovlev. *Neutron stars 1: Equation of state and structure*, volume 326. Springer, New York, USA, 2007.

[45] A. Hewish, S.J. Bell, J.D.H Pilkington, P.F. Scott, and R.A. Collins. Observation of a rapidly pulsating radio source. *Nature*, 217:709–713, 1968.

[46] W. Baade and F. Zwicky. Remarks on super-novae and cosmic rays. *Phys. Rev.*, 46:76–77, Jul 1934.

[47] J. R. Oppenheimer and G. M. Volkoff. On massive neutron cores. *Phys. Rev.*, 55:374–381, Feb 1939.

[48] K. Hebeler, J.M. Lattimer, C.J. Pethick, and A. Schwenk. Equation of state and neutron star properties constrained by nuclear physics and observation. *Astrophys. J.*, 773:11, 2013.

[49] K. Hebeler, J.M. Lattimer, C.J. Pethick, and A. Schwenk. Constraints on neutron star radii based on chiral effective field theory interactions. *Phys. Rev. Lett.*, 105:161102, 2010.

[50] Hsin-Yu Chen, Paul M. Chesler, and Abraham Loeb. Searching for exotic cores with binary neutron star inspirals. *Astrophys. J. Lett.*, 893(1):L4, 2020.

[51] Mark G. Alford, Steven P. Harris, and Pratik S. Sachdeva. On the stability of strange dwarf hybrid stars. *Astrophys. J.*, 847(2):109, 2017.

[52] James M. Bardeen, Kip S. Thorne, and David W. Meltzer. A Catalogue of Methods for Studying the Normal Modes of Radial Pulsation of General-Relativistic Stellar Models. , 145:505, August 1966.

[53] B. P. Abbott et al. Observation of Gravitational Waves from a Binary Black Hole Merger. *Phys. Rev. Lett.*, 116(6):061102, 2016.

[54] B. P. Abbott et al. GW170817: Observation of Gravitational Waves from a Binary Neutron Star Inspiral. *Phys. Rev. Lett.*, 119(16):161101, 2017.

[55] Eanna E. Flanagan and Tanja Hinderer. Constraining neutron star tidal Love numbers with gravitational wave detectors. *Phys. Rev.*, D77:021502, 2008.

[56] Kip S. Thorne. Tidal stabilization of rigidly rotating, fully relativistic neutron stars. *Phys. Rev. D*, 58:124031, Nov 1998.

[57] R. Shankar. Renormalization group for interacting fermions in d ¿ 1. *Physica A: Statistical Mechanics and its Applications*, 177(1):530 – 536, 1991.

[58] D.T. Son. Superconductivity by long range color magnetic interaction in high density quark matter. *Phys. Rev. D*, 59:094019, 1999.

[59] D. V. Deryagin, Dmitri Yu. Grigoriev, and V. A. Rubakov. Standing wave ground state in high density, zero temperature QCD at large N(c). *Int. J. Mod. Phys.*, A7:659–681, 1992.

[60] E. Shuster and D.T. Son. On finite density QCD at large N(c). *Nucl. Phys. B*, 573:434–446, 2000.

[61] Sean A. Hartnoll, Christopher P. Herzog, and Gary T. Horowitz. Building a Holographic Superconductor. *Phys. Rev. Lett.*, 101:031601, 2008.

[62] Riccardo Apreda, Johanna Erdmenger, Nick Evans, and Zachary Guralnik. Strong coupling effective Higgs potential and a first order thermal phase transition from AdS/CFT duality. *Phys. Rev. D*, 71:126002, 2005.

[63] Heng-Yu Chen, Koji Hashimoto, and Shunji Matsuura. Towards a Holographic Model of Color-Flavor Locking Phase. *JHEP*, 02:104, 2010.

[64] Anton F. Faedo, David Mateos, Christiana Pantelidou, and Javier Tarrio. Towards a Holographic Quark Matter Crystal. *JHEP*, 10:139, 2017. [Erratum: JHEP 07, 058 (2019)].

[65] Adith Ramamurti, Edward Shuryak, and Ismail Zahed. Are there monopoles in the quark-gluon plasma? *Phys. Rev. D*, 97(11):114028, 2018.

[66] Barry A. Freedman and Larry D. McLerran. Fermions and Gauge Vector Mesons at Finite Temperature and Density. 3. The Ground State Energy of a Relativistic Quark Gas. *Phys. Rev. D*, 16:1169, 1977.

[67] Edward Witten. Multitrace operators, boundary conditions, and AdS / CFT correspondence. 2001.

[68] Thomas Faulkner, Gary T. Horowitz, and Matthew M. Roberts. Holographic quantum criticality from multi-trace deformations. *JHEP*, 04:051, 2011.

[69] Nick Evans and Keun-Young Kim. Holographic NambuJona-Lasinio interactions. *Phys. Rev.*, D93(6):066002, 2016.

[70] Barry A. Freedman and Larry D. McLerran. Fermions and Gauge Vector Mesons at Finite Temperature and Density. 1. Formal Techniques. *Phys. Rev. D*, 16:1130, 1977.

[71] Barry A. Freedman and Larry D. McLerran. Fermions and Gauge Vector Mesons at Finite Temperature and Density. 2. The Ground State Energy of a Relativistic electron Gas. *Phys. Rev. D*, 16:1147, 1977.

[72] Veselin G. Filev, Clifford V. Johnson, R. C. Rashkov, and K. S. Viswanathan. Flavoured large N gauge theory in an external magnetic field. *JHEP*, 10:019, 2007.

[73] Carlos Hoyos, David Rodrguez Fernndez, Niko Jokela, and Aleksi Vuorinen. Holographic quark matter and neutron stars. *Phys. Rev. Lett.*, 117(3):032501, 2016.

[74] I. Tews, T. Krger, K. Hebeler, and A. Schwenk. Neutron matter at next-to-next-to-next-to-leading order in chiral effective field theory. *Phys. Rev. Lett.*, 110(3):032504, 2013.

[75] A. Gezerlis, I. Tews, E. Epelbaum, S. Gandolfi, K. Hebeler, A. Nogga, and A. Schwenk. Quantum Monte Carlo Calculations with Chiral Effective Field Theory Interactions. *Phys. Rev. Lett.*, 111(3):032501, 2013.

[76] A. Vuorinen. The Pressure of QCD at finite temperatures and chemical potentials. *Phys. Rev. D*, 68:054017, 2003.

[77] Aleksi Kurkela and Aleksi Vuorinen. Cool quark matter. *Phys. Rev. Lett.*, 117(4):042501, 2016.

[78] Kenji Fukushima and Chihiro Sasaki. The phase diagram of nuclear and quark matter at high baryon density. *Prog. Part. Nucl. Phys.*, 72:99–154, 2013.

[79] Christian Ecker, Carlos Hoyos, Niko Jokela, David Rodrguez Fernndez, and Aleksi Vuorinen. Stiff phases in strongly coupled gauge theories with holographic duals. *JHEP*, 11:031, 2017.

[80] Eemeli Annala, Christian Ecker, Carlos Hoyos, Niko Jokela, David Rodrguez Fernndez, and Aleksi Vuorinen. Holographic compact stars meet gravitational wave constraints. *JHEP*, 12:078, 2018.

[81] Niko Jokela, Matti Jrvinen, and Jere Remes. Holographic QCD in the Veneziano limit and neutron stars. *JHEP*, 03:041, 2019.

[82] Kazem Bitaghsir Fadafan, Farideh Kazemian, and Andreas Schmitt. Towards a holographic quark-hadron continuity. *JHEP*, 03:183, 2019.

[83] Raul Alvares, Nick Evans, and Keun-Young Kim. Holography of the Conformal Window. *Phys. Rev. D*, 86:026008, 2012.

[84] Matti Jarvinen and Elias Kiritsis. Holographic Models for QCD in the Veneziano Limit. *JHEP*, 03:002, 2012.

[85] Nick Evans, Astrid Gebauer, Keun-Young Kim, and Maria Magou. Holographic Description of the Phase Diagram of a Chiral Symmetry Breaking Gauge Theory. *JHEP*, 03:132, 2010.

[86] Nick Evans, Astrid Gebauer, Maria Magou, and Keun-Young Kim. Towards a Holographic Model of the QCD Phase Diagram. *J. Phys. G*, 39:054005, 2012.

[87] Nicolas Kovensky and Andreas Schmitt. Heavy Holographic QCD. *JHEP*, 02:096, 2020.

[88] Tadakatsu Sakai and Shigeki Sugimoto. Low energy hadron physics in holographic QCD. *Prog. Theor. Phys.*, 113:843–882, 2005.

[89] Takaaki Ishii, Matti Jrvinen, and Govert Nijs. Cool baryon and quark matter in holographic QCD. *JHEP*, 07:003, 2019.

[90] Oren Bergman, Gilad Lifschytz, and Matthew Lippert. Holographic Nuclear Physics. *JHEP*, 11:056, 2007.

[91] Si-wen Li, Andreas Schmitt, and Qun Wang. From holography towards real-world nuclear matter. *Phys. Rev. D*, 92(2):026006, 2015.

[92] Nick Evans, Keun-Young Kim, Maria Magou, Yunseok Seo, and Sang-Jin Sin. The Baryonic Phase in Holographic Descriptions of the QCD Phase Diagram. *JHEP*, 09:045, 2012.

[93] Bob Holdom. Raising the Sideways Scale. *Phys. Rev. D*, 24:1441, 1981.

[94] V.A. Miransky and Koichi Yamawaki. Conformal phase transition in gauge theories. *Phys. Rev. D*, 55:5051–5066, 1997. [Erratum: Phys.Rev.D 56, 3768 (1997)].

[95] David B. Kaplan, Jong-Wan Lee, Dam T. Son, and Mikhail A. Stephanov. Conformality Lost. *Phys. Rev. D*, 80:125005, 2009.

[96] Nick Evans and Kimmo Tuominen. Holographic modelling of a light technidilaton. *Phys. Rev. D*, 87(8):086003, 2013.

[97] Paulo Bedaque and Andrew W. Steiner. Sound velocity bound and neutron stars. *Phys. Rev. Lett.*, 114(3):031103, 2015.

[98] Tianqi Zhao and James M. Lattimer. Tidal Deformabilities and Neutron Star Mergers. *Phys. Rev.*, D98(6):063020, 2018.

[99] Sergey Postnikov, Madappa Prakash, and James M. Lattimer. Tidal Love Numbers of Neutron and Self-Bound Quark Stars. *Phys. Rev.*, D82:024016, 2010.

[100] Tanja Hinderer, Benjamin D. Lackey, Ryan N. Lang, and Jocelyn S. Read. Tidal deformability of neutron stars with realistic equations of state and their gravitational wave signatures in binary inspiral. *Phys. Rev.*, D81:123016, 2010.

[101] Luis A.H. Mamani, Cesar V. Flores, and Vilson T. Zanchin. Phase diagram and compact stars in a holographic QCD model. 6 2020.

[102] Timo Alho, Nick Evans, and Kimmo Tuominen. Dynamic AdS/QCD and the Spectrum of Walking Gauge Theories. *Phys. Rev. D*, 88:105016, 2013.

[103] Nick Evans and Marc Scott. Hyper-Scaling Relations in the Conformal Window from Dynamic AdS/QCD. *Phys. Rev. D*, 90(6):065025, 2014.

[104] Nick J. Evans and Michela Petrini. Superfluidity in the AdS / CFT correspondence. *JHEP*, 11:043, 2001.

[105] Feryal zel and Paulo Freire. Masses, Radii, and the Equation of State of Neutron Stars. *Ann. Rev. Astron. Astrophys.*, 54:401–440, 2016.

[106] H. Thankful Cromartie et al. Relativistic Shapiro delay measurements of an extremely massive millisecond pulsar. *Nature Astron.*, 4(1):72–76, 2019.